



<http://researchspace.auckland.ac.nz>

ResearchSpace@Auckland

Copyright Statement

The digital copy of this thesis is protected by the Copyright Act 1994 (New Zealand).

This thesis may be consulted by you, provided you comply with the provisions of the Act and the following conditions of use:

- Any use you make of these documents or images must be for research or private study purposes only, and you may not make them available to any other person.
- Authors control the copyright of their thesis. You will recognise the author's right to be identified as the author of this thesis, and due acknowledgement will be made to the author where appropriate.
- You will obtain the author's permission before publishing any material from their thesis.

To request permissions please use the Feedback form on our webpage.

<http://researchspace.auckland.ac.nz/feedback>

General copyright and disclaimer

In addition to the above conditions, authors give their consent for the digital copy of their work to be used subject to the conditions specified on the [Library Thesis Consent Form](#) and [Deposit Licence](#).

Note : Masters Theses

The digital copy of a masters thesis is as submitted for examination and contains no corrections. The print copy, usually available in the University Library, may contain corrections made by hand, which have been requested by the supervisor.

Design Studies Towards Mixers and Pumps Based on Electrochemically Active Conducting Polymers for Microfluidic Devices

Karthik Kannappan

A thesis submitted in fulfilment of the requirements for the degree of
Doctor of Philosophy
The University of Auckland
2011

ABSTRACT

This thesis concerns the design of mixers and pumps for microfluidic devices, based on the actuation and ion-exchange properties of electrochemically active conducting polymers (ECP). Electrochemical oxidation or reduction of these polymers is accompanied by ion-exchange with the electrolyte and an associated change of volume. The thesis proposes that this volume change can be utilised for the purpose of mixing and pumping, in which the electrochemical cell is formed within a microfluidic structure and the motion is induced in the electrolyte as a consequence of redox reaction of the polymer.

The thesis falls into three parts. The first part explores theoretically the propagation of composition waves along a strip of ECP upon electrochemical stimulation, and the use of such waves as a means of mixing and pumping. For the theoretical description of the propagation of composition waves, an efficient solution of the electro-neutral Nernst–Planck equations in 2-D for electromigration and diffusional transport in the solution is developed. Under some circumstances, waves reflecting back from the end of the strip are predicted. We then demonstrate theoretically how such waves, associated as they are with expansion of the polymer, could be employed to enhance mixing or induce pumping in microfluidic systems. The anticipated effects of using ECP alone, based on known volume changes for ECP as a consequence of the redox reaction, seemed quite small. Therefore, the second part of the thesis explores the idea that, by using an ion sensitive polyelectrolyte gel as the electrolyte surrounding the ECP, a significant amplification of motion could be achieved. The hydrogel and ECP are assumed formed as a uniformly mixed composite. A 1-D model incorporating both diffusion and migration of ions and accounting for the space- and time-dependent variation in both ionic and electronic conductivity is set up and solved using the COMSOL multi-physics solver package. The importance for achieving a significant and long-lasting change in local ionic composition of the composite of the volume fraction of the two phases, the electronic conductivity contrast between oxidised and reduced states of the ECP, the ionic mobilities in the hydrogel and the ion-exchange capacity of the ECP are demonstrated. The final part presents experimental studies directed at depositing and actuating such ECP based composites in a miniature electrochemical cell.

ACKNOWLEDGEMENTS

First and foremost I would like to express my sincere gratitude to my supervisor Professor David Williams for his unwavering support and patient guidance over the last four years. He is an excellent supervisor and a wonderful person and I am grateful for the time I spent under his mentorship.

I would like to thank my co supervisor Dr Gib Bogle for his support all through my degree. He helped me learn a lot about mathematical modelling and I am grateful for his guidance during the first year of my degree. I am also thankful for the guidance provided by my co supervisor Associate Professor Jadranka Travas-Sejdic throughout my degree. I would also like to acknowledge Dr. Bryon Wright for all his help during my degree, particularly with clean room fabrication and AFM studies.

Special thanks to my friends who helped me on this project; Alex and Marsilea for their help in the laboratory, Angela for synthesising the hydrogel and helping with the experiments and Jin for his help in laser machining for microfluidics design.

I would also like to thank all my awesome friends and family who have supported me throughout my degree. I could not have done it without all of you.

Lastly, I would like to thank my dad, my mom, my sister Anu and my brother Vignesh for their love and constant support.

TABLE OF CONTENTS

ABSTRACT	i
ACKNOWLEDGEMENTS	ii
TABLE OF CONTENTS	iii
ABBREVIATIONS AND SYMBOLS	vi
CHAPTER 1: INTRODUCTION	1
1.1 Thesis Objectives	3
CHAPTER 2: LITERATURE REVIEW	
2.1 Micro-Devices	5
2.2 Microfluidics and its Application in Biology	7
2.3 Microfluidic Mixers and Pumps	10
2.4 Electrochemically-active Conducting Polymers	12
2.4.1 Electrochemical Polymerisation	14
2.4.2 Chemical Polymerisation	15
2.4.3 Mechanical Swelling Mechanism	15
2.5 ECP-Based Microfluidic Devices	18
2.6 ECP Composites	21
2.6.1 ECP-Hydrogel Composites	22
2.6.2 Physical Mixing	22
2.6.3 Chemical Polymerisation	23
2.6.4 Electrochemical Polymerisation	24
2.6.5 Applications	24
2.7 Thesis Structure	27
CHAPTER 3: EXPERIMENTAL METHODS	
3.1 PDMS Soft Lithography	29
3.2 Characterisation Techniques	31
3.2.1 Experimental Setup	31
3.2.2 Electrochemical Cells	32
3.2.3 Conductivity Measurement	33
3.2.4 Optical Microscopy	33
3.2.5 Scanning Electron Microscopy	33
CHAPTER 4: MODELLING THE OXIDATION WAVE PROPOGATION IN ELECTROCHEMICALLY ACTIVE CONDUCTING POLYMERS	
4.1 Introduction	34
4.2 Modelling Oxidation Wave Velocity in ECPs	38
4.2.1 Assumptions	38
4.2.2 Relationship Between Local Current Density and Electric Potential in the Polymer	40

4.2.3	Interfacial Potential Difference	41
4.2.4	Ion Flux at the Interface	41
4.2.5	Ion Flux and Potential Gradient in the Solution	42
4.3	Numerical Model	43
4.3.1	Solver Sequence	45
4.3.2	Scharfetter-Gummel Scheme	46
4.3.3	Alternating Direction Implicit Method	52
4.3.4	Calculating Solution Potential and Polymer Current from Concentration and Ion Flux	55
4.4	Results and Discussion	57
4.4.1	Variation of Oxidation Wave with Conductivity Change	60
4.4.2	Variation of Oxidation Wave Propagation with Cell Geometry	63
4.4.3	Model comparison with experimental data	64
4.5	Conclusion	66

CHAPTER 5: COMPUTATIONAL DESIGN OF MICROMIXERS AND MICROPUMPS BASED ON ELECTROCHEMICALLY ACTIVE CONDUCTING POLYMER OXIDATION WAVE

5.1	Introduction	67
5.2	Design of a Micropump	68
5.3	Design of a Micromixer	72

CHAPTER 6: MODELLING ELECTROCHEMICALLY ACTIVE CONDUCTING POLYMER -HYDROGEL COMPOSITES

6.1	Introduction	76
6.2	Mathematical Modelling	77
6.3	Numerical Modelling	82
6.3	Results and Discussion	83
6.4	Conclusions	89

CHAPTER 7: ELECTROCHEMICALLY ACTIVE CONDUCTING POLYMER COMPOSITES – PREPARATION AND CHARACTERISTICS

7.1	Introduction	90
7.2	Patterning of Polyaniline Thin Films	91
	7.2.1 Experimental	91
	7.2.2 Characterisation	92
7.3	Polypyrrole-PDMS Composites	94
	7.3.1 Experimental	94
	7.3.2 Results and Discussion	94
7.4	Polypyrrole-Carbon Fibre Composites	97
	7.4.1 Chemical Polymerisation	98
	7.4.2 Characterization	98
	7.4.3 Electrochemical Polymerization	102
7.5	Polypyrrole-Hydrogel Composites	
	7.5.1 Hydrogel Synthesis	103
	7.5.2 Hydrogel Characterisation	104
	7.5.3 Hydrogel-Polypyrrole Composite Preparation	105

7.6	Discussion	114
	CHAPTER 8: CONCLUSION	115
8.1	Future Work	116
	REFERENCES	118

ABBREVIATIONS AND SYMBOLS

1D	One dimensional
2D	Two dimensional
A	Ampere
AC	Alternating current
ADI	Alternating Direction Implicit
AFM	Atomic Force Microscopy
APS	Ammonium persulphate
C_0	Initial Concentration
C	Concentration of the solution
C_A	Concentration of the positive ions
C_B	Concentration of negative ions
C_I	Concentration of ions in phase 1
C_{s1}	Concentration of the solution in phase 1
CV	Cyclic Voltammetry
cm	centimetre
Δy	Thickness of the polymer
D_A	Diffusion coefficient of the positive ions
D_B	Diffusion coefficient of the negative ions
DBS	Dodecyl Benzene Sulphonate
DBSA	Dodecyl benzenesulphonic acid
DMPA	2,2-dimethoxy-2-phenylacetophenone
DNA	Deoxyribonucleic acid
$^{\circ}\text{C}$	Degree celsius
ε	Oxidation state
ε_t	Oxidation state at which the transition occurs
ECP	Electrochemically-active Conducting Polymers
EDC	1-Ethyl-3-(3-dimethyl-laminopropyl) carbodiimide hydrochloride
EDOT	Ethylenedioxythiophene
ELSIA	Enzyme-linked immunosorbent assay
EQCM	Electrochemical quartz crystal microbalance
F	Faraday's constant
FET	Field Effect Transistor
γ_B	Activity coefficient
ζ	Volume fraction of hydrogel
g	gram
h	Distance between the electrodes
HEMA	Hydroxyethylmethacrylate
HIV	Human immunodeficiency virus
HPLC	High Pressure Liquid Chromatograph
I_P	Current along the polymer
IC	Integrated Circuit
ITO	Indium Tin Oxide
i_s	Current density in the solution
$i_{s,,y,0}$	Current density across the interface
J_A	Flux due to positive ions
J_B	Flux due to negative ions
$J_{A,0}$	Flux due to positive ions at the interface

$J_{B,0}$	Flux due to negative ions at the interface
KPS	Potassium persulphate
KCl	Potassium Chloride
L	Characteristic distance
LEDs	Light Emitting Diodes
M	Ion capacity of the film
MEMS	Micro Electro Mechanical Systems
MPa	mega pascal
M	metre
mm	millimetre
μ	Micro, 10^{-6}
mg	milligram
ml	milliliter
nm	nanometre
NMP	N-methyl 2pyrrolidone
ϕ_p	Potential along the polymer
ϕ_s	Potential in the solution
$\Delta\phi^0$	Standard potential difference
$\Delta\phi$	Potential difference at the interface
PA	Polyacetylene
PAAc/ PAA	Poly (acrylic acid)
PVSA	Poly vinyl sulphonic acid
PAAm	Polyacrylamide
PAMPS	Poly (2-acrylamido-2-methyl-1-propanesulfonic acid)
PANI	Poly(aniline)
PC	Propylene Carbonate
PCR	Polymerase Chain Reaction
PDMS	Poly(dimethyl siloxane)
PEDOT	Poly(ethylenedioxythiophene)
PSS	Poly(styrenesulfonate)
PET	Poly(ethylene terephthalate)
P-HEMA	Poly(hydroxyethylmethacrylate)
PMMA	Poly(methyl methacrylate)
PPy	Polypyrrole
PPy-Cl	Chloride doped polypyrrole
PPy-DBS	DBS doped polypyrrole
PPy-PPS	p-phenol sulfonate
PPy-pTS	Polypyrrole -paratoluenesulphonate
PPy-PVS	Polypyrrole -polyvinylsulphonate
PT	Polythiophene
PVA	Poly vinyl alcohol
PVDF	Polyvinylidene fluoride
Q	Total charge
ρ	Density of the fluid
R	Gas constant
RE	Reference Electrode
Re	Reynolds number
RF-MEMS	Radio Frequency –Micro Electro Mechanical Systems
RIE	Reactive Ion Etching
SAW	Surface Acoustic Waves

SICM	Scanning Ion Conductance Microscopy
σ_p	Conductivity of the polymer
σ_{max}	Maximum polymer conductivity
σ_{min}	Minimum polymer conductivity
SEM	Scanning Electron Microscope
T	Temparatue
t	Time
U_A	Mobility of the positive ions
U_B	Mobility of the negative ions
UV	Ultra Violet
v	Mean velocity of the fluid
V	Voltage
W_T	σ_{min} to σ_{max} transition width in units of oxidation state
w	Width of the polymer
WE	Working Electrode
z	Ionic charge

CHAPTER 1: INTRODUCTION

Micro-devices are fast transforming into an important part of biological studies. Currently, they are used in various biological applications, from pathogen detection to cell culture and metabolomics. The majority of the micro devices used in biology are the ones that handle very small amounts of fluids such as samples and reagents. These *microfluidic devices* offer a number of advantages over the traditional devices that perform these functions¹:

- High sensitivity and precision with the control, measurement, and manipulation of small amounts of liquids^{2,3}.
- Speed in comparison to the traditional devices⁴.
- Convenience, as they occupy less space and can be made into portable hand held devices that consume little power.

A microfluidic system usually contains inlets and outlets to introduce and extract the samples, micro-channels, and a pumping mechanism for transporting the samples to different parts of the system. It also contains valves and mixers to direct the flow and mix different liquids. By integrating these functions into one small system, a functioning laboratory in a miniature chip can be achieved. In the design of single-use devices for biomedical measurement, towards which much current effort in the development of microfluidic systems is directed, mixing is a particularly important issue⁵. In such devices, the prototype of which is the home-use pregnancy test or the rapid assay test for cardiac markers, reagents and labels that were previously dried into a device must be thoroughly mixed into a small sample in some simple way that can be implemented within a robust and compact instrument. In the present generation of tests, the labels are typically dried within a porous pad and a capillary driven flow of the sample through the pad achieves re-suspension of the labels in the sample. A degree of mixing then occurs by virtue of the complex flow pattern through the pad. Poor, slow mixing is one major reason for the limited measurement precision attained by the current generation of instruments. One of the defining characteristics of microfluidic devices is that flow is laminar and mixing is by diffusion only. When it comes to re-suspension of a particulate label in a fluid or mixing of reagents within a

short time, diffusion alone is not an effective mechanism. Furthermore, mixer designs⁵ that rely on pressure-driven flows across patterned surfaces (e.g.,^{6,7}), induce chaotic motion in suitably designed channels (e.g.,^{8,9}), use flow splitting and recombination (e.g.,¹⁰), or use mechanically-induced motion (e.g.,¹¹⁻¹³) have significant barriers to their implementation in a practical form in devices where major design constraints are reliability, simplicity, low cost, and single use.

These considerations led us to consider the mechanical response of Electrochemically-active Conducting Polymers (ECP) to an electrochemical stimulus, on which there is a large literature¹⁴⁻¹⁷, as a means for inducing mixing and pumping in a micro-chamber. Approaches to the construction of actuators and valves utilizing the redox switching phenomenon of the ECP have been reported¹⁸⁻²⁰. These have generally involved multiple fabrication steps, typically of a composite of an elastomer deposited on top of a porous membrane that supports an electrochemical cell. In contrast, we have explored the possibilities for mixing and pumping stimulated by direct actuation of the ECP using the fluid itself as the electrolyte.

There are different means by which solution movement in a micro-chamber might conceivably be stimulated by actuation of an ECP. The simplest is an expansion and contraction of polymer deposited in the chamber in the form of pads. An issue with such a scheme is that the relative expansion is generally small (e.g., on the scale of 10%, although with choice of exchangeable ion, larger strains can be attained²¹). From this limitation, a large polymer thickness would be needed to facilitate significant movement, which would, in turn, limit the achievable rate of movement. To overcome these issues, we have explored two different design methods in this thesis, by which ECP can directly be used to fabricate microfluidic mixers and pumps.

In the first method, we designed a peristaltic mixer and a pump utilising an oxidation wave phenomenon that is unique to ECP. Peristaltic pumps and mixers do not require actuators with large expansion and contraction. First, we studied and modelled the oxidation wave phenomenon in ECP and computationally designed different pump and mixer configurations to utilise this wave.

In the second method, we explored the possibility of enhancing the expansion and

contraction of the ECP by preparing composites of it with polyelectrolyte hydrogels. Polyelectrolyte hydrogels are known for their swelling properties. They swell or shrink to more than 100% of the original volume upon change of pH or salt concentration. It has been shown that the stimuli response time of the hydrogels can be greatly improved by reducing its size in microfluidic channels²². We formulated a 1D model to compute the salt concentration changes in the ECP-hydrogel composite upon electrochemical actuation and thereby were able to predict the enhancement in the actuation that can be achieved for different compositions. ECPs are mechanically poor and fragile²³. They are insoluble in most solvents, making them difficult to process. ECP-hydrogel composites, in comparison, have an advantage, as they can be made more mechanically stable and processable. It has indeed been reported in the literature, that it is possible to incorporate ECP within other stable polymers and still retain the electrochemical properties²⁴⁻²⁷.

Though the major focus of the thesis is on modeling and designing of ECP-based actuators for microfluidic devices, in the final part we also discuss some experimental studies done towards preparing, processing, and characterising ECP-based composites. We believe these experimental studies will not only help the design of ECP based microfluidic mixers and pumps, but will also help validate our modelling results.

1.1 Thesis Objectives

The objectives of the thesis are as follows:

- 1) Identify the importance of microfluidic devices and discuss existing pumping and mixing mechanisms.
- 2) Study the role of ECP as actuators in microfluidic devices.
- 3) Examine the existing methods to prepare ECP-based composites and study their properties and applications.
- 4) Understand the phenomenon of oxidation wave in ECP by building a 2-D numerical model.
- 5) Computationally design a microfluidic mixer and a pump that utilises the ECP oxidation wave and find its efficiency to mix or pump electrolytes.
- 6) Build a 1D numerical model of a ECP hydrogel composite and find the

compositional changes of the composite during electrochemical actuation.

7) Explore the methods to prepare and characterise various ECP composites and study the electrochemical behaviour in a microchannel.

8) Recommend further studies that can be done utilising the results from this thesis.

CHAPTER 2: LITERATURE REVIEW

2.1 Micro-Devices

Modern micro-device have their origins from the field of electronics when the first integrated circuit (IC) was developed at Texas Instruments in the late 1950s²⁸. The idea of creating functional devices at micro scale was then discussed by R.P Feynman in his talk in 1959²⁹. This idea opened up the fields of microfabrication, micromachining, and micro devices. A functioning resonant gate transistor was soon developed in 1967³⁰, and a decade later, an accelerometer containing a moving loading beam was developed by Roylance and Angell³¹. Reduction in the size of mechanical parts created an increase in the frequency response and in precision. This invention later led to the creation of successful commercial devices such as airbag sensors in cars and sensors in modern electronic equipments. A few years later, a fully functional motor, in the scale of 100 micrometers, was developed at Berkeley³². This development marked the beginning of the Micro Electro Mechanical Systems (MEMS) or Microsystems field.

Image removed for copyright reasons. The image can be accessed at <http://www.sciencedirect.com/science/article/pii/S0250687489871008>

Figure 2.1. SEM image of 24 step stepper motor developed by Fan et al at Berkeley³². The gap between stator and rotor is 2 micrometers. Image is taken from their paper.

Due to its origins from the electronics industry, the initial choice of material for micro devices was silicon. Silicon has strength and reliability, and can be machined precisely. Moreover, it can be can be fabricated using the same techniques used by the

semiconductor industry and can be integrated with the electronics components³³. These properties made it a good choice of material for making micro-devices. But now, a variety of materials that includes polymers, metals, and ceramics is being used in fabrication. These other materials have overcome some of the shortcomings of silicon and furthered the usage of micro-devices in new fields.

In recent years, polymers have been increasingly used for a wide variety of micro-devices. Silicon, though strong, is brittle³⁴ and is problematic in devices that require flexibility. Polymers, in comparison, are flexible and can be deformed to a greater extent. In addition, they are cheaper as materials than silicon. Some polymers are also permeable to air, which is useful for applications in the field of biology. In addition, polymers open up a variety of new fabrication techniques that are impossible with silicon, such as moulding, casting, screen printing, and hot embossing. These new techniques are cheaper and easier than the traditional techniques used to process silicon.

Traditionally, microdevices are made using a method called microfabrication. Microfabrication is a broad term to describe a set of techniques employed to create micrometer size range patterns or structures. There are two main categories of microfabrication methods: surface micromachining and bulk micromachining. Surface micromachining is the process by which thin films of materials are deposited on the surface of the substrate and are etched selectively to form structures³⁵. A sacrificial layer is often used to create a moving part such as a cantilever or a piston³⁶. In comparison to surface micromachining, bulk micromachining involves processing or selectively removing the substrate directly using etching processes to create structures or devices^{35,37}.

Both these methods typically involve techniques such as laser patterning, optical lithography, material doping, deposition, etching, and bonding. Initially, these methods enabled the electronic industry to fabricate components such as transistors, resistors, and capacitors in the scale of micrometers or less. Later the same techniques were adopted to fabricate microdevices. Optical lithography, or photolithography, is one of the main processes involved in the process of microfabrication. The process is simple and fast and involves transferring a material's required pattern on to a substrate by using a photo mask³⁸. The minimum feature size of the patterns is limited by the resolution of the mask. The masks are usually created by etching a chrome plated glass by laser machining.

Currently, although photolithography is still widely used, the advent of ultra short pulse lasers with nanometre range resolutions has allowed researchers to directly create micro patterns on to substrates without the need for the intermediate step of photolithography.³⁹ This method is often called *mask-less microfabrication*^{40,41} making laser machining into another major microfabrication technique alongside photolithography^{42,43}.

Owing to many advantages of miniaturisation, the field of micro devices has given rise to many subfields such as Optical-MEMS, RF-MEMS, and Bio-MEMS.

2.2 Microfluidics and its Application in Biology

*Microfluidics*¹ is a branch of MEMS that handles very small amount of fluids, using channels with dimensions of tens to hundreds of micrometers. The early reported micro-devices that handled liquids were the inkjet printing nozzle arrays in silicon, developed by researchers at IBM⁴⁴, and the High Pressure Liquid Chromotography (HPLC) devices with micro capillaries, developed at Stanford for chemical analysis⁴⁵. Though the initial microfluidic devices were fabricated in silicon, the majority of the current devices use polymers. Poly (dimethyl siloxane)(PDMS) is one of the mainly used polymers for research purposes. PDMS is a soft transparent polymer and is generally considered to be chemically inert. It is nonflammable and nontoxic. It is biocompatible and is also inert to most of the biological compounds and living cells. PDMS is impermeable to liquids and can be crosslinked at low temperatures. These properties make it an ideal material to fabricate microfluidic channels. The process by which PDMS-based microfluidic devices are fabricated is called soft lithography. The process is explained in detail in chapter 3. Currently, microfluidic systems are used in wide variety of fields such as in chemistry⁴⁶, pharmacy⁴⁷, biology⁴⁸, physics⁴⁹, and medicine⁵⁰. Of these, biology and medicine are two important fields which have great potential. Some of the applications in these fields, where the current research interests lie, are briefly discussed here.

Laboratory diagnosis, in which a patient's biological samples are tested for pathogens or abnormalities, is an important step in medical diagnostics. Currently a majority of these tests are done manually in instruments that occupy large space, require large expenses, and take long diagnostics times. Microfluidics has the potential to replace many of these instruments with a single small chip that is cheaper and faster. In recent years, many such

microfluidic devices have been developed. In a recent paper, for example, Chin et al⁵⁰ developed a microfluidic chip that can detect HIV and syphilis simultaneously. They used a simple syringe to create vacuum and draw the fluids into the microfluidic channels. They successfully demonstrated that their small chip can perform the standard ELSIA (Enzyme-linked immunosorbent assay) test done in the laboratories to detect protein based biomarkers. In another recent paper, Ma et al⁵¹ developed a microfluidic chip that can evaluate single immune cells to detect tumour. In yet another study, Devadhasan et al⁵² discussed the methods for early detection of Alzheimer's disease using microfluidic devices.

Image removed for copyright reasons. The image can be accessed at <http://www.nature.com/nature/journal/v442/n7101/abs/nature05064.html>

Figure 2.2. Example of an microfluidic disposable diagnostic card developed by T Edwards et al at University of Washington⁵³ for detection of small molecule analytes in saliva.

Microfluidics is also widely used in the field of systems biology. DNA sequencing rate has been vastly improved by the use of microfluidic devices⁵⁴. DNA sequencing requires parallel capillary channels, which can be fabricated and automated by the use of microfluidic chips. Polymerase Chain Reaction (PCR) is the process by which DNA can be amplified. It requires cycling the solution containing the DNA between different temperature zones. Microfluidic systems are currently used to perform these functions. Micro heater arrays can be fabricated in the chip along with the microchannels⁵⁵. Proteomics⁵⁶ and metabolomics⁴⁸ are two other fields of systems biology where microfluidic systems are currently used. The ease with which a single cell or a protein can

be manipulated or analysed using microchannels is advantageous for using microfluidic chip for these functions. Microfluidic technology is also used in the field of synthetic biology⁵⁷

Drug discovery is another major area of application for microfluidic devices. Drug discovery traditionally involves a laborious process of screening thousands of drug compounds on cells. The use of microfluidic systems in this process has vastly improved the screening time⁴⁷ through an automated screening process that uses micro wells, microchannels, and electrophoresis for cell sorting and analysis⁵⁸. It has also significantly reduced the sample consumption, thereby reducing the cost. These applications demonstrate the role of microfluidics as an important tool in the field of biology.

It is important to note that fluid flow in micrometer size channels has very different behaviour from the fluid flow in macro channels. It is common to calculate Reynolds number to evaluate the type of fluid flow in channels. Reynolds number (Re) is defined as the ratio of inertial forces to viscous forces

$$Re = \frac{\rho v L}{\mu} \quad (2.1)$$

Where,

ρ - Density of the fluid

v - Mean velocity of the fluid

L - Characteristic distance

μ - Viscosity

Smaller sizes are associated with greater viscous forces acting on the fluid. Because of this association, the fluid flow in the micro channel is predictable and nonchaotic. This type of flow is called laminar flow, as compared to flow in macro channels where the flow is turbulent and chaotic. Typically, when the calculated Reynolds number is less than 2300, the fluid flow is laminar. In microchannels the typical distance scale L is very small and the velocities of the fluids are in millimetre per second ranges, bringing Reynolds number down to a very small number, making the flow laminar. One of the characteristics of laminar flow is that when two or more liquids are introduced in a channel, they do not mix, except through diffusion. This property has many advantages

and has been exploited in many microfluidic applications like fuel cells⁵⁹, electroporation systems⁶⁰, and particle sorting⁶¹. Even though it is useful for many applications, when it comes to mixing fluids in microchannels, which is important for many bio-diagnostic applications, laminar flow poses a problem. The mixing of fluids by diffusion only requires longer times, especially when the diffusion coefficients of the fluids differ greatly. Thus the microfluidic devices require special components built in them for mixing fluids.

2.3 Microfluidic Mixers and Pumps

Mixers for microfluidic systems can be classified into two main categories: passive mixers and active mixers. Passive mixers require no external energy source; they simply manipulate the flow in such way to aid the mixing of fluids⁶². A simple passive micro mixer is a T-junction mixer, where two different channels with the mixable fluids meet at a T junction and form a single channel. Because in a microchannel the flow is laminar, the fluids that meet at the junction do not mix immediately but rather slowly through diffusion. Thus, the mixer needs a long mixing channel after the junction. Stiles et al⁶³ used a plus junction mixer, where one liquid is pumped in one of the channels while the other liquid is pumped in two other channels which meet and surround the first liquid at the junction. Another method of improving the mixing is by creating serpentine channels. This method reduces the footprint of the mixer while increasing the length of the mixing channel. Malecha et al⁶⁴ and Kim et al⁶⁵ designed and fabricated such a mixer. Mixing can also be increased by creating chaotic advection in the microchannel by fabricating structures that obstruct the fluid flow. Lin et al⁶⁶ fabricated a mixer with cylindrical structures along the channel. One example of a complex design is the 3D vortex structure created by Hsin et al⁶⁷, which can improve mixing.

Another category of mixers that are used in microfluidic devices are active mixers, where an external stimulus is applied to enhance the mixing of fluids. The external stimulus can be applied in many different ways. One approach is to apply pressure perturbations along the sides of the channel, as done by Niu et al⁶⁸. Nyguen et al⁶⁹ induced mixing by using Surface Acoustic Waves (SAW) as an external stimulus. Electrokinetic and electroosmotic forces are two other commonly used external stimuli. Campisi⁷⁰ et al fabricated a micromixer where the fluids were displaced by an AC electroosmotic rolling

force which created a mixing effect. Chen et al⁷¹ designed a mixer that creates chaotic electric fields that aid in the mixing of fluids. Magnetic stimuli have also been used to mix fluids in a microfluidic system. Affanni et al⁷² designed a mixer that uses magneto-hydrodynamic force to stir fluids in a microchannel. Mixing has also been performed using thermal disturbances. Francais et al⁷³ fabricated a micromixer by heating the liquid at certain parts of the channel using heating resistors. This process causes rapid volume change cycles in the liquid which enhances mixing.

Another method of mixing fluids in channels is by using mechanical actuators in the channel, which physically stir the fluid. A variety of materials have been used as actuators. Prettyman et al⁷⁴ have used the stimulus response swelling and shrinking property of hydrogels to enhance mixing. They fabricated cylindrical structures of the hydrogel in the channel and stimulated it by changing the pH of the flowing fluids. Himstedt et al⁷⁵ used a magnetic responsive membrane as an actuator. Ryu et al.⁷⁶ fabricated a micro magnetic stirrer that rotates along its axis when magnetic stimulus is applied. Similarly, Williams et al⁷⁷ have used nafion polymer as an actuator to create mechanical disturbance at the base of the channel to enhance the mixing.

Another important component of a microfluidic device is the micropump which is required to manipulate fluids around the micro channel. There are a number of methods to pump fluids in microchannels. One method uses a mechanical actuator to physically push or create a pressure that pumps the fluids. Usually a diaphragm and a chamber are designed with incoming and outgoing valves. When the diaphragm is actuated, the pump draws in the liquid through the incoming valve and fills the chamber; when the diaphragm is relaxed back, the chamber is emptied by pumping the fluid through outgoing valve. Peristaltic pumping is another pumping technique used in microfluidic devices. In this method a peristaltic wave is generated along the walls of the microchannel which induces fluid motion. Chao et al⁷⁸ and Hwang et al⁷⁹ induced a peristaltic wave by using three different piezoelectric actuators in line and actuating them one after another. Trenkle et al⁸⁰ fabricated three successive diaphragms and wells whereby they actuated one after another in a peristaltic motion to pump fluids. Numerous other methods that do not involve mechanical displacement have been reported to pump fluids in microchannels. They use different actuation methods such as electrophoresis, electrohydrodynamics, electroosmotic, magnetohydrodynamics, and acoustic actuation.

A number of materials have been used as actuators to induce fluid motion in microchannels. These materials include piezoelectric materials⁸¹, electrochemically active conducting polymers⁸² (ECP), and hydrogels⁸³. In this thesis, we will focus only on ECPs, hydrogels, and their composites.

2.4 Electrochemically active Conducting Polymers

Since first reported in 1977, electrochemically active conducting polymer (ECP) materials have been extensively studied for their chemical, physical, and mechanical properties. ECP exhibit electrical properties similar to inorganic semiconductors while retaining the mechanical properties of conventional polymers. The electrical properties of ECP can be varied significantly by changing the band gap between the valence band and the conductance band through doping. Unlike in semiconductors, the process of doping in ECP is relatively easy and can be reversed. In addition to the changes in the electrical properties during doping, ECP also undergo changes in chemical and mechanical properties, such as ion exchange capacity, hydrophobicity, and stress and strain. ECPs are currently used in a wide variety of applications such as electrochemical sensors⁸⁴, electronic transistors⁸⁵, light emitting diodes (LEDs)⁸⁶, drug delivery devices⁸⁷, fuel cell⁸⁸ batteries, electro chromic displays⁸⁹, and as actuators in microdevices.

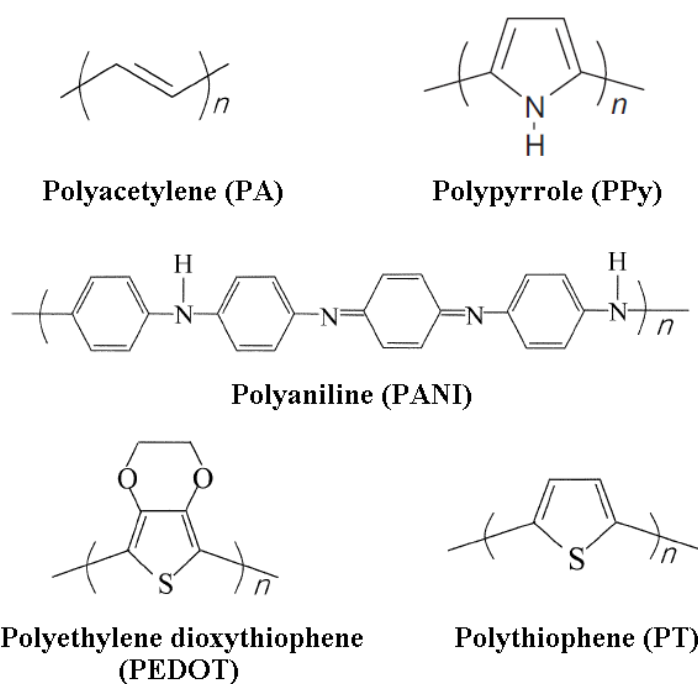


Figure 2.3. Chemical structures of few commonly studied ECPs.

ECP can be synthesised either chemically or electrochemically by oxidative polymerisation of appropriate monomer units. Different mechanisms have been proposed to explain the polymerisation process of the ECP. Sadki et al⁹⁰ wrote a detailed review of different electrochemical polymerisation mechanisms. Of all the different proposed mechanisms, the most commonly accepted mechanism, given by Diaz et al⁹¹, is briefly discussed here. Though most proposed mechanisms are for the electrochemical polymerisation, Bjorklund et al⁹² and Rosseinsky et al⁹³ have concluded that chemical polymerisation follows a similar mechanism. Polymerisation is an oxidative process and the oxidation is initiated either by applying an oxidative potential (electrochemical polymerisation) or by adding an oxidising agent (chemical polymerisation) to the monomer solution. The initial step in the polymerisation process is the creation of the monomer radical due to the removal of electron by oxidation. The scheme for both electrochemical and chemical polymerisation of pyrrole is given in Figure 2.4.

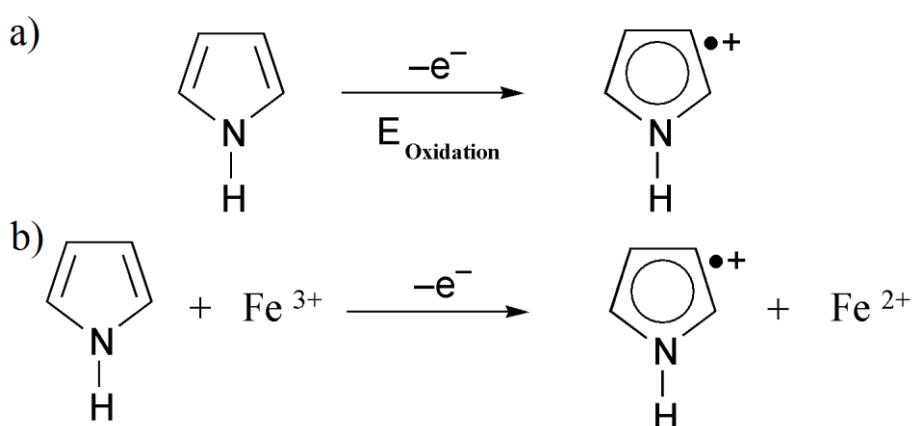


Figure 2.4. Scheme for the initial step of pyrrole polymerisation (a) Electropolymerisation (b) Chemical polymerisation with Fe^{3+} as oxidant. Schemes adopted from papers cited in this section.

The monomer radical formed is unstable and it reacts with another monomer radical to form an intermediate dimer which then undergoes deprotonation to form the stable dimer. The dimer undergoes further oxidation to form a dimer radical. The dimer radical couples with another dimer radical or a monomer radical to form an intermediate tetramer or trimer, which again undergoes deprotonation reaction to stabilize. This sequence of oxidation, coupling, and deprotonation continues until the final polymer is formed.

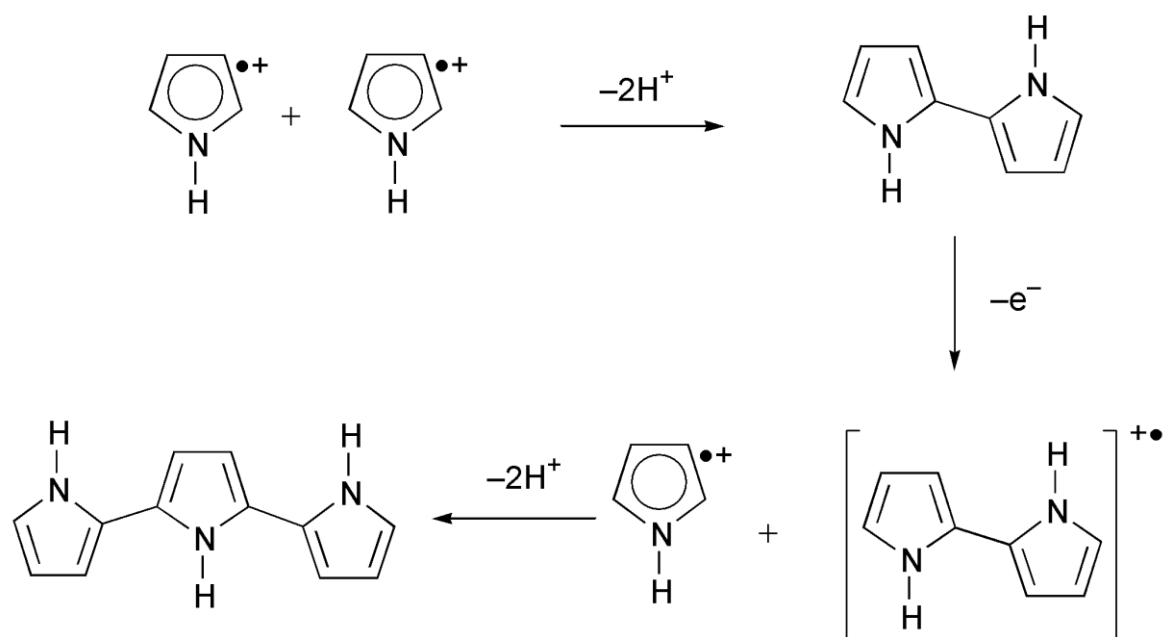


Figure 2.5. Mechanism by which pyrrole oligomers are formed. Scheme adopted from papers cited in this section.

2.4.1 Electrochemical Polymerisation

Electrochemical polymerisation is usually performed using a three electrode setup which contains a working, counter, and a reference electrode placed in a solution containing monomer and an electrolyte. When an oxidative potential is applied between the working and the counter electrodes, the monomer solution in contact with the working electrode polymerises on the surface of the electrode and forms a film. This polymerisation process is more controllable than chemical oxidation and thin films of ECP can be synthesised using this method. The oxidation potential of the oligomers gradually reduces as the length of the chain increases. This reduction is evident from the fact that the potential drops over time during the electrochemical polymerisation⁹⁴. During the electrochemical polymerisation reaction, there is a continuous production of H^+ ions near the electrode thus reducing the pH of the solution near the electrode. Though pH of the solution does not have any influence on the oxidation potential, it influences the reactivity and the stability of the polymer. Lower pH makes the surface of the deposited polymers smooth and the polymer less conductive⁹⁰. There are also number of other parameters that affect the morphology of the ECP during electrochemical polymerisation, such as the type of solvent, electrolyte, and electrodes used, alone with deposition time and deposition

charge. The final product of the electrochemical polymerisation is a positively charged polymer, which gets neutralised by bonding with the anions present in the solution.

2.4.2 Chemical Polymerisation

Chemical polymerisation involves adding an oxidant such as ferric chloride (FeCl_3) or ammonium persulphate ($(\text{NH}_4)_2\text{S}_2\text{O}_8$) to the monomer solution. This method is more useful in synthesising bulk quantities of ECP. The yield of the ECP obtained by this method depends on different parameters such as the oxidant to monomer ratio, type of solvent/oxidant, and the reaction time. Bjorklund et al⁹² noted that the pH of the solution partially determines the rate of the polymerisation in chemical polymerisation. The polymerisation rate increases with decrease in the pH. From this finding, they suggested that the ferric ions are better solvated in water when the pH is low and thus are better at oxidising the pyrrole monomers which are slightly basic.

2.4.3 Mechanical Swelling Mechanism

The ECP obtained from both chemical and electrochemical polymerisation are in the oxidised state and thus incorporate anions from the solution to balance the charge. The structure of the final polymerised polypyrrole is given in Figure 2.6. The process of addition of an anion to the polypyrrole (PPy) backbone is called doping. The doped polymer is electrically conductive.

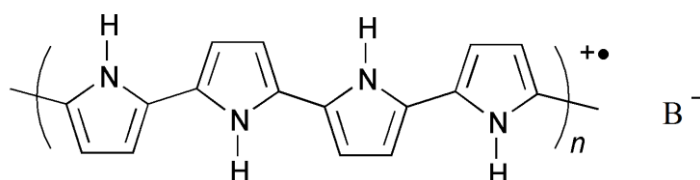


Figure 2.6. Polypyrrole in its oxidised state doped with an anion (B^-).

One of the interesting properties of ECP is the ability to easily switch between oxidised and reduced states. When an ECP is reduced, to keep the total charge neutral the anion is expelled from the ECP. If the ECP is doped with a larger anion such as Dodecyl benzene sulphonate (DBS), the anion gets trapped in the polymer and cannot be expelled. In this case, a cation from the solution is absorbed to keep the system neutral. The process is reversible so when the ECP is re-oxidised, it again absorbs an anion or expels the absorbed cation to keep the system neutral⁹⁵. The redox processes are given in Figure 2.7.

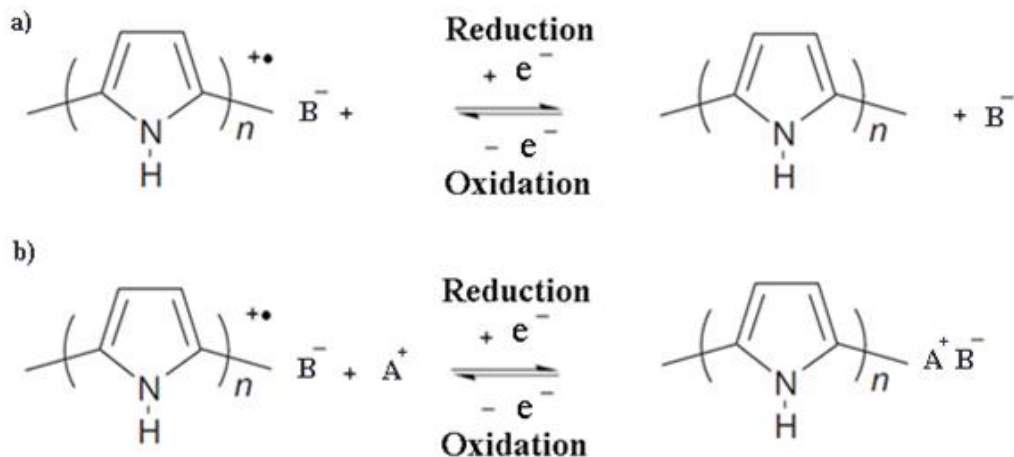


Figure 2.7. The redox processes of the ECP (a) when doped with a small anion (b) doped with a large anion

Another important property of ECP is that during the process of oxidation and reduction, they can mechanically swell or shrink. There have been many theories proposed to explain this property. Pei et al⁹⁶ in their paper have studied two different ECP: a chloride doped polypyrrole (PPy-Cl) and a DBS doped polypyrrole (PPy-DBS). They studied the volume change of the ECP by using the bending beam method. In this method, PPy is electrochemically grown on a gold-polyethylene thin film. When actuated, the bilayer immersed in electrolyte solution bends due to the compressive stress caused by the swelling and shrinking of the ECP. They proposed that the volume change of the ECP is due to the ion exchange. When the PPy-Cl is reduced, since chloride ion is smaller, PPy expels the ion and shrinks. When oxidised, the Cl ion is absorbed back into the polymer and thereby it swells. But when PPy-DBS is reduced, because the DBS ion is larger, it gets trapped in the PPy chains so the polymer thus absorbs the cation from the surrounding electrolyte and swells. This mechanism was confirmed through the observed bending behaviour of the PPy-Cl and PPy-DBS polymers during oxidation and reduction. Figure 2.8 shows that the bending direction is opposite for PPy-Cl and PPy-DBS upon oxidation or reduction.

Image removed for copyright reasons. The graphs can be accessed at <http://pubs.acs.org/doi/abs/10.1021/j100124a041>

Figure 2.8. The swelling and shrinking behaviour of the ECP during the oxidation and reduction for (a) PPy-Cl ECP and (b) PPy-DBS ECP as observed by Pei et al⁹⁶. Graphs reproduced from the publication.

Gandhi et al⁹⁷ in their paper have proposed a similar mechanism. They studied two different polymers: PPy-pTS (polypyrrole -paratoluenesulphonate) and PPy-PVS (polypyrrole-polyvinylsulphonate). They used a tensile testing method to study the swelling and shrinking behaviour. They observed that both the polymers swell upon reduction and shrink upon oxidation. In their experiments they used different kinds of electrolyte solutions and found that the magnitude of the swelling and shrinking depends upon the type of cation used in the solvent. In some cases when polymers were reduced, they swelled first and then shrank over time. This occurrence is due to a process called *salt draining*, which occurs when the ECP is reduced, the cation moves into the polymer to neutralise the doped anion, and the anion forms a salt molecule. Over time, this salt diffuses out of the polymer and causes it to shrink. This process happens only when both the cation and the anion are mobile.

Suarez et al⁹⁸ have used AFM to study the changes in the morphology of the ECP during deposition and also during the redox reaction. They prepared PPy-ClO₄ films electrochemically and measured the volume change during oxidation and reduction.

When reduced in NaClO₄ solution, the films swelled, but the swelling was not reversible upon oxidation. They suggested that the prolonged reduction cycle might have altered the structure of the polymer. The films experienced reversible swelling and shrinking behaviour when cycled in Na (pTS) solution. This process suggests that the PPy swelling mechanism is strongly dependent on the type of anion present in the solution.

Bay et al⁹⁹ have suggested that the swelling of the polymer is caused not only by the ion movement but also by the osmotic intake of solvent molecules along with the ions. This osmotic intake might be one of the reasons for the large swelling behaviour seen in ECP during oxidation and reduction. In the experiments they obtained the elongation length measurement along with the EQCM frequency measurement of the polymer during the oxidation and reduction and they correlated the dimension changes with the mass changes of the polymer. They also found that when the concentration of the surrounding electrolyte was increased, the swelling of the ECP decreased by 30%. This finding suggests that Donnan potential at the polymer interface reduces when the concentration of the ions increases, thus reducing the osmotic intake of the surrounding solution.

2.5 ECP-Based Microfluidic Devices

ECPs have been used before as actuators in microfluidics devices. One of the simplest methods is by utilizing the volume change property of the polymer directly in the microchannel. Smela et al¹⁰⁰ have used this method to construct simple valves. They electrochemically actuated the ECP in a microchannel causing it to swell or shrink and thereby closing or opening the channel.

Image removed for copyright reasons. The image can be accessed at <http://onlinelibrary.wiley.com/doi/10.1002/adma.200390113/abstract>

Figure 2.9. A simple microfluidic valve that utilises the volume change property of the ECP, developed by Smela et al¹⁰⁰. The image is taken from their review paper.

A different method for creating an ECP based actuator is by fabricating an ECP bilayer, by which an ECP layer is bonded to another material that does not change volume. When the ECP is oxidised or reduced, the swelling causes a stress on the other material that is bonded to it. This stress causes a concave bend in the bilayer. When the ECP actuation is reversed, the material shrinks back to its original size, causing the bi-layer to relax back to its original position. Smela et al.¹⁰¹ fabricated a microactuator that utilises this principle with a PPy-gold bilayer. Pettersson et al.¹⁰² used this actuator as valves for microfluidics system. They attached a rigid plate to the bilayer and used it as a hinge to open or close the microchannel. Casadevall et al.¹⁰³ fabricated this bilayer actuator to be used as a mixer in a microfluidic channel. Fang et al⁸² fabricated a trilayer actuator using a similar principle, where they sandwich a PVDF layer in between two ECP layers. They oxidised one layer of ECP while reducing the other. This treatment causes one ECP to swell and the other ECP to shrink thus causing the actuator to bend. They designed a micropump using this actuator. Fuchiwaki et al¹⁰⁴ created a bi layer with two different ECP (PPy-DBS and PPy-PPS). One of the polymers is anion driven while the other is cation driven. When actuated, one of the polymers swells while the other shrinks, causing the actuator to bend. They also used it to fabricate a micropump. Alici et al¹⁰⁵⁻¹⁰⁷, in their series of papers, modelled and optimised the bending behaviour of these multi-layered composites.

Image removed for copyright reasons. The image can be accessed at <http://www.springerlink.com/content/j5827163t7595625/>

Figure 2.10. Actuation mechanism of ECP-gold bi-layer actuator. Here the polymer is doped with NaDBS salt. When applied voltage the polymer oxidises and expels the Na ions, thus shrinking and causing a compressive stress. The image is taken from the review paper by Casadevall et al¹⁰³

Other authors have reported the use of the swelling and shrinking property of an ECP to move a diaphragm that is in contact with a microchannel. The most commonly used material for the diaphragm is PDMS. Lefevre et al¹⁰⁸ fabricated a PPy layer under a very thin PDMS layer. When the ECP was actuated, it swelled and pushed the PDMS layer to close the microchannel, thus acting as a valve. Ho Kim et al¹⁰⁹ and Wei et al¹¹⁰ also created similar actuators with a PDMS-PPy diaphragm, but they designed a micropump using the diaphragm as a piston. Naka et al¹¹¹ designed a more complicated micropump which uses the bilayer effect, discussed previously, to move a PDMS based diaphragm.

Along with the volume change property, hydrophobicity of the ECP also changes when it is oxidised or reduced. Causley et al¹¹² have explored the idea of creating a micropump using this property of the ECP. Hansen et al¹¹³ designed an electro-osmotic micropump that uses PEDOT as electrodes to cause the ionic imbalance.

2.6 Electrochemically active Conducting Polymer Composites

Electrochemically active Conducting Polymers (ECPs) are difficult to process and they have poor mechanical properties. One way to process ECP is by creating a dispersion of the ECP in a host solution. Haba et al¹¹⁴ were able to prepare polyaniline(PANI) films that have a conductivity of 0.03 S/cm, prepared from aqueous dispersions obtained by a unique method of aniline polymerization in the presence of DBSA. Jayashree and others¹¹⁵ have studied a wide range of PANI blends prepared by the method of dispersing monomers in organic liquid or water and polymerizing it.

Another method for processing ECP is by creating a composite with another stable polymer that can be processed. By preparing this composite, the mechanical properties of the ECP can also be improved. There have been previous studies creating processable ECP composites with other polymers, which have good mechanical strength and also retain the properties of the ECP. A wide variety of materials have been used as the supporting materials for the ECP. Ruckenstein and Park¹¹⁶ have used polystyrene as a binder. They made a composite by adding pyrrole monomer to the porous host polystyrene and then polymerising the pyrrole inside the polystyrene by adding oxidants to it. They were able to achieve a very highly conductive composite (0.8 S/cm). Bhat et al²³ have used cellophane as a supporting polymer. They polymerised the ECP chemically by pouring solution containing pyrrole monomer over oxidant soaked cellophane.

ECP composites are widely used as super capacitive materials and electrodes. An et al¹¹⁷, used carbon aerogel as an additive. They chemically polymerised the pyrrole monomer in a solution containing carbon aerogel. The resulting composite contained PPy-coated carbon aerogel with good super capacitive properties. A similar method was used by Park et al¹¹⁸. Instead of carbon aerogels, they chemically polymerised the pyrrole on graphite fibre matrix sheets. The resulting composite not only had a good super-capacitive property but was also highly conductive. Coffey et al¹¹⁹ have used graphite fibre matrix sheets as an additive, but instead of chemical polymerisation, they electrochemically grew the PPy onto the sheet for use of the composite material as an electrode.

2.6.1 ECP-Hydrogel Composites

Polyelectrolyte gels (hydrogels) are known for their swelling properties. These hydrogels swell by osmotic intake of water until reaching equilibrium. The osmotic pressure is due to the Donnan potential created by the free charges in the hydrogel. When water is replaced by ionic salt solution, the swelling of the polyelectrolyte gel reduces as a result of the change in the Donnan equilibrium and repulsion of charges in the hydrogel network^{120,121}. This process is reversible. Composites of ECP with hydrogels are a means of coupling the electrical properties of ECPs with the swelling properties of hydrogels. The proposed applications that have driven this effort are reviewed later (section 2.6.5). The most commonly used hydrogels for this purpose have been poly (acrylic acid), poly (acrylamide), poly (HEMA), and their co polymers. Chitosan, poly (vinyl alcohol), poly (vinyl pyridine), and poly (vinyl pyrrolidone) have also been used in some cases.

ECPs – hydrogel composites can be prepared in several ways. One method involves mechanically mixing ECP with the monomer or polymer solution of the hydrogels and cross linking the solution to obtain a composite^{27,122}. Sometimes ECP monomer and hydrogel monomer are mixed together with the cross linker and the initiator/oxidising agent is added to polymerise both the polymers together.¹²³ Another method involves soaking the hydrogel in a monomer solution of ECP and polymerising the ECP either chemically^{124,125} or electrochemically^{24,26}. For chemical polymerisation, the ECP monomer-loaded hydrogel is soaked in an oxidant, usually ammonium persulphate (APS) or potassium persulphate (KPS), to get the composite. For electrical polymerisation, along with the ECP monomer, the hydrogel is loaded with a salt; then a constant potential or constant current is applied to get the ECP to grow in the hydrogel matrix

2.6.2 Physical Mixing

Wallace et al²⁷ prepared an extrudable composite by physical mixing of PPy colloids with PAA and glycerol and cross linking them. The equilibrium water uptake of the composite was less than that of the pure hydrogel. When the colloid content was increased, the rate of dehydration decreased. Tao et al¹²² synthesised sulphonated polyaniline and polymerised PAA with it. Their composite was pH sensitive and equilibrium water uptake of the composite was slightly higher than that of the pure hydrogel. The addition of the sulphonated polyaniline, a charged polymer, created more free ions in the hydrogel, increasing the osmotic pressure thus increasing the swelling. The gel was also pH

sensitive. The swelling decreased 17 times when the pH was reduced from 12 to 1. This again was because of the interaction of the charged sulphonated polyaniline with the hydrogel networks. They also found that the composite retained the ECP better in acidic and neutral solutions. In alkali medium, the ECP chains slowly diffused into the solution. Aouada et al¹²⁶ prepared a composite by polymerising PAAm in a solution containing PEDOT-PSS. The water uptake of the composite did not significantly change due to the ECP addition. However, increase in the crosslinking density and PAAm concentration decreased the water uptake significantly. This decreased water uptake stemmed from the tighter structure and smaller pore sizes of the formed hydrogel because of the increase in the cross linking density¹²⁷.

2.6.3 Chemical Polymerisation

Siddhanta et al¹²⁸ have prepared two different composites by preparing hydrogels (PAAm and PAMPS) with aniline monomer in it and then soaking it in APS. They observed that, when the hydrogel sample was thicker, the polyaniline was not uniformly formed in the hydrogel. The outer regions had more polyaniline than the inner core. However, thinner slabs of hydrogel formed uniform polyaniline. PAMPS –PANI composite had a higher water uptake capacity than the pure PAMPS. The researchers suggested that PANI impedes the crosslinking of the hydrogel to a certain extent, causing the composite to swell more. The swelling of the composites decreased considerably when the solution was replaced with NaCl solution. Tang et al¹²⁹ also prepared a composite by chemical polymerisation of aniline soaked in PAA hydrogel. They observed that the composite swelling was affected by the temperature. When the temperature increased from 5°C to 45°C, the water intake capacity decreased by around 25%. The swelling of the hydrogel decreased when the amount of crosslinking agent added to the mixture was increased. This process again shows that the swelling depends on the crosslinking density of the hydrogel. Owino et al¹²⁵ prepared the composite by soaking the pyrrole monomer loaded P-HEMA in APS solution, and found that the concentration of APS plays an important role in the formation of the PANI network in the hydrogel. When the concentration of the APS was higher, there was over-oxidation of PANI, turning it black. When the APS concentration was low, the PANI formed rapidly on the surface of the hydrogel, blocking the diffusion of APS into the hydrogel; hence PANI did not grow inside the hydrogel.

2.6.4 Electrochemical Polymerisation

In their series of papers, Wallace et al reported^{24,26,130} the preparation and characterisation of a wide range of ECP- hydrogel composites by electrochemical polymerisation. These researchers were able to prepare large slabs of composites that were electrochemically active. They noted that it is difficult to prepare large sized pure ECP slabs because of its fragile mechanical properties. The water intake property of the hydrogel was not affected by the ECP network. However, the rate of hydration and dehydration reduced as the ECP content was increased. The electrochemical property of the composite increased as the composite was dehydrated. This reaction is attributable to the increased conductivity of the composite as it dried. The mechanical property of the composite degraded and oxidation/reduction peaks disappeared when the electro-polymerisation time was increased. The authors also found that pH played an important role in the homogeneity of the ECP grown in the hydrogel. During the electrochemical reaction, there was a release of protons from the ECP, thus decreasing the pH inside the gel. At the same time, the pH in the solution increased due to the reduction reaction at the counter electrode. The ECP growth slowed down when it reached the outer edge of the hydrogel because of the higher pH in the solution. These authors were able to grow uniform ECP in the hydrogel by maintaining the pH stable at around 6.0.

Brahim and Guiseppi-Elie¹³¹ have prepared a PPy-P-HEMA composite through electrochemical polymerisation. After the composites were prepared they oxidised the composite for 2 hours with 0.7V potential. They found that the charge consumed by the hydrogel composite is much higher than the pristine PPy subjected to the same oxidation. This, they concluded, is due to the capacitive charging of the PPy in the hydrogel matrix.

2.6.5 Applications

Controlled drug release. ECP – hydrogel composites have been studied for use in controlled drug delivery. In these systems, the drug component is often loaded in the hydrogel and the ECP is used to stimulate the release of the drug molecule. Following this approach, Li et al.¹³² have mixed the drug molecule into PVA hydrogel solution when prepared. The hydrogel was then covalently bonded onto a PPy film. Chansai et al¹³³ also mixed the drug molecule directly in to the PAA solution when preparing it and

chemically polymerised the hydrogel with ECP. Others^{25,134-136} have prepared the composite and later soaked it in the aqueous solutions of the drug molecule to load it. In all the cases applying electric potential to the composite increased the release of the drug component. Chasai et al. attributed this behaviour to the electrostatic attraction of the charged drug towards the electrode. In their study, the diffusion coefficient of the drug increased from $5 \times 10^{-9} \text{ cm}^2 \text{ s}^{-1}$, in the absence of electric field, to a value of around $7.3 \times 10^{-7} \text{ cm}^2 \text{ s}^{-1}$, when an electric potential was applied. Another factor that has influenced the release of drug under electric field is the electrochemical reactions of the ECP and the hydrogel. Li et al¹³² suggested that this reaction may introduce a pH gradient in the composite which might aid in the release of drug molecule. They also considered the temperature change, which might occur because of the applied current. Studies have shown that higher temperature causes hydrogel to swell, causing the release of drug molecules. Lira et al¹³⁴ have suggested that when a potential is applied, the ECP oxidise and swell, occupying more space, thus expelling more drug molecules.

Actuators. ECP hydrogel composites have been used as actuators¹³⁷⁻¹⁴². In previous research, the composite prepared were placed in between two electrodes in a salt solution and subjected to an electric field. The composite was observed to bend towards the positive electrode. When the polarity of the electrode was switched, the bending direction switched. The measured bending angle increased with the increase in the applied voltage. The ranges of applied voltages for the actuation varied from 3 V¹³⁹ up to 25 V in some cases¹³⁷

Image removed for copyright reasons. The image can be accessed at

<http://pubs.acs.org/doi/abs/10.1021/cm049921p>

Figure 2.11. PPy-hydrogel composite bending behaviour as reported by Moschou et al¹³⁹. The composite (1) is placed in between two electrodes (2,3) in 0.15 M NaCl solution. When a voltage of 3 V was applied for 2 minutes the composite bent from position (A) to position (B). Image taken from their paper.

Moschou et al^{139,140} observed the actuation time response to be around 2 minutes and lowering the applied voltage increased the response time. When the salt concentration was below 1.5×10^{-4} M, the hydrogel stopped responding. Bajpai et al¹³⁸ observed an increase in bending angle when the ECP content (PANi) was increased. Bending angle also increased when salt concentration of the surrounding electrolyte was increased. Dai et al¹⁴¹ demonstrated a similar actuator and found that the mechanical strength of the hydrogel can be improved from 0.1 MPa to 1.2 MPa by adding PEDOT-PSS to the hydrogel network. Yamuchi et al¹⁴² observed a similar increase in mechanical strength when PAMPS composite was prepared with PPy.

The bending mechanism is attributed to the unequal swelling on each side of the hydrogel. When electric potential is applied, the free ions in the hydrogel move toward the electrode, which creates an osmotic pressure that swells the hydrogel on the other side¹⁴³. When the number of free ions in the solution is increased, osmotic pressure increases, thus causing more bending when salt concentration is increased. Hydrogel on its own displays this bending behaviour; however, the presence of the ECP in the composite increases the bending. Lin et al. attributed this phenomenon to the fact that the carboxylic acid group in the PAA hydrogel creates a strong hydrogen bond with PANi, thus releasing more H⁺ and Cl⁻ free ions in the composite, increasing the osmotic pressure. One other factor might be the oxidization of the ECP when electric potential is applied and thus becomes positive. This oxidization creates repulsion with the positively charged hydrogel causing the bending¹³⁷.

Han et al¹⁴⁴ prepared a PAAc/PVSA –PANi composite by chemical oxidation of aniline inside the hydrogel network. They studied the actuation behaviour of the composite by applying voltage directly to the composite placed in a salt solution instead of subjecting it to an electric field as in previous studies. Here they observed that the composite swells when subjected to different potentials and the swelling behaviour is linearly related to the applied potential. When the polarity of the applied potential was switched, the composite shrank. The swelling and shrinking behaviour is due to a change in the local pH of the hydrogel, which was due to the oxidation or reduction reaction the ECP. Because the hydrogel is pH sensitive, it swells or shrinks when positive or negative voltage is applied to the composite.

Table 2.1

Summary of ECP – Hydrogel Composites Reviewed in Section 2.6.1

S.No	Hydrogel	ECP	Preparation method	Maximum Conductivity	Reference
1	PAA/ Glycerol	PPy	Physical mixing	$14 \text{ e}^{-6} \text{ S/cm}$	Wallace et al ¹²⁷
2	PAA	Sulphonated PANI	Physical mixing	-	Tao et al ¹²²
3	PAAm	PEDOT-PSS	Physical mixing	$160 \text{ e}^{-6} \text{ S/cm}$	Aouada et al ¹²⁶
4	PAAm	PANI	Chemical polymerisation	$1 \text{ e}^{-3} \text{ S/cm}$	Siddhanta et al ¹²⁸
5	PAA	PANI	Chemical polymerisation	$15 \text{ e}^{-3} \text{ S/cm}$	Tang et al ¹²⁹
6	P-HEMA	PANI	Chemical polymerisation	-	Owino et al ¹²⁵
7	PAA	PPy	Electro-polymerisation	6 S/cm (Dried state)	Wallace et al ^{24,26,130}
8	P-HEMA	PPy	Electro-polymerisation	-	Guilessi et al ¹²⁵
9	P-HEMA	PPy	Electro-polymerisation	-	Guiseppi- et al ¹³¹
10	P (AA-AAM)	PPy	Physical mixing	-	Moschou et al ^{139,140}
11	P (AAm)	PEDOT-PSS	Chemical polymerisation	$2.6 \text{ e}^{-3} \text{ S/cm}$	Dai et al ¹⁴¹
12	P (AAm)/ P (AMPS)	PANi	Chemical polymerisation	-	Lin et al ¹³⁷
13	P (AMPS)	PPy	Chemical polymerisation	$2 \text{ e}^{-4} \text{ S/cm}$	Yamauchi et al ¹⁴²
14	PVA-g- PAA	PANi	Chemical polymerisation	$9.1 \text{ e}^{-2} \text{ S/cm}$	Bajpai et al ¹³⁸

ECP –hydrogel composites have also been used in other applications such as biosensors¹⁴⁵ and neural prosthetics¹⁴⁶. A summary of the ECP –hydrogel composites discussed in this section is given in table 2.1

2.2 2.7 Thesis Structure

The structure of the thesis to be followed is briefly discussed here. The experimental setup and methods, used to prepare and characterise various ECP composites, are discussed in **chapter 3**. To understand the oxidation wave phenomenon in ECP, a complete 2D numerical model is formulated and solved in **chapter 4**. Various designs for

micromixers and micropumps, utilising the oxidation wave of ECP, are discussed in **chapter 5**. A numerical model to compute the compositional changes in ECP – hydrogel composite during electrochemical actuation is formulated and solved in **chapter 6**. Various methods to prepare and characterise ECP composites are discussed in **chapter 7**. A conclusion with an overall discussion and future work that can be developed based upon this work is discussed in **chapter 8**.

CHAPTER 3: EXPERIMENTAL METHODS

3.1 PDMS Soft Lithography

We used poly (dimethylsiloxane) (PDMS) to fabricate microfluidic electrochemical chambers. These microfluidic chambers were used to characterise the Electrochemically active Conducting Polymer (ECP) composites. Dimethylsiloxane monomer and curing agent were purchased from Dow Corning Inc. The monomer was then mixed with the curing agent in the ratio of 10:1. The mixture was degassed in a vacuum desiccator for one hour. The degassed mixture was poured over a mould and crosslinked at 65°C for one hour to form the PDMS. This crosslinked PDMS was peeled off the mould and its surface was modified to hydrophilic surface by exposing it to oxygen plasma. This patterned PDMS was then adhered to another flat cross linked PDMS to get the desired micro channel. Because PDMS is a soft elastomer, access holes to the micro channel were punched straight through its surface. This process of creating microfluidic devices is called soft lithography and the process is explained in Figure 3.1.

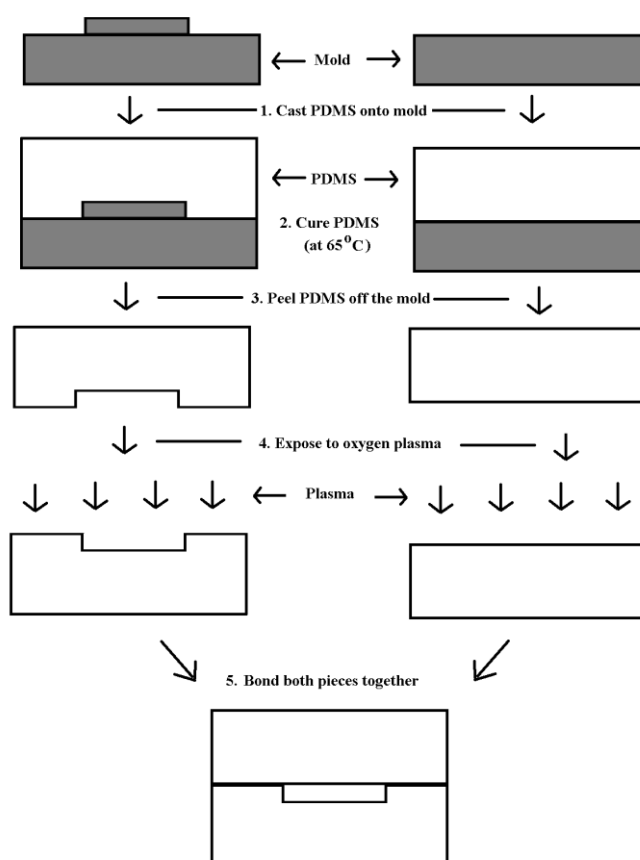


Figure 3.1. PDMS soft lithography process steps.

A simple machining process was used to create the moulds. In this method, a thin sheet of PMMA (1mm) is cut into desired channel shape using laser machining. This design was then bonded to another thicker PMMA slab (5mm) by attaching the pieces together with clips and heating it to 120⁰C for one hour. This method is fast and moulds can be fabricated within few hours. The laser machining method to create moulds is described in Figure 3.2.

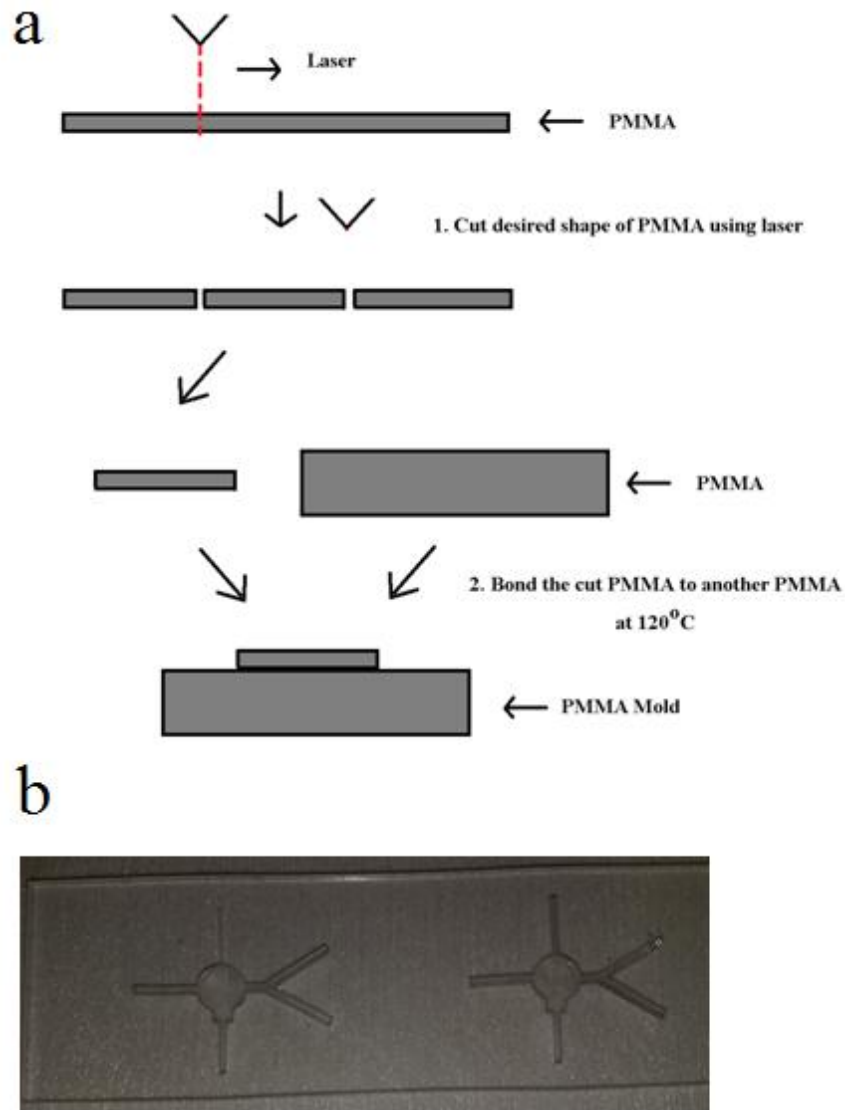


Figure 3.2. (a) Fabrication steps to create PMMA moulds and (b) Fabricated PMMA mould.



Figure 3.3. PDMS based microfluidic chip with the inlet and outlet. The depth of the channel was 1 mm.

3.2 Characterisation Techniques

3.2.1 Experimental Setup

In order to study the behaviour of ECP hydrogel composites in the microchannels, the composites were deposited in the microchannel and were subjected to electrochemical studies. In experiments done in section 7.4.2, ECPs were grown chemically and electrochemically inside the hydrogel network deposited in the microchannel. During these experiments, the composites were analysed using the optical microscope. The setup is illustrated in Figure 3.4.

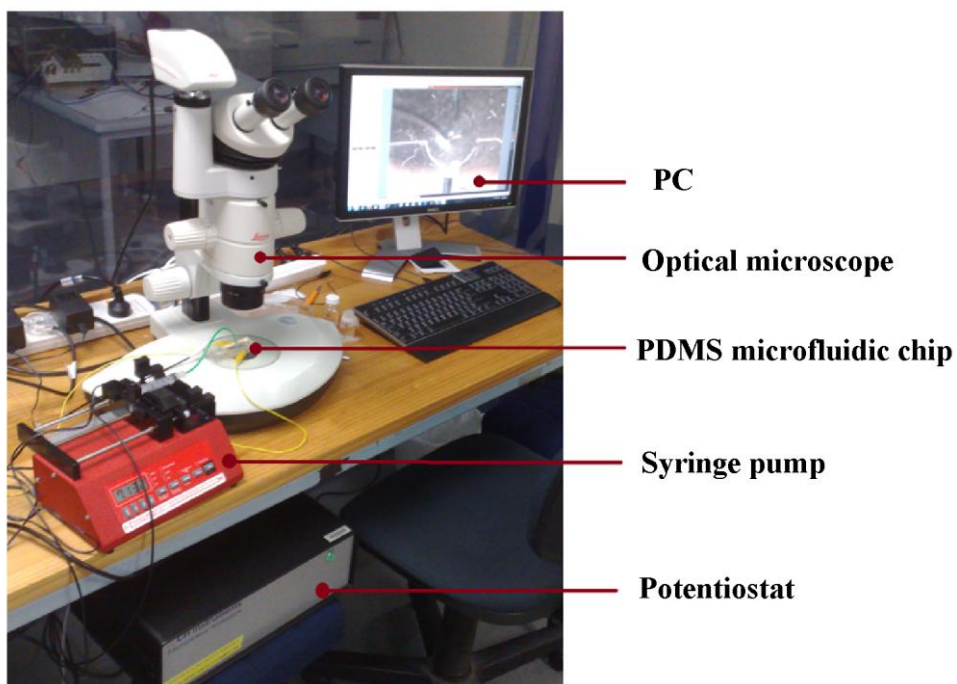


Figure 3.4. Setup for electrochemical studies of ECP-hydrogel composite in a micro-channel.

3.2.2 Electrochemical Cells

Various electrochemical techniques were used to prepare and characterise the ECP composites. Two different electrochemical cells were used. One was a standard cell with glassy carbon working electrode, platinum wire counter electrode and silver/silver chloride wire reference electrode; the second was a PDMS microfluidic cell with graphite rods as working and counter electrodes and silver/silver chloride wire as reference electrode. The Ag/AgCl reference electrode was prepared by soaking silver (Ag) wire in bleach for 3 hours. Both the electrochemical cells are illustrated in Figure 3.5. Standard cell is used in all electrochemical studies except for the experiments described in section 7.4.2.

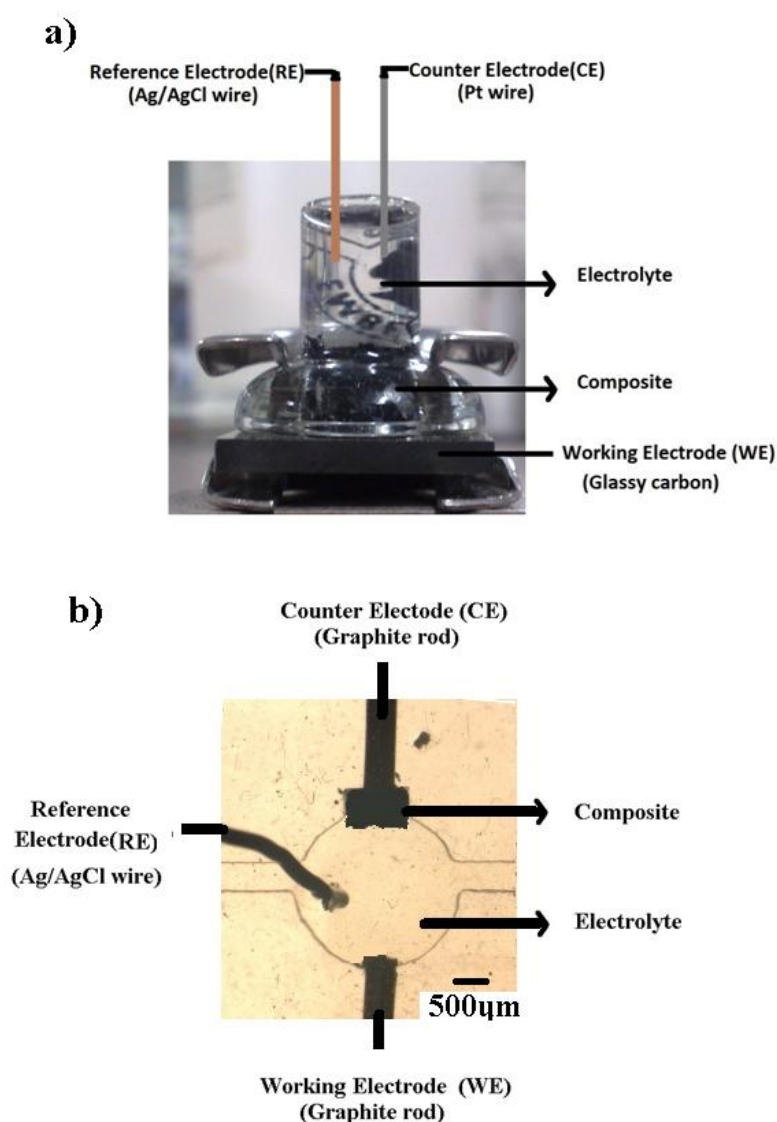


Figure 3.5. Electrochemical cells used in the experiments (a) Standard cell and (b) Microfluidic cell.

3.2.3 Conductivity Measurement

Conductivity measurements for the ECP composite films were performed using Jandel RM2 four point conductivity meter. The instrument has four equally spaced probes and passes current between the two outer probes and measures the voltage developed between the inner probes. From the set current and the measured voltage, the conductivities of the films were calculated using the following formula (Equation 3.1):

$$\text{Conductivity} = \frac{\text{Current}(A)}{4.532 * \text{Thickness}(cm) * \text{Voltage}(V)} S \text{ cm}^{-1} \quad (3.1)$$

3.2.4 Optical Microscopy

The ECP composites and hydrogels were analysed using Leica MZ 7.5 optical microscope. Images obtained from the microscope were analysed in the computer to obtain the volume change data. In some cases, time lapse images were obtained and compared

3.2.5 Scanning Electron Microscopy

The morphology of the conducting polymer composites was analysed using Philips XL30S Scanning Electron Microscope. The samples were mounted on aluminium studs using adhesive graphite tape and sputter coated with platinum.

CHAPTER 4: MODELLING THE OXIDATION WAVE PROPOGATION IN ELECTROCHEMICALLY ACTIVE CONDUCTING POLYMERS

4.1 Introduction

To induce fluid motion of the electrolyte in a microfluidic channel using Electrochemically-active Conducting Polymers (ECP), one interesting idea is to consider the possible coupling of solution movement to a mechanical wave motion, as in peristalsis. Such ideas have been explored using piezoelectric or acoustic actuators^{147,148}. The effect could be achieved using an ECP either with a suitable set of pad electrodes, or by induction of a mechanical wave along a single electrode appropriately connected.

Tezuka and others¹⁴⁹⁻¹⁵¹ first demonstrated composition wave propagation along an ECP strip. When an anodic potential was applied to a contact attached to one end of a reduced PPy strip, the oxidation process started from the contact and proceeded along the polymer, propagating as a wave. The movement of the composition front would be associated with a moving mechanical wave; as such, this association is of interest because it would couple with movement of the solution. When the polymer was reduced, it reduced uniformly.

The key to the behaviour is the variation in electrical conductivity of the polymer, from low in the reduced state to high in the oxidised state. Warren and Madden¹⁵² simulated the wave front propagation using an empirical variable resistance transmission line model, in which one arm was the solution, the other was the polymer, and the two arms were capacitively coupled. The capacitor represented the ionic charge stored in the polymer when it was electrochemically oxidised. The general features of the experimental results were reproduced. However, an important part of their model is the empirically assigned value for the capacitance and resistance coupling the two arms of the transmission line, so the model's usefulness is slightly restricted to explanation of a particular set of experimental results rather than as a general design tool. Wang et al.^{153,154} recently described a different experiment in which they constrained the ionic flux into the polymer: a strip of polymer was uniformly contacted by an electrode but covered with an ion barrier so that ions could

only enter by the edge.

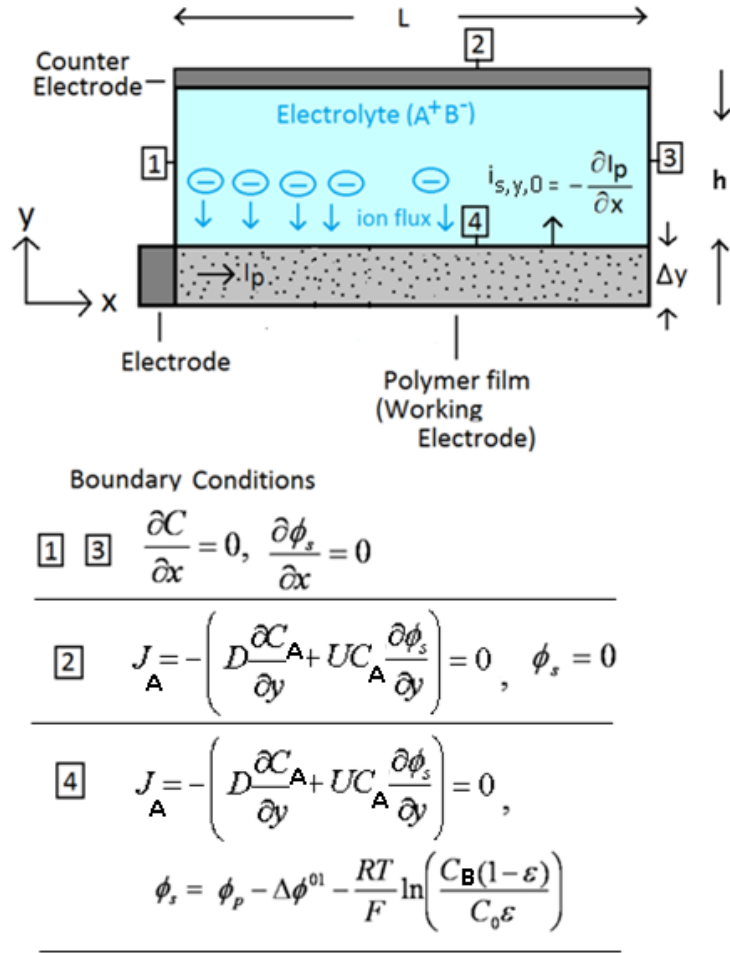


Figure 4.1. Geometry and boundary conditions of the system, showing the current in the polymer and current density across the interface. The concentration boundary conditions are required for the nonexchanged ion, A, only. The concentration field for ion B is determined by the assumption of electroneutrality throughout the solution (see text).

A compositional and mechanical wave propagated from the edge to the centre when the polymer was switched from an insulating to a conducting state. The wave propagation was simulated¹⁵⁵ by solution of the 1-D Nernst-Planck-Poisson equations to account for both electro-migration and diffusion as contributors to the ionic transport into the polymer film. Brumleve and Buck¹⁵⁶ showed the equivalence between transmission line models and the Nernst-Planck-Poisson equations.

There are two subtle questions relating to whether fluid motion could be induced as a consequence of an electrochemical actuation of a ECP in a micro-chamber. The first is: What is the net change in volume of the electrolyte-polymer system occurring as a

result of the electrochemical reaction? Solvent is incorporated into the polymer to a degree which depends upon the state of oxidation of the polymer, but solvent has a different partial molar volume within the polymer to that which it has in the solution. The second question is: To what degree is the motion of the polymer within the chamber constrained by transport limitations in the electrolyte? That is, where are the ions coming from and how quickly? In this chapter, we address the second question, with a view to optimizing the design of the chamber and the arrangement of the electrodes. A 1-D model, as used in previous works, cannot be applied. The major purposes of this work are thus to (a) present a 2-D solution of the Nernst-Planck transport equations for a complete electrochemical cell formed in a micro-chamber, (b) study the characteristics of composition waves propagated along an electrochemically-active conducting polymer electrode in the chamber, and (c) examine the effect of some aspects of the geometry of the cell on the compositional response of the electrochemically-active conducting polymer electrode. We then make the simplifying assumption that solvent is not incorporated into the polymer in order to explore the best possible mixing and pumping that might be achieved in a microchamber using these wave propagation effects. Again, we explore some different configurations.

There are some specific aspects of our treatment that differ from the general literature in this area^{155,157} and which are applicable to the design problem at hand. We use boundary conditions based on the fluxes of ions rather than the concentration, and we assume an ionic electrochemical equilibrium between polymer and solution, using the Nernst equation to describe the potential difference across the polymer-solution interface. This boundary condition allows us to study the dependence of the wave propagation on the potential difference applied to the cell. We use the Scharfetter-Gummell method¹⁵⁸ for computing the concentration field, since this method, being flux-based, conserves the mass in the system, and is numerically stable. The numerical scheme for extending this method to 2-D is given in the later section. Rather than solve the Poisson equation for the potential, which causes some significant difficulties associated with different distance scales for the region around the electrode and the region in the bulk of the solution, we impose electro-neutrality and extend the method of Cohen and Cooley¹⁵⁹ to 2-D. Also, because our emphasis is on the design of the electrochemical cell and the limitations that this imposes, for this

version of our model, like Warren and Madden¹⁵², we have assumed that the polymer electrode is very thin and so have not treated the diffusion-migration problem within the polymer electrode itself. We establish that the surface wave propagation can be controlled by altering the solution conductivity, the conductivity contrast between oxidised and reduced states of the polymer, and the arrangement of the electrodes. We then explore the fluid flows expected in response to these surface waves and discuss designs for pumps and mixers to be deposited in microchambers.

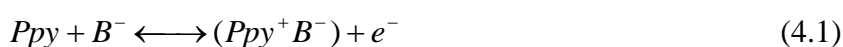
4.2 Modelling Oxidation Wave Velocity in Electrochemically active Conducting Polymers

In this section, we present the principles of the model. The full computational details can be found in section 4.4. We consider a thin slab of electronically ECP in contact with the electrolyte solution. When an anodic potential is applied at one end of the polymer slab, the polymer will be oxidised there, releasing electrons to the external circuit and exchanging ions with the solution in order to balance the charge. The oxidation of the polymer increases its electrical conductivity, so that this part acts as a contacting electrode to the rest of the polymer strip. The process continues until the entire polymer strip is oxidised. Qualitatively, one can observe that the way in which the polymer transformation propagates along the strip should depend on the conductivity of the polymer in the initial state, whether the polymer conductivity increases or decreases in response to the electrochemical change, and the ion transport in the solution. Under some conditions, the transformation should occur as a wave front propagating along the strip.

4.2.1 Assumptions

The geometry considered is that of Figure 1. The polymer layer is considered long in comparison to its thickness and is assumed to be uniform in composition in the z direction (right angles to its long axis). The electrolyte solution (represented as A^+B^-) has an initial concentration C_0 . For simplicity, all the equations derived here assume that A^+ and B^- are the only ions in the solution. The solution of the Nernst-Planck equations for transport, where both diffusion and electro-migration terms are included, is a difficult problem in a 2-D domain. This will be our focus since we are interested particularly in the effects of the overall geometry of the electrochemical cell on the observation or otherwise of propagating waves of composition change. Thus we make two important simplifications

in the treatment of the polymer part of the problem. First, we assume that the polymer layer is thin enough, and that the charge transport rate within the polymer is fast enough, that the layer can be considered uniform in composition in the direction normal to the polymer-solution interface (the y direction of Figure 4.1). This is an important assumption. The task of lifting it by considering the transport problem within the polymer layer itself, coupled to transport in the bulk solution phase, is significant. We consider the assumption justified because by using it we obtain the upper limit of performance of the system. The second assumption is that the polymer is in electrochemical equilibrium with the solution adjacent to it and that only one ion of the electrolyte is exchanged with the polymer. That is, we express the polymer-solution reaction as follows:



where Ppy denotes the polymer (e.g., PPy), with degree of oxidation, ε . Certainly, the polymer reaction can involve insertion and ejection of either anions or cations or both. The simplification introduced by equation 4.1 means that everywhere on the polymer-solution interface the potential difference across the interface is given by the Nernst equation, relating the local degree of oxidation to the local solution composition and the polymer-solution interfacial potential difference. There will be effects on the ionic transport in the solution due to convection in the solution induced by the swelling and shrinkage of the polymer. The task of incorporating such effects into the model is also significant and we have not addressed it.

While the negative ion B^- is being absorbed into or ejected from the polymer, in order to keep the system electrically neutral and balanced, we consider that the same ion B^- is injected into or removed from the system at the counter electrode at the same rate as it is being absorbed or ejected at the polymer working electrode. We do not consider the case where the counter electrode reaction results in different ions being injected into the solution. In practice, cells that satisfy this condition could be constructed where the counter electrode is also an ECP. Later in the thesis, we consider the consequences for fluid motion when both electrodes are constructed from ECP.

4.2.2 Relationship Between Local Current Density and Electric Potential in the Polymer

When the potential at one end of the polymer is changed, current flows into the polymer from the contact at one end and out across the polymer-solution interface, as a consequence of which the local degree of oxidation of the polymer, ε , changes. The potential gradient in the polymer is dependent on the local current and on the local conductivity, σ , which is itself dependent on the local degree of oxidation. The purpose of this section is to derive the relationship between potential in the polymer and the degree of oxidation. Consider a small segment of polymer with width w and thickness Δy , in contact with electrolyte. When a potential difference is created at the interface the polymer is oxidised (or reduced), releasing (or taking) electrons from the external circuit. Balancing this electron flux, there is a flux of negative ions into (or out of) the polymer (Equation 4.1). The position-dependent rate of oxidation of the polymer is related to the flux of the ions into the polymer which is related to the local current density across the polymer-solution interface, $i_{S,y,0}$:

$$i_{S,y,0} = MF\Delta y \frac{\partial \varepsilon}{\partial t} \quad (4.2)$$

where F is the Faraday constant and M is the ion capacity of the polymer film expressed in moles.m⁻³. Equation 4.2 expresses the assumption of uniformity of composition of the polymer in the y -direction. Note that the width in the z -direction, w , is assumed sufficiently large that the problem can be considered as a 2-D one, with variations only along the x - and y -axes. Similarly there will be a position-dependent current flow I_P along the length of the polymer, removing the charge consumed by oxidation resulting from the ion flux into the polymer.

$$\frac{\partial I_P}{\partial x} = -i_{S,y,0}w \quad (4.3)$$

The potential gradient in the polymer film is determined by this current I_P :

$$\frac{\partial \phi_P}{\partial x} = -\left(\frac{1}{w\Delta y\sigma}\right)I_P \quad (4.4)$$

where σ is the conductivity of the polymer. The conductivity switches when the state of oxidation increases through a transition threshold¹⁶⁰. Warren and Madden¹⁵² proposed an empirical sigmoidal function model relating the conductivity σ_p of the polymer to its fractional oxidation state:

$$\sigma_P = \frac{\sigma_{\max} - \sigma_{\min}}{1 + e^{(\varepsilon - \varepsilon_T)/W_T}} + \sigma_{\min} \quad (4.5)$$

where ε_T is the oxidation state at which the transition occurs and W_T is the transition width. Note that $i_{S,y,0}$, I_P , ϕ_p , ε , and σ are all functions of x

4.2.3 Interfacial Potential Difference

Warren and Maddent treated the ion absorption into the polymer as a potential-dependent capacitance¹⁶¹ – that is, considering the polymer as a matrix carrying one sign of charge with the ions as the balancing charge on the other side of an internal interface within the polymer structure. This view is indeed appropriate for an empirical description, but does not assist in the development of a model where the chemistry of the ion insertion process is explicitly considered. Therefore we have adopted an approach similar to that of Albery *et al*^{162,163} who used the idea of a Donnan potential to describe the ionic distribution between solution and polymer. We propose that we can determine the potential difference across the polymer-solution interface at any position by the Nernst equation. The chemical potential, μ , of the polymer-ion system in its oxidised and reduced state can be determined by making an assumption that the charge carriers in the polymers do not interact, and thinking about the polymer-ion system as an ideal solid solution of ions in polymer, with the fully reduced and fully oxidised states as the end members. This model can be extended in a number of standard ways to account for the interactions between the charges in the system, for ordering of charges, and so forth. With the simple ideal solid-solution model:

$$\mu[PPy^+ B^-] = \mu^0[PPy^+ B^-] + RT \ln(\varepsilon) \quad (4.6)$$

$$\mu[PPy] = \mu^0[PPy] + RT \ln(1 - \varepsilon) \quad (4.7)$$

Here, R denotes the gas constant and T the Kelvin temperature. Hence we can write the Nernst equation for the reduction reaction,

$$\phi_p - \phi_s = \Delta\phi^0 - \frac{RT}{F} \ln\left(\frac{A_B(1 - \varepsilon)}{\varepsilon}\right) \quad (4.8)$$

where ϕ_p denotes the potential on the polymer side of the interface and ϕ_s that on the solution side of the interface at the same position; $\Delta\phi^0$ is a standard potential difference determined by the Gibbs energy change on insertion of an ion into the polymer and A_B denotes the activity of the salt in the solution at the interface. Equation 4.8 assumes that the polymer is throughout its thickness in equilibrium with the solution. We can convert

this relation in terms of concentration of ion B⁻ (C_B) by assuming that the activity coefficient of ions in solution do not vary within our concentration range, i.e.

$$\Delta\phi = \phi_P - \phi_S = \Delta\phi^{01} - \frac{RT}{F} \ln\left(\frac{C_B(1-\varepsilon)}{C^0\varepsilon}\right) \quad (4.9)$$

Where

$$\Delta\phi^{01} = \left[\Delta\phi^0 - \frac{RT}{F} \ln(\gamma_B) \right] \quad (4.10)$$

γ_B is the activity coefficient, assumed constant, and C^0 specifies the concentration scale. Later, we render concentrations dimensionless by scaling them to the bulk concentration of salt in the solution, before the electrochemical process is started, and set $C^0/C_0=1$. Note that this scaling would also change the value of γ_B and hence of $\Delta\phi^{01}$ since the bulk concentration would not in general be the same as the unit concentration of the scale of measurement.

4.2.4 Ion Flux at the Interface

The rate of change of the degree of oxidation of the polymer is related to $J_{B,0}$, the flux (mole/unit area) of negative ions in the solution, perpendicular to the interface, at the polymer-solution interface. Note that $J_B < 0$ corresponds to a flow of negative ions into the polymer (i.e., $i_{S,y,0} > 0$). The negative ion flux at the interface is the sum of the electro-migration effect due to the potential gradient and the diffusion effect, which can be expressed by the Nernst-Planck equation. Hence:

$$J_{B,0} = M \Delta y \frac{\partial \varepsilon}{\partial t} = - \left(D_B \frac{\partial C_B}{\partial y} \Big|_{y=0} - U_B C_B \frac{\partial \phi_s}{\partial y} \Big|_{y=0} \right) \quad (4.11)$$

Equation (4.11) relates the change in the degree of oxidation to the ionic concentration and the electric potential field in the solution near the interface. The positive ion A⁺ is not incorporated into the polymer and hence the flux of the A⁺ ion at the interface is zero:

$$J_{A,0} = - \left(D_A \frac{\partial C_A}{\partial y} \Big|_{y=0} + U_A C_A \frac{\partial \phi_s}{\partial y} \Big|_{y=0} \right) = 0 \quad (4.12)$$

Here U_A , U_B and D_A , D_B are the mobility and diffusion coefficients of the positive and negative ions respectively. The mobility and the diffusion coefficient are related through the Nernst-Einstein equation:

$$D = \frac{RTU}{|z|F} \quad (4.13)$$

Where z denotes the ionic charge (here, we have assumed $z = 1$)

4.2.5 Ion Flux and Potential Gradient in the Solution

The rates of change of ionic concentrations in the solution are related to the ion fluxes by:

$$\frac{\partial C_i}{\partial t} = -\nabla \cdot J_i = \nabla \cdot (D_i \nabla C_i + U_i z_i C_i \nabla \phi_s) \quad (4.14)$$

In principle we can solve these equations together with Poisson's equation for the potential within the solution. One popular way of handling the difficulty of very different distance scales for the variations of potential and concentration is to use a spatially varying grid for the numerical solution of the differential equations. Extended to 2-D such methods become computationally cumbersome. An approximate method to handle this situation was developed by Cohen and Cooley¹⁵⁹ for the 1-D case. We have adapted their method to solve our 2-D problem.

First, we take advantage of our assumption that the electrolyte is just one salt, with just two ions. Since the current in the solution is carried by the ions, the current density vector anywhere in the solution, i_S , is proportional to the difference between the fluxes of the two ions:

$$i_S = (J_A - J_B)F \quad (4.15)$$

Second, we treat the steady state: that is, charge does not accumulate anywhere in the solution so by continuity, the divergence of i_S vanishes everywhere in the solution:

$$\nabla \cdot i_S = \nabla \cdot (J_A - J_B) = 0 \quad (4.16)$$

The key assumption made by Cohen and Cooley¹⁵⁹ is charge neutrality, i.e. the concentrations of the positive and negative ions remain the same throughout the solution. Setting $C_A = C_B = C$, we can also simplify the boundary conditions since all boundaries are no-flux for species A. Using (4.14) and (4.16), we have

$$\nabla \cdot (J_A - J_B) = \nabla \cdot (D_A \nabla C + U_A C \nabla \phi_s - D_B \nabla C + U_B C \nabla \phi_s) = 0 \quad (4.17)$$

which with the Nernst-Einstein equation (4.13) gives

$$(U_A - U_B) \frac{RT}{F} \nabla^2 C + (U_A + U_B) \nabla \cdot (C \nabla \phi_s) = 0 \quad (4.18)$$

This is the equation that we solve instead of Poisson's equation, together with the drift-diffusion equation that results from combining (4.13) and (4.14):

$$\frac{\partial C}{\partial t} = U_A \nabla \cdot \left(\frac{RT}{F} \nabla C + C \nabla \phi_s \right) \quad (4.19)$$

Note that the assumption of electro-neutrality does not imply that the right hand side of Poisson's equation goes to zero; that is, that Laplace's equation holds for the potential¹⁶⁴. Laplace's equation is valid only if the mass transfer of the ions does not contribute to the current flow, which in our case is not true.

We can now relate the gradients of concentration and potential at the interface to the current density across the interface and thence to the current flowing in the polymer at any given position. Equation 4.2 relates the change of composition of the polymer to the current density in the bulk solution at the polymer-solution interface, $i_{S,y,0}$. However, we also have, from 4.12, 4.13, and 4.15:

$$i_{S,y,0} = F \left[- (U_A - U_B) \frac{RT}{F} \frac{\partial C}{\partial y} \Big|_{y=0} - (U_A + U_B) C \frac{\partial \phi_s}{\partial y} \Big|_{y=0} \right] \quad (4.20)$$

The polymer potential ϕ_p and the polymer current I_p together satisfy Ohm's law (4.4), where the conductivity, σ , is a function of ε , given by (4.5). The difference between ϕ_p and ϕ_s at the polymer interface, $\Delta\phi$, is a function of C and ε (4.9), while the rate of change in oxidation ε at a point is proportional to $i_{S,y,0}$ (4.2 and 4.20). For a given set of boundary conditions, the coupled equations (4.2), (4.3), (4.4), (4.5), (4.9), (4.19) and (4.20) completely describe the time evolution of the system.

4.3 Numerical Model

The set of equations to be solved is nonlinear and involves partial differential equations in both spatial and time domains. We assume that the diffusion constants and hence the ionic mobility of the A^+ ion and the B^- ion are the same.

This assumption conveniently decreases the number of parameters that have to be specified, but could also be removed in order to explore the effects that very different ionic mobilities might cause. The boundary conditions are shown on Figure 4.1. Here we consider no-flux boundaries for the concentration on all boundaries. Note that the no-flux boundary condition applies only for the A^+ ions. Our use of the Cohen-Cooley

method and assumption of electroneutrality allows us to solve for the concentration of A^+ assuming no flux on all boundaries, then to set the concentration of B^- equal to that of A^+ everywhere, as noted above. The B^- ions will cross into the polymer, and we assume that there will be an equal flux of B^- ions flowing into the solution from the counter electrode to keep the system electrically neutral.

In each time step, we first solve for the ion concentration (C) and then for the potential (ϕ_S) in the solution and the current in the polymer (which implicitly determines the solution-polymer current at the boundary). The current at the solution boundary sets the rate of oxidation of the polymer. The rate of oxidation determines the oxidation state of the polymer at the next time step which in turn determines the resistivity of polymer, Nernst potential and the solution boundary potential. The new solution boundary potential changes the potential and concentration distribution in the solution. The current falls to zero everywhere when the polymer is completely reacted to the degree of oxidation specified by the applied potential and bulk solution concentration. The usual method of solution is to compute the fluxes from the concentrations at each mesh point. However, as noted by Scharfetter and Gummell¹⁵⁸, this approach can lead to numerical instability when the potential gradient is large and to an accumulation of numerical errors that lead to nonconservation of mass inside the computational domain. The Scharfetter-Gummell scheme in contrast applies an analytical solution for concentrations at the grid points, derived from the fluxes assuming that at each step the fluxes and potential gradients are constant across each pair of adjacent points. Mass conservation in the system is guaranteed and the method is robust against the accumulation of small numerical errors. We used the Alternating Direction Implicit (ADI) method to extend the method to 2-D. In order to verify the correct functioning of the code for the different blocks of the problem, at each stage artificial model cases were generated for which analytical solutions were found and compared. Typically, the error due to numerical approximation was found to be in the range of 0.1% to 0.5%.

4.3.1. Solver Sequence

The nonlinear time-dependent partial differential equations linking the spatial distributions of potential, ionic concentrations, and polymer oxidation were solved in

Matlab using finite difference methods. The parameters were solved separately in the sequence explained in Figure 4.2

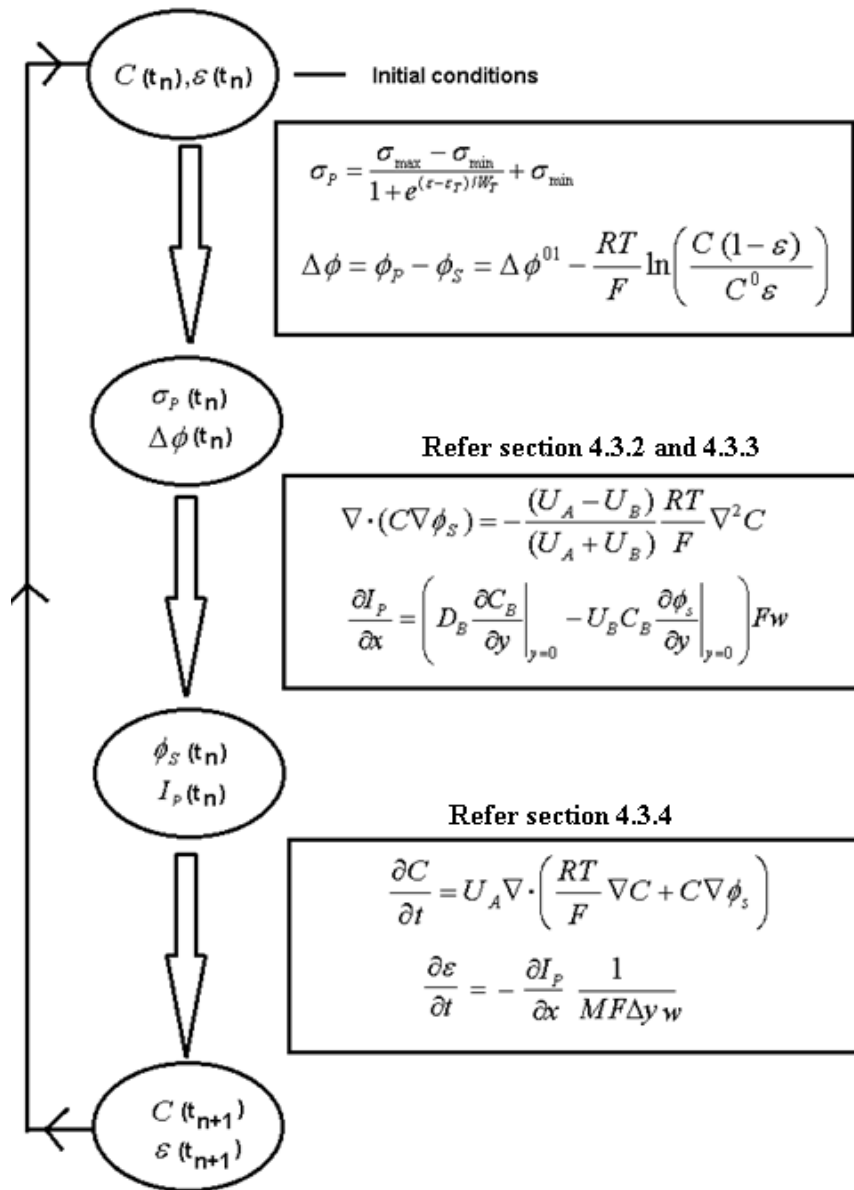


Figure 4.2. Solver sequence used to solve the partial differential equations.

Solution concentration and oxidation state values were stepped through time and all the other parameters were updated instantaneously. The finite difference schemes used to solve solution potential, polymer current, and solution concentration are explained in the following sections. Splitting up the solution of this complex nonlinear system into separate steps makes the problem tractable, but in some cases the disconnection between the concentration and potential solvers can lead to ripples that tend to grow. This effect is readily suppressed with a simple smoothing procedure. Holding the end-point values

fixed, a sliding-average smoother was applied to each row of the concentration matrix, not touching the rows near the upper and lower boundaries. There undoubtedly are more sophisticated iterative solution procedures that will not require this smoothing step.

4.3.2 Scharfetter-Gummel Scheme

In order to solve the convection-diffusion problem for concentration over time with the finite difference method (Equation 4.14), we used the Scharfetter-Gummel scheme. This exponential fitting discretization method converges faster than the conventional equidistance central difference method and it can handle rapid variations of concentration between two mesh points. This method is derived assuming that the potential gradient is constant between grid points, and has the virtue of guaranteeing mass conservation. We first derived this scheme for a positive ion in one dimension and then extended it to 2-D using the Alternating Direction Implicit method. The drift diffusion equation for the positive ion in one dimension is given by

$$\frac{\partial C}{\partial t} = U \frac{\partial}{\partial x} \cdot \left(\frac{RT}{F} \frac{\partial C}{\partial x} + C \frac{\partial \phi}{\partial x} \right)$$

Here C is the concentration of the ion, and ϕ is the voltage potential.

The original dimensions of the system are normalized using the following parameters.

$$C_0 = 0.1 \text{ (moles L}^{-1}\text{, the bulk concentration)}$$

$$x_0 = 0.001 \text{ (meters , typical width of the system)}$$

$$D_A = D_B = D = 2 \times 10^{-9} \text{ (m}^2\text{s}^{-1}\text{, diffusion constant)}$$

$$t_0 = \frac{x_0^2}{D} \text{ (s, as unit time)}$$

$$\phi_0 = \frac{RT}{F} \text{ (V)}$$

(T is absolute room temperature, R is the gas constant and F is Faraday's constant)

The nondimensionalised form of the equation is

$$\frac{\partial C}{\partial t} = \frac{\partial}{\partial x} \cdot \left(\frac{\partial C}{\partial x} + C \frac{\partial \phi}{\partial x} \right)$$

This can also be written as

$$\frac{\partial C}{\partial t} = - \frac{\partial J}{\partial x} \quad (4.21)$$

Where $J = - \left(\frac{\partial C}{\partial x} + C \frac{\partial \phi}{\partial x} \right)$ is the flux of the positive ion.

The x axis is discretized with $NX+1$ equally spaced points, $i=1 \dots NX+1$, with spacing Δx . Consider two points i and $i+1$, where the concentrations are C_i and C_{i+1} . The flux between the two grid points is assumed to be constant, $J_{i+1/2}$.

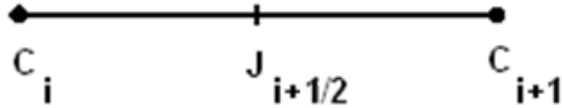


Figure 4.3. Flux between two grid points.

We assume that the potential gradient between the two grid points is constant, and refer to it as K

$$\frac{\partial C}{\partial x} = -KC - J_{i+1/2} \quad (4.22)$$

$$K = \frac{\partial \phi}{\partial x}$$

$$J_{i+1/2} = - \left(\frac{\partial C}{\partial x} + CK \right)$$

This first order equation can be integrated with an integrating factor, which in our case is an exponential function.

$$J_{i+1/2} e^{-K(x-x_i)} = - \left(\frac{\partial C}{\partial x} + CK \right) e^{-K(x-x_i)}$$

$$J_{i+1/2} e^{-K(x-x_i)} = - \left(\frac{\partial (C e^{-K(x-x_i)})}{\partial x} \right)$$

Integrating both sides

$$\int_{x_i}^{x_i+\Delta} J_{i+1/2} e^{-K(x-x_i)} dx = - \int_{x_i}^{x_i+\Delta} \left(\frac{\partial(Ce^{-K(x-x_i)})}{\partial x} \right) dx$$

$$J_{i+1/2} = \frac{K(C_i - e^{-K\Delta x} C_{i+1})}{(1 - e^{-K\Delta x})}$$

$$J_{i+1/2} = \frac{K}{(1 - e^{-K\Delta x})} C_i - \frac{Ke^{-K\Delta x}}{(1 - e^{-K\Delta x})} C_{i+1}$$

$$J_{i+1/2} = \alpha C_i - \beta C_{i+1} \quad (4.23)$$

Where $\alpha = \frac{K}{(1 - e^{-K\Delta x})}$ and $\beta = \frac{Ke^{-K\Delta x}}{(1 - e^{-K\Delta x})}$

Thus we have the flux between the two grid points, given the concentrations at the grid points and the assumed constant potential gradient K . Now the equation 4.21 can be converted into finite difference formulation and can be solved numerically as below. Consider three points: $i-1$, i , and $i+1$.

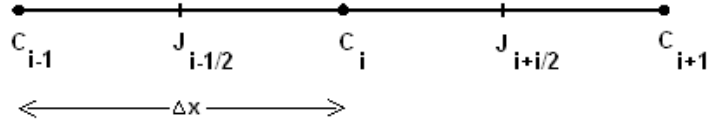


Figure 4.4. Scharfetter-Gummel 1-D discretization.

The equation $\frac{\partial C}{\partial t} = - \frac{\partial J}{\partial x}$ can be written in finite difference form as

$$\frac{\partial C}{\partial t} = - \frac{(J_{i+1/2} - J_{i-1/2})}{\Delta x}$$

Then substituting equation 4.23 $J_{i+1/2} = \alpha C_i - \beta C_{i+1}$ and $J_{i-1/2} = \alpha C_{i-1} - \beta C_i$ we get

$$\frac{\partial C}{\partial t} = - \frac{(\alpha C_i - \beta C_{i+1} - \alpha C_{i-1} + \beta C_i)}{\Delta x}$$

$$\frac{\partial C}{\partial t} = - \frac{(\alpha + \beta)C_i - \beta C_{i+1} - \alpha C_{i-1}}{\Delta x}$$

Here we use the implicit finite difference method for time domain discretization. By incrementing from the time step n to $n+1$, we have the following discretization.

$$\begin{aligned}
\frac{C_i^{n+1} - C_i^n}{\Delta t} &= \frac{\left[-\frac{(\alpha + \beta)C_i^{n+1} - \beta C_{i+1}^{n+1} - \alpha C_{i-1}^{n+1}}{\Delta x} \right] + \left[-\frac{(\alpha + \beta)C_i^n - \beta C_{i+1}^n - \alpha C_{i-1}^n}{\Delta x} \right]}{2} \\
C_i^{n+1} + \frac{\Delta t}{2} \left[\frac{(\alpha + \beta)C_i^{n+1} - \beta C_{i+1}^{n+1} - \alpha C_{i-1}^{n+1}}{\Delta x} \right] &= C_i^n + \frac{\Delta t}{2} \left[-\frac{(\alpha + \beta)C_i^n - \beta C_{i+1}^n - \alpha C_{i-1}^n}{\Delta x} \right] \\
\left(1 + \frac{\Delta t}{2\Delta x} (\alpha + \beta) \right) C_i^{n+1} - \frac{\Delta t}{2\Delta x} \beta C_{i+1}^{n+1} - \frac{\Delta t}{2\Delta x} \alpha C_{i-1}^{n+1} &= \left(1 - \frac{\Delta t}{2\Delta x} (\alpha + \beta) \right) C_i^n + \frac{\Delta t}{2\Delta x} \beta C_{i+1}^n + \frac{\Delta t}{2\Delta x} \alpha C_{i-1}^n
\end{aligned} \tag{4.24}$$

This equation is the finite difference formulation, where $\alpha = \frac{K}{(1 - e^{-K\Delta x})}$, $\beta = \frac{Ke^{-K\Delta x}}{(1 - e^{-K\Delta x})}$

and $K = \frac{\partial \phi}{\partial x}$. Note that K , α , and β are computed for each grid interval. The ion flux is specified at each boundary, $J_{x=0}$ and $J_{x=1}$. We need to derive a special form of the equation for these points. At the left boundary $x = 0$

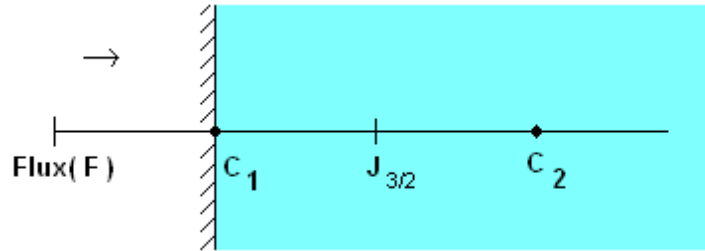


Figure 4.5. Flux boundary at $y = 0$.

$$\frac{\partial C_1}{\partial t} = -\frac{\partial J}{\partial x}$$

$$\frac{\partial C_1}{\partial t} = -\frac{(F - J_{3/2})}{\Delta x}$$

$$\frac{\partial C_1}{\partial t} = -\frac{(F - \alpha C_1 + \beta C_2)}{\Delta x}$$

Using the implicit finite difference method for time domain discretization

$$\frac{C_1^{n+1} - C_1^n}{\Delta t} = \frac{\left[-\frac{(F - \alpha C_1^{n+1} + \beta C_2^{n+1})}{\Delta x} \right] - \left[\frac{(F - \alpha C_1^n + \beta C_2^n)}{\Delta x} \right]}{2}$$

$$\frac{C_1^{n+1} - C_1^n}{\Delta t} =$$

$$\frac{\left[-\frac{(F - \alpha C_1^{n+1} + \beta C_2^{n+1})}{\Delta x} \right] - \left[\frac{(F - \alpha C_1^n + \beta C_2^n)}{\Delta x} \right]}{2}$$

$$\frac{C_1^{n+1} - C_1^n}{\Delta t} =$$

$$\frac{\Delta t}{2\Delta x} (-F + \alpha C_1^{n+1} - \beta C_2^{n+1} - F + \alpha C_1^n - \beta C_2^n)$$

$$C_1^{n+1} \left(1 - \alpha \frac{\Delta t}{2\Delta x} \right) + \beta \frac{\Delta t}{2\Delta x} C_2^{n+1} =$$

$$\left(1 + \alpha \frac{\Delta t}{2\Delta x} \right) C_1^n - \beta \frac{\Delta t}{2\Delta x} C_2^n - \frac{\Delta t}{\Delta x} F \quad (4.25)$$

This gives us the finite difference formulation for the left boundary.

At the right boundary $x=1$

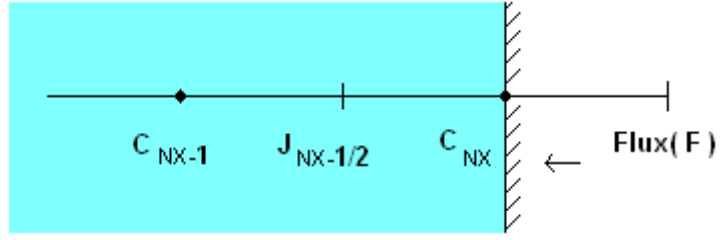


Figure 4.6. Flux Boundary at $x=1$.

$$\frac{\partial C_{NX}}{\partial t} = -\frac{\partial J}{\partial x}$$

$$\frac{\partial C_{NX}}{\partial t} = -\frac{(J_{NX-1/2} - F)}{\Delta x}$$

$$\frac{\partial C_{NX}}{\partial t} = -\frac{(\alpha C_{NX-1} - \beta C_{NX} - F)}{\Delta x}$$

Using the implicit finite difference method for time domain discretization

$$\frac{C_{NX}^{n+1} - C_{NX}^n}{\Delta t} = \frac{-\left[\frac{(\alpha C_{NX-1}^{n+1} - \beta C_{NX}^{n+1} - F)}{\Delta x}\right] - \left[\frac{(\alpha C_{NX-1}^n - \beta C_{NX}^n - F)}{\Delta x}\right]}{2}$$

$$\frac{C_{NX}^{n+1} - C_{NX}^n}{\Delta t} = \frac{\frac{\Delta t}{2\Delta x}(F - \alpha C_{NX-1}^{n+1} + \beta C_{NX}^{n+1} + F - \alpha C_{NX-1}^n + \beta C_{NX}^n)}{2}$$

$$C_{NX}^{n+1} \left(1 - \beta \frac{\Delta t}{2\Delta x}\right) + \alpha \frac{\Delta t}{2\Delta x} C_{NX-1}^{n+1} =$$

$$\left(1 + \beta \frac{\Delta t}{2\Delta x}\right) C_{NX}^n - \alpha \frac{\Delta t}{2\Delta x} C_{NX-1}^n + \frac{\Delta t}{\Delta x} F$$

(4.26)

At each time step, the set of linear equations given by 4.24, 4.25, and 4.26 can be solved for the concentrations at the $NX+1$ grid points, given the potential ϕ as a function of x and the concentrations at the previous time step. The way we solve for P and C together is discussed below in the description of the method used for the 2-D case.

4.3.3 Alternating Direction Implicit Method

Now we can extend this 1-D finite difference method to two dimensions in x and y directions using alternate direction implicit method. Alternating Direction Implicit (ADI) method uses two half step time intervals in order to progress one time step. The time interval is divided into two. During the first half step, from time t to $t + \frac{\Delta t}{2}$ only x direction values are integrated while the y direction values are held fixed. During the second half of the time step (i.e., from $t + \frac{\Delta t}{2}$ to $t + \Delta t$) the y direction values are updated using the previous results as base values, while the x direction values are held fixed. Figure 4.7 is the 5 point ($C_{i,j}, C_{i-1,j}, C_{i+1,j}, C_{i,j-1}, C_{i,j+1}$) stencil representation of the system in a two dimensional domain. The fluxes in the system can be represented using the Scharfetter-Gummel method explained above. Using the equation 4.23 we can derive the fluxes at the points $J_{i-1/2,j}, J_{i+1/2,j}, J_{i,j+1/2}, J_{i,j-1/2}$.

In the x direction the flux depends on the potential gradient along the x direction given by

$K_x = \frac{\partial \phi}{\partial x}$ and in y direction it depends on the potential gradient along the y direction given by $K_y = \frac{\partial \phi}{\partial y}$. Thus the α and β in the equation 4.23 for x direction are given by

$$\alpha_x = -\frac{K_x}{(1 - e^{K_x \Delta x})} \text{ and } \beta_x = -\frac{K_x e^{K_x \Delta x}}{(1 - e^{K_x \Delta x})} \text{ and for } y \text{ direction are given by } \alpha_y = -\frac{K_y}{(1 - e^{K_y \Delta y})}$$

$$\beta_y = -\frac{K_y e^{K_y \Delta y}}{(1 - e^{K_y \Delta y})}$$

Thus the fluxes are given by

$$J_{i-1/2,j} = \alpha_x C_{i-1,j} - \beta_x C_{i,j}$$

$$J_{i+1/2,j} = \alpha_x C_{i,j} - \beta_x C_{i+1,j}$$

$$J_{i,j-1/2} = \alpha_y C_{i,j-1} - \beta_y C_{i,j}$$

$$J_{i,j+1/2} = \alpha_y C_{i,j} - \beta_y C_{i,j+1}$$

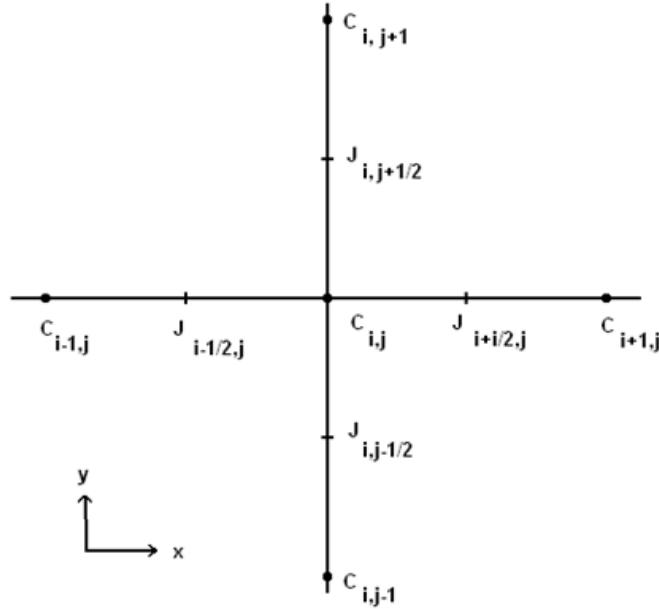


Figure 4.7. 2-D Stencil for alternating direction implicit method.

We know that $\frac{\partial C_{i,j}}{\partial t} = -\nabla \cdot J_A$. This equation is solved implicitly from time n to time $n+1$. First, the time step is divided into two as n to $n+1/2$ and $n+1/2$ to $n+1$. During the first half of the time step,

$$\frac{C_{i,j}^{n+1/2} - C_{i,j}^n}{\Delta t} = \frac{\left(\frac{J_{i-1/2,j}^{n+1/2} - J_{i+1/2,j}^{n+1/2}}{\Delta x} \right) + \left(\frac{J_{i,j-1/2}^n - J_{i,j+1/2}^n}{\Delta y} \right)}{2} \quad (4.27)$$

only the x direction values are integrated over the time while the y direction values are held as same in the previous time step. Over the next half of the time step we use the results from the previous calculation and integrate the system over time only in the y direction while holding the x direction values same. Thus we get the integrated final values in both the directions for the time $n+1$.

$$\frac{C_{i,j}^{n+1} - C_{i,j}^{n+1/2}}{\Delta t} = \frac{\left(\frac{J_{i,j-1/2}^{n+1} - J_{i,j+1/2}^{n+1}}{\Delta y} \right) + \left(\frac{J^{n+1/2}_{i-1/2,j} - J^{n+1/2}_{i+1/2,j}}{\Delta x} \right)}{2} \quad (4.28)$$

The boundaries are treated same as the 1D method. The stencil for the lower boundary is given in the Figure 4.8. Here we have a specified flux F instead of $J_{i,j-1}$. The derivation for the lower boundary with the specified flux F is given below in the equations 4.29 and 4.30. Similarly we can derive finite difference equations for all the other three boundaries.

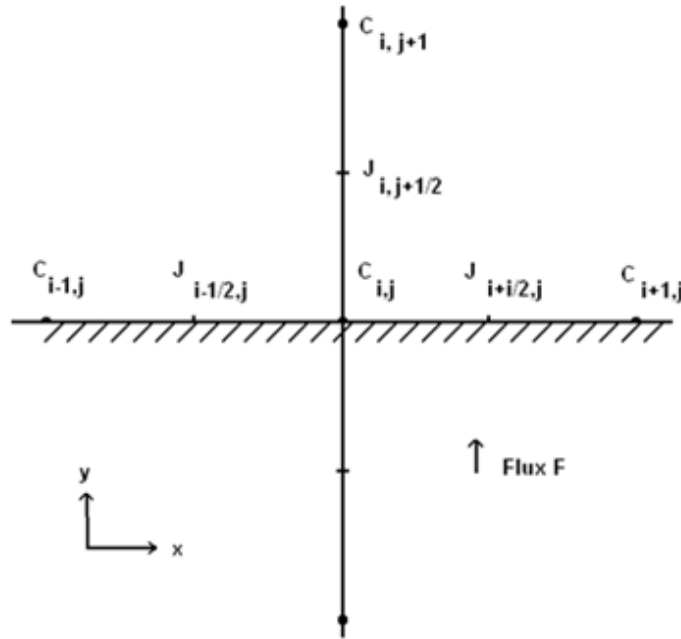


Figure 4.8. Lower boundary.

$$\frac{C_{i,j}^{n+1/2} - C_{i,j}^n}{\Delta t} = \frac{\left(\frac{J_{i-1/2,j}^{n+1/2} - J_{i+1/2,j}^{n+1/2}}{\Delta x} \right) + \left(\frac{F - J^n_{i,j+1/2}}{\Delta y} \right)}{2} \quad (4.29)$$

$$\frac{C_{i,j}^{n+1} - C_{i,j}^{n+1/2}}{\Delta t} = \frac{\left(\frac{F - J_{i,j+1/2}^{n+1}}{\Delta y} \right) + \left(\frac{J^{n+1/2}_{i-1/2,j} - J^{n+1/2}_{i+1/2,j}}{\Delta x} \right)}{2} \quad (4.30)$$

The two systems of linear equations that result from the finite difference formulation, one for each half time step, are solved in the usual way. In our current application we solve

for the concentration of the positive ion (A), for which the boundary conditions are zero flux on all the boundaries. As discussed before, the concentration of the negative ion B equals the concentration of A everywhere.

4.3.4 Calculating Solution Potential and Polymer Current from Concentration and Ion Flux

Potential in the solution and the polymer current can be calculated from the solution concentration and ion flux at the interface using the following equations (equations 4.2, 4.3, 4.11, 4.18).

$$\nabla \cdot (C \nabla \phi_s) = - \frac{(U_A - U_B) RT}{(U_A + U_B) F} \nabla^2 C \quad (4.31)$$

$$\frac{\partial I_p}{\partial x} = -i_{s,y,0} w \quad (4.32)$$

$$i_{s,y,0} = MF \Delta y \frac{\partial \varepsilon}{\partial t} \quad (4.33)$$

$$J_{B,0} = M \Delta y \frac{\partial \varepsilon}{\partial t} = - \left(D_B \frac{\partial C_B}{\partial y} \Big|_{y=0} - U_B C_B \frac{\partial \phi_s}{\partial y} \Big|_{y=0} \right) \quad (4.34)$$

From equations 4.12, 4.13, and 4.14, we arrive at the equation 4.15: defining polymer current in terms of the ion flux at the interface.

$$\frac{\partial I_p}{\partial x} = \left(D_B \frac{\partial C_B}{\partial y} \Big|_{y=0} - U_B C_B \frac{\partial \phi_s}{\partial y} \Big|_{y=0} \right) F w \quad (4.35)$$

We have solved equation 4.11 and 4.15 together to find I_p and ϕ_s . We use the finite difference method with the matrix formulation described as in figure 7.

$$\Delta \phi = \phi_p - \phi_s = \Delta \phi^{01} - \frac{RT}{F} \ln \left(\frac{C_B (1 - \varepsilon)}{C^0 \varepsilon} \right) \quad (4.36)$$

We solve for the polymer currents $I_p(k)$ at the same time as solving for the solution potential, by including in our linear system equations that combine equation 4.16 with Ohm's law to relate the polymer currents to the solution potential values at the boundary. In place of the usual stencil, for $\phi_s(k, 1)$ equation 4.15 is used to provide a linear equation linking the I_p values to the solution potential (a three-point formula is used to estimate the gradient of ϕ_s at the boundary). Updating of oxidation ε at each time step is performed using a simple explicit discretization of equation 4.13.

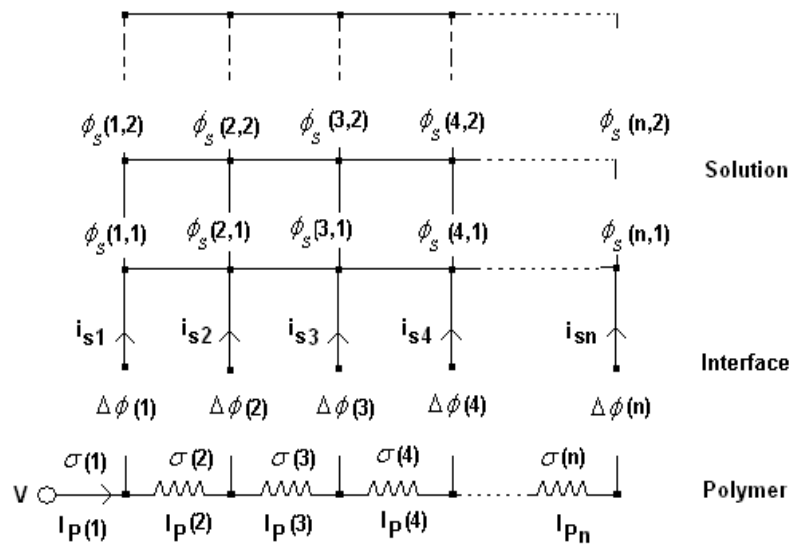


Figure 4.9. Matrix formulation for solving polymer current (I_p) and solution potential (ϕ_s).

4.4 Results and Discussion

Figure 4.10. shows the results of typical simulations. The current across the polymer-solution interface had a maximum at the moving boundary of the zone where the polymer was being transformed from its reduced (low conductivity) to its oxidised (high conductivity) state. The moving front was also associated with strong gradients of potential and concentration in the solution (Figure 4.11). The total current flowing into the polymer for different cases is displayed in Fig 4.10. Immediately following the application of a potential high enough to essentially completely transform the polymer from its initial, reduced, low-conductivity state to its final, oxidised, high-conductivity state, the current increased rapidly then more slowly, then rose to a plateau and remained almost constant until the oxidation wave front had reached the end of the strip.

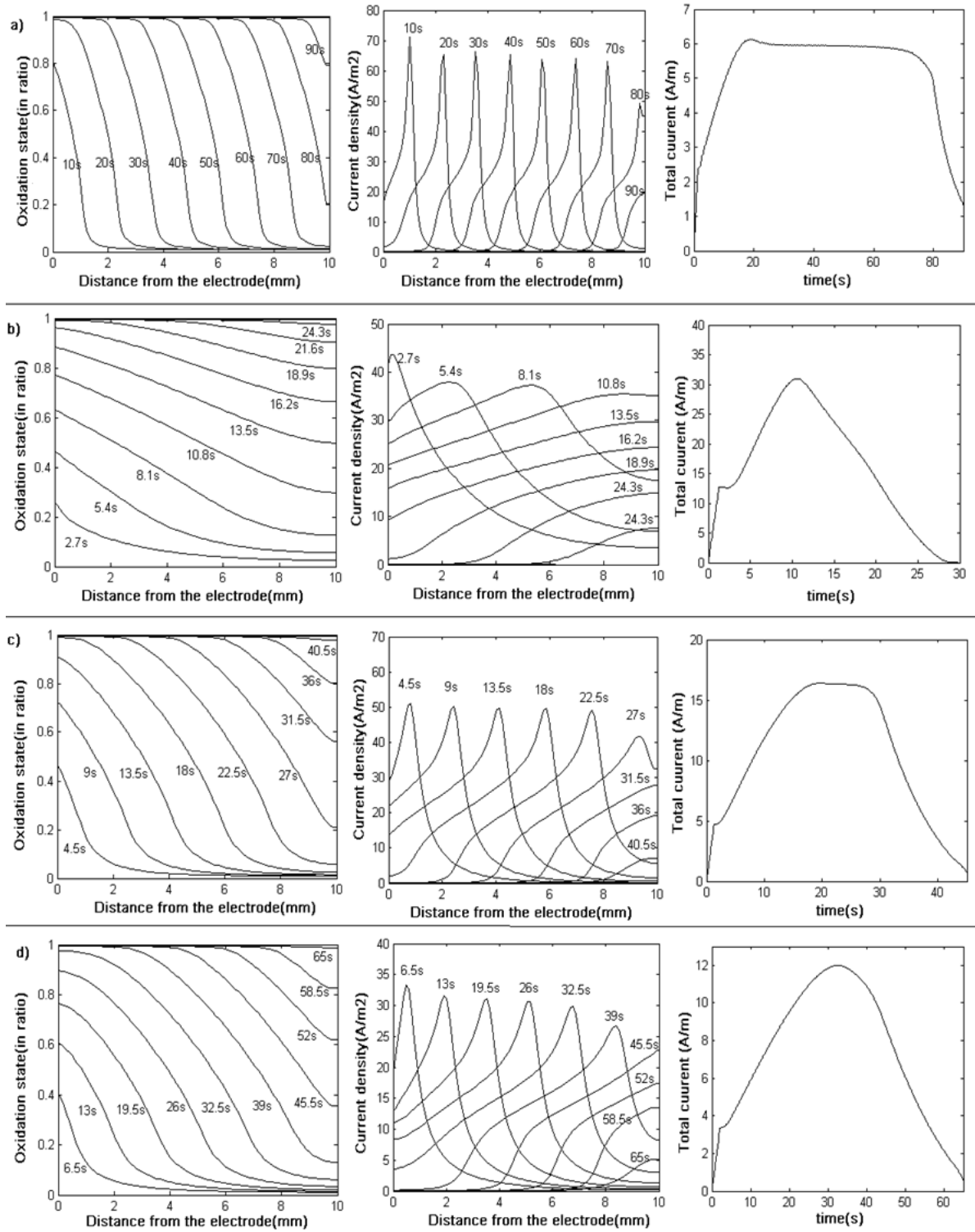


Figure. 4.10. Effects of conductivity and cell thickness on the oxidation wave propagation . (a) and (b) show the effect of altering the minimum polymer conductivity with $h=1\text{mm}$ (a) $\sigma_{min} = 1.49 \times 10^2 \text{ S m}^{-1}$ (b) $\sigma_{min} = 1.4 \text{ S m}^{-1}$. (c) and (d) show the variation of oxidation wave profile with geometry. (c) $h = 1\text{mm}$; (d) $h=2\text{mm}$. when $\sigma_{min} = 14.9\text{S m}^{-1}$. *Other conditions $L = 1\text{cm}$, $\sigma_{max} = 1.4 \times 10^3 \text{ S m}^{-1}$, $\varepsilon_T = 0.5$, $W_T = 0.03$, $C_0 = 0.01\text{mol liter}^{-1}$, $U_A = U_B = 7.75 \times 10^{-8} \text{ m}^2 \text{ s}^{-1} \text{ V}^{-1}$, thickness $\Delta y = 1\mu\text{m}$, applied potential = 0.25V , $\Delta\phi^{01} = 0.115\text{V}$

The current then decayed slowly as the polymer completed oxidation to the final state along the whole length of the strip. In contrast, no wave appears on reduction, from the high-conductivity to the low-conductivity state. The strip reduced uniformly (Fig. 4.12). The final stage of reduction was very slow and at the end of the simulation run time some 30% of the strip remained un-transformed. The essential details of the experimental observations presented by Tezuka *et al*^{149,150} have been captured by the simulation

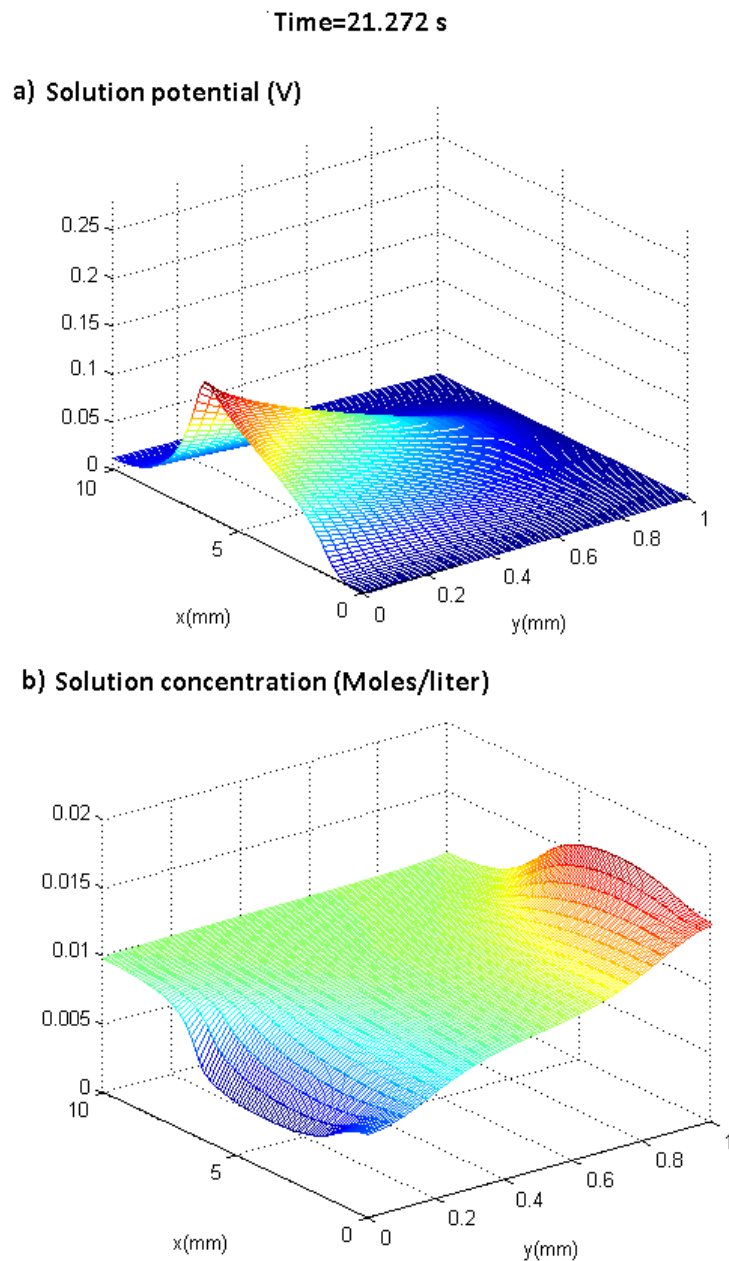


Figure 4.11. Variation of concentration and potential fields during the simulation.

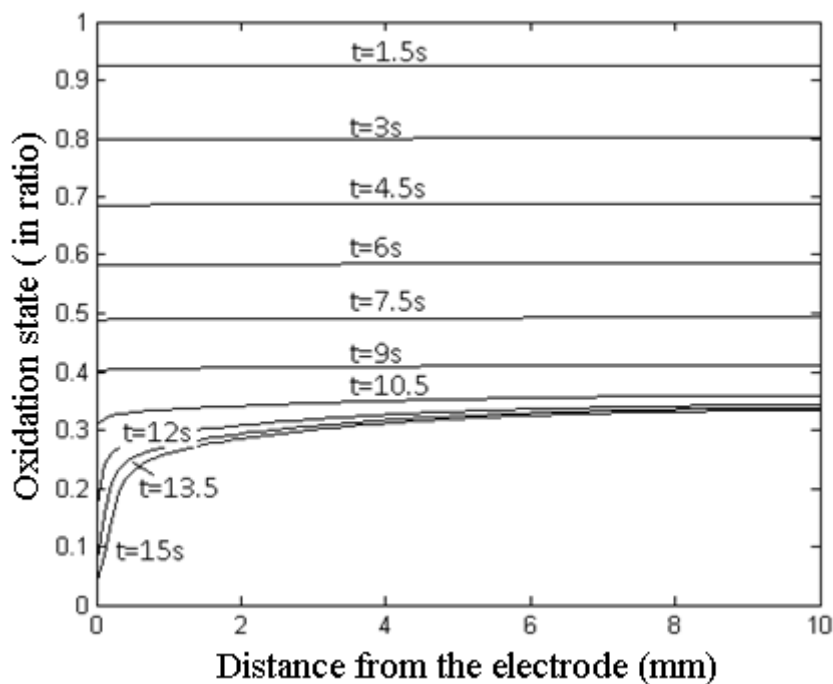


Figure 4.12 Reduction of the fully oxidised film: step from 0 to -0.25 V. ($\sigma_{min} = 14 \text{ S m}^{-1}$, $h=1\text{mm}$, L , σ_{max} , ε_T , W_T , C_0 , U_A , U_B as of Figure 4.10).

4.4.1 Variation of Oxidation Wave with Conductivity Change

There are two parameters that define the behaviour of oxidation wave propagation: the conductivity of the polymer in the low-conductivity state, σ_{min} , and solution conductivity. The minimum, σ_{min} and maximum, σ_{max} conductivity of the polymer largely define the shape of the moving front. When σ_{min} is sufficiently increased the oxidation wave ceases to exist and the oxidation state of the polymer increases uniformly over the length of the polymer. The same effect is found when the concentration of the solution species and consequently the conductivity of the solution is decreased. Hence the conductivity of the solution and the conductivity of the polymer in the reduced state (σ_{min}) together determine whether the oxidation proceeds as a wave along the polymer.

These parameters also affect the time it takes for the polymer to get completely oxidised. When the minimum conductivity of the polymer is reduced, the rate at which the polymer oxidises increases but when the concentration of the electrolyte is decreased, the rate at

which the wave propagates decreases. The concentration of the electrolyte also affected the total current flowing into the polymer: The higher the concentration, the higher the current into the polymer. As noted above, the wave also became less well-defined. These effects are illustrated in Figure 4.10 and Figure 4.13.

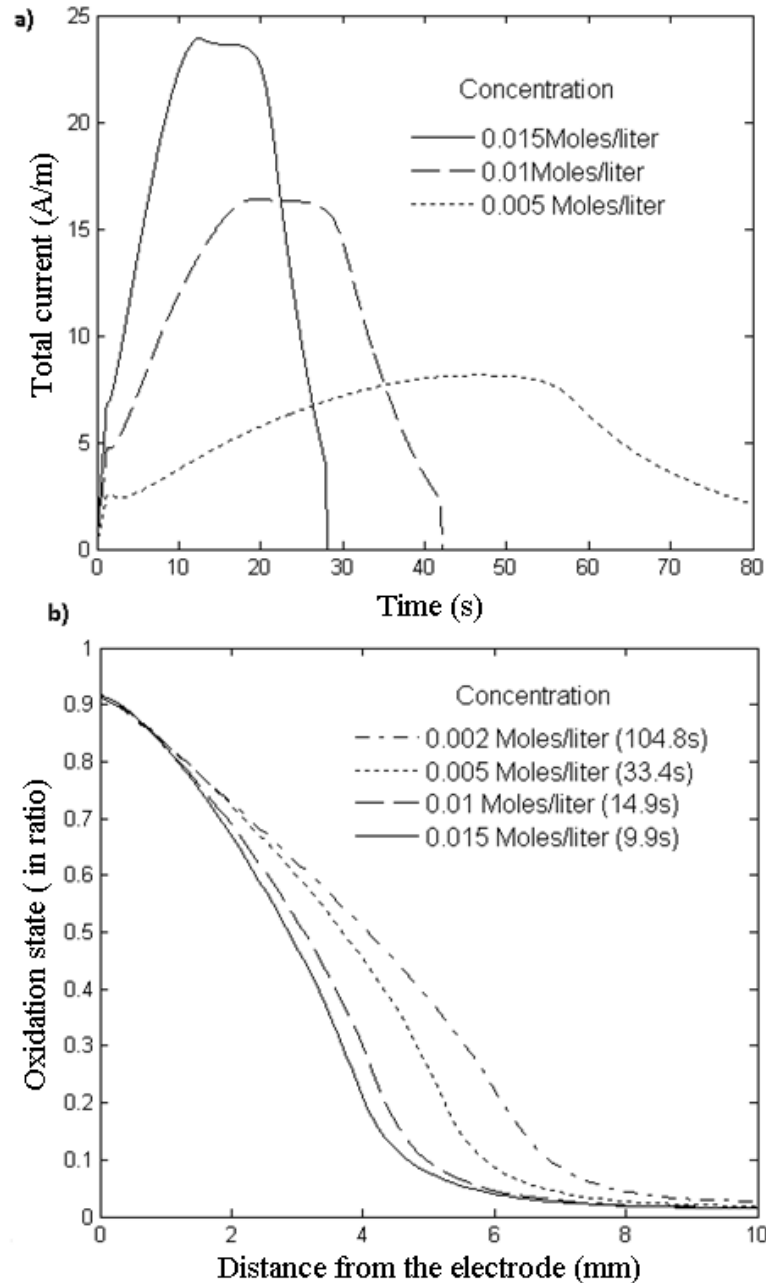


Figure 4.13. Variation of total current (a) and oxidation wave shape (b) with the electrolyte concentration. The wave shape is shown at a time such that the wave had passed approximately halfway along the strip. ($\sigma_{min} = 14 \text{ S m}^{-1}$, $h=1\text{mm}$, L , σ_{max} , ε_T , W_T , U_A , U_B and applied potential as for Figure 4.9).

When the initial polymer conductivity is high, then the wave accelerates as it progresses along the strip. With decreasing initial polymer conductivity, the wave velocity is significantly lower, the acceleration becomes less marked and the wave velocity becomes relatively constant. This effect is illustrated in Figure 4.14

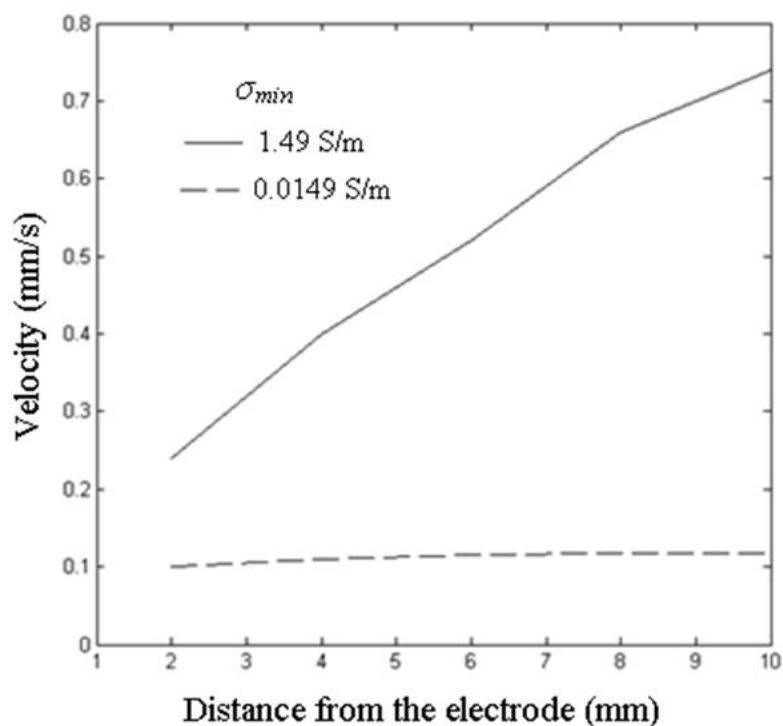


Figure 4.14. Variation of the velocity along the length of the polymer with different initial conductivities.

Change in the minimum polymer conductivity changed the shape of the oxidation wave profile and because of that the velocity of the progressing wave also changed. When the initial polymer conductivity is high, the wave accelerates as it progresses along the strip. With decreasing initial polymer conductivity, the wave velocity is significantly lower, the acceleration becomes less marked, and the wave velocity becomes relatively constant, as shown in Figure 4.16. The velocity of the oxidation wave was linearly influenced by the applied voltage. When we increased the applied voltage the oxidation process was faster and the wave velocity increased, but the velocity was inversely proportional to the ion capacity and thickness of the film. These effects are illustrated in Figure 4.17.

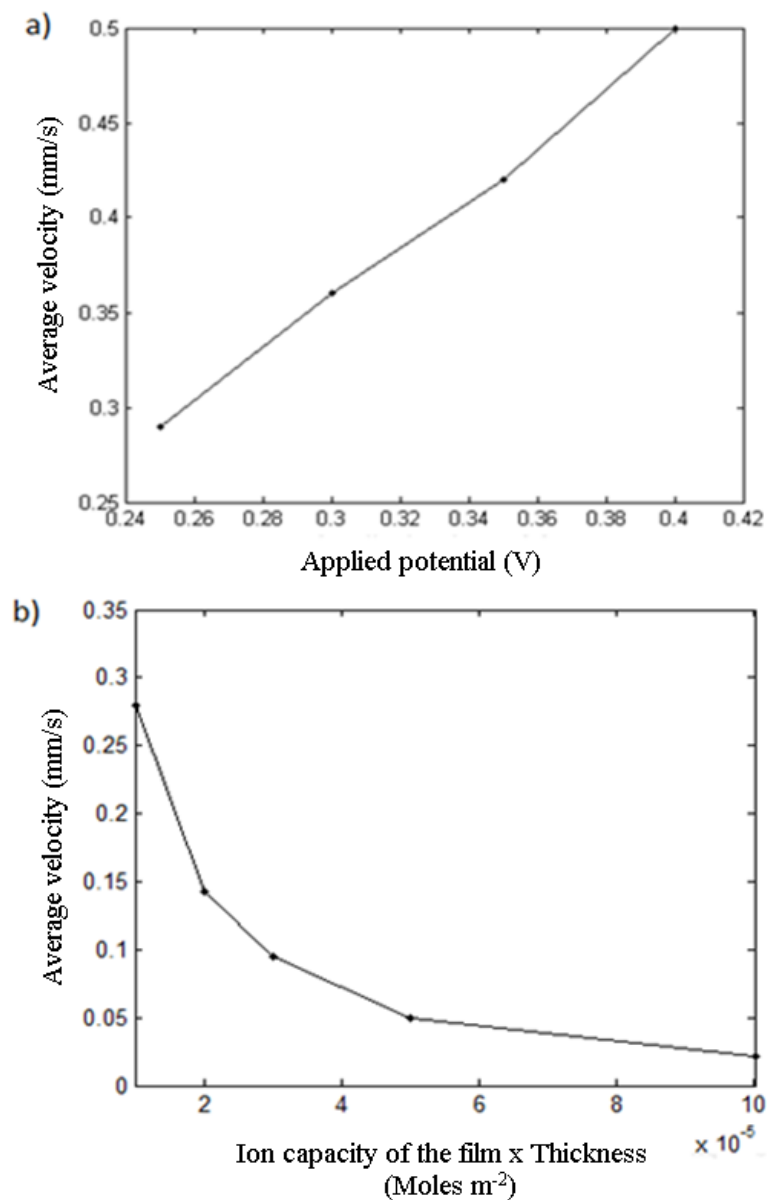


Figure 4.15 . Variation of wave velocity with (a) applied potential and (b) the product of ion capacity of the film time its thickness. Minimum polymer conductivity is 0.149S/m (Other conditions as in Figure 4.10).

4.4.2 Variation of Oxidation Wave Propagation with Cell Geometry

The effects of electromigration ensure that the wave propagation is dependent on the cell geometry, specifically, the thickness of the electrolyte layer between the working and counter electrodes and the length and position of the counter electrode within the cell. Figure 4.10 illustrates the effect of changing the cell thickness. When the distance between polymer and counter electrode is increased, the electric field in the solution is decreased so the rate of the oxidation is reduced and the wave propagates

more slowly. Figure 4.16 illustrates the effect of changing the counter electrode geometry. When the counter electrode was 50% of the length of the polymer (Figure 4.16a), the oxidation wave proceeded slowly until the oxidised zone came directly underneath the counter electrode. When the composition change reached directly underneath the counter electrode, the wave velocity increased very rapidly; full oxidation was achieved underneath the counter electrode. A reflected wave, completing the oxidation, then moved back towards the contact point on the polymer. If the counter electrode was made small (just 10% of the entire length of the polymer for the case illustrated in Figure 4.16b), the phenomenon of a reflected wave was more pronounced. The oxidation wave moved very slowly and with a pronounced gradient of composition until it reached the location of the counter electrode at the end of the strip. The wave then reversed and moved backwards slower than it proceeded forward. However, full oxidation of the film was not achieved. Instead, the reverse oxidation wave proceeded only half the way back along the strip before the whole oxidation process slowed down.

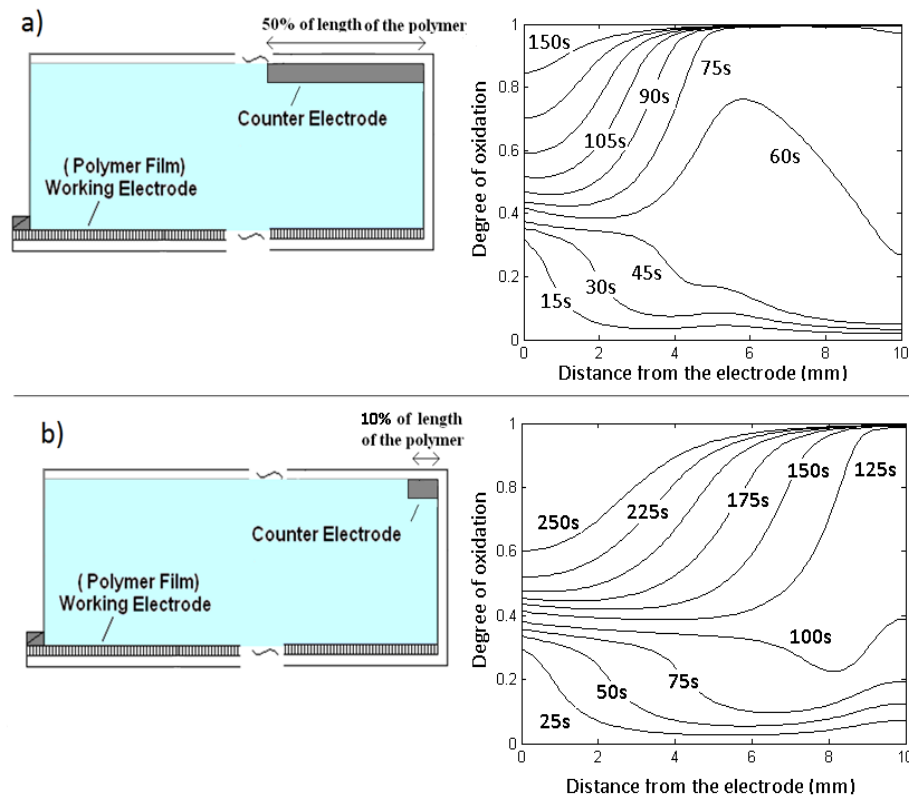


Figure 4.16. Variation of oxidation wave profile with size and position of counter electrode ($\sigma_{min} = 14 \text{ S m}^{-1}$, $h=1\text{mm}$, σ_{max} , ϵ_T , C_0 , W_T , U_A , U_B and applied potential as for Fig.4.10)

4.4.3 Model comparison with experimental data:

In this section we compare the oxidation wave profile obtained through simulations with the Tezuka et al experimental data¹⁵⁰. In their experimental setup, an electrochemically grown polypyrrole film (6mm x 1mm) was placed on an insulating glass plate with a stainless steel electrode clamped at the edge. It was then oxidised in an electrochemical cell (1cm x 1cm quartz cell) with a counter electrode (platinum plate) and a reference electrode (Saturated calomel electrode) as shown in figure 4.17a. The oxidation state of the polymer film was determined by measuring its absorbance over time.

Image removed for copyright reasons. The image can be accessed at

http://www.journalarchive.jst.go.jp/english/jnlabstract_en.php?cdjournal=bcsj1926&cdvol=64&noissue=7&startpage=2045

Figure 4.17. a) Experimental setup used in Tezuka et al experiment¹⁵⁰ b) Oxidation wave profile observed in the experiment by measuring the conducting polymer film absorbance along the distance of the film over time. Figures taken from their experimental paper¹⁵⁰

In order to make the comparison, the length of the polymer film in the model was modified to 5mm to fit the experimental setup. The simulations were performed and the oxidation wave propagation was plotted against the experimental data as shown in figure 4.18. The results show that the simulated wave propagation follows the experimental data, although the wave velocity was somewhat higher in the experiment than in the simulation. After the wave has passed half way through the polymer, the experimental wave propagation slower and the wave shape becomes flatter.

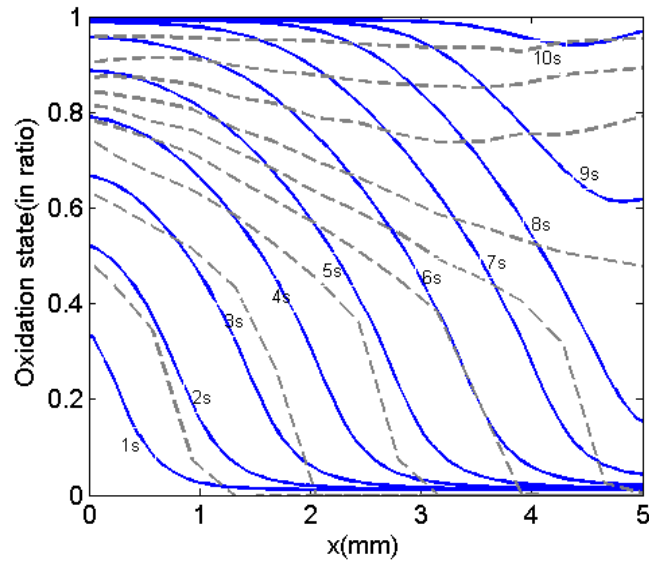


Figure 4.18. Simulated oxidation wave profile plotted against the experimental data. The grey dotted line showing the experimental data from Tezuka et al¹⁵⁰ and blue lines showing the simulated data for a similar length of polymer film. ($\sigma_{min} = 14.9 \text{ S m}^{-1}$, $C_0 = 0.01 \text{ mol liter}^{-1}$ applied potential $= -0.2 \text{ V}$, Ion capacity $= 0.8 \text{ mol liter}^{-1}$, $L = 5 \text{ mm}$, $h = 2 \text{ mm}$, σ_{max} , ε_T , W_T , Δy , U_A , and U_B as for Fig.4.10)

The discrepancies observed in the simulation data as compared to the experiment might be due to several factors listed below

1. The geometry of the system plays an important role in determining oxidation wave profile. Specifically, the position of the counter electrode and its size determine the current flow and the oxidation wave profile. The experimental study used a three electrode system with reference electrode defining the potential boundary and counter electrode defining the concentration boundary; our model, however, is based on a two electrode system as it is difficult to model concentration and potential boundaries separately. In the experimental setup, the counter electrode extends from the start (the electrical contact point) of the polymer film to a position a short distance down the film. As the simulations presented earlier show (section 4.4.3), the wave propagates slower, and oxidation goes only slowly to final completion, in the region of the polymer film that is not directly underneath the counter electrode.
2. The Nernst equation defining the potential difference between solution potential and polymer potential in the model assumes electrochemical equilibrium at the boundary. This assumption leads to faster kinetics as compared to the experiment.

3. The polymer in the model is assumed to have a uniform composition across its thickness which might not be true in the case of the experiment.

4.6 Conclusions

A propagating wave of deformation of an ECP can be launched along a polymer strip as a consequence of the electrochemical reaction. The shape of the wavefront and its velocity depend upon the relative conductivities of the electrolyte and of the polymer in its oxidised and reduced states. A key element determining the wave propagation is the proportion of the ionic flux in the solution near the interface that is carried by electromigration rather than diffusion, giving an interesting dependence on the cell geometry.

CHAPTER 5: COMPUTATIONAL DESIGN OF MIXERS AND PUMPS BASED ON ELECTROCHEMICALLY ACTIVE CONDUCTING POLYMER OXIDATION WAVE

5.1 Introduction

In chapter 4, we studied the propagation of expansion waves of an electrochemically active conducting polymer (ECP), deposited on one side of a channel. In this chapter, we study the fluid motion stimulated as a result of an expansion wave, moving along one or both sides of a channel. Chapter 4 simulation results showed that the expansion front could be approximated as a sigmoidal wave moving a constant velocity. Therefore, in this chapter, the sigmoidal form has been assumed and the pumping rate induced by motion has been explored for different amplitude and steepness of the wave front. We also explored different conceptual designs for pumps utilising these expansion waves.

5.2 Design of a Micro-Pump

Figure 5.1 illustrates some different conceptual configurations for a micro-pump utilising the oxidation wave property discussed in the previous sections. In each of these configurations, volume is not conserved in the channel, thus causing a fluid motion through the channel. We first analysed the simplest case, shown in Figure 5.1a, in which we assume a chloride electrolyte and the polymer is faced by a counter electrode such as Ag/AgCl which can act as an ion source/sink without change of dimension. Rather than use the exact wave shape derived from the previous analysis, we simplified the problem by approximating the wave front as a sigmoid function, which allowed us to explore the effect of the wave amplitude and wave front slope on the pumping rate. We used the finite element method to solve the Navier-Stokes Equation to predict the fluid velocity in the microchannel. The model was created using the Comsol multiphysics finite element solver. All the boundaries were considered as no slip boundaries except for the inlet and outlet. The inlet and outlet were set as open boundaries with zero stress. The boundaries that define the polymer swelling were made into a moving mesh boundary. Here we have set the polymer swelling to move with a defined velocity of $150\mu\text{m/s}$. This velocity is a reasonable expected average velocity for the front, given expected values for polymer and solution conductivity, as indicated in Figure 4.10.d. The polymer wave velocity for different parameter values is illustrated in Figure 4.15.

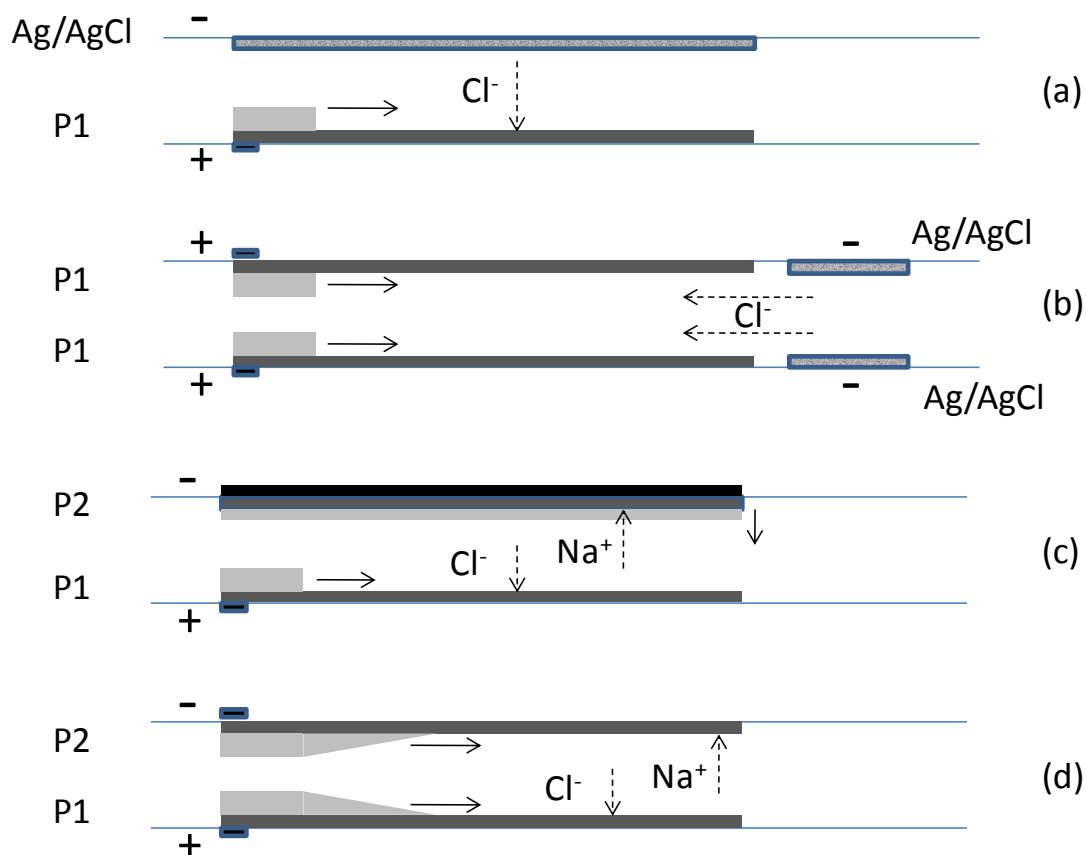
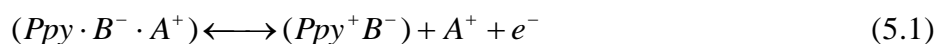


Figure 5.1. Possible configurations for a micropump based on the wave propagation phenomenon in ECP: (a) A nonpolymer counter-electrode without volume change supplies the ions for insertion into the polymer. Ag/AgCl is an example and NaCl as the electrolyte; (b) The same ECP (labelled P1) is on both faces of the channel and the counter-electrode is further along the channel. The performance is limited because of the appearance of a reflected wave, as shown in Figure 5.1. (c) Two different polymers facing one another constitute the electrodes; One (P1) swells on oxidation, by anion insertion and the other (P2) swells on reduction, by cation insertion. Since the conductivity decreases on reduction, P2 swells uniformly. In this configuration, the electrode contact for P2 extends the full length of the polymer; (d) This configuration differs from (c) only in that the contact to P2 is at one end of the polymer, opposite to that on P1. The current flow and wave propagation in this case is complex, as discussed in the text.

We fixed the channel width and height at 30 μ m, and calculated the pumping rate by integrating the total amount of material passing across the outlet and the inlet boundaries during the passage of the wave and then subtracting these and dividing by the wave passage time. The detailed results for the configuration illustrated in Figure 5.1 (a) are shown in Figure 5.2. The fluid velocity was maximum for a wave front-slope of 45°. The flow rate increased slightly more than linearly with the wave amplitude. If the wave amplitude (10 μ m) was 30% of the channel height, then the net

flow rate obtained with a front-slope of 45° , 30pL s^{-1} , was approximately 67% of the total volume displaced by the polymer expansion (45pL s^{-1}), falling to 14pL s^{-1} (62% of the volume displaced) for a wave amplitude ($5\mu\text{m}$) that was 17% of the chamber height. Practically achievable swelling for electrochemically- actuated ECPs are in the range 10-30% of the polymer thickness^{21,165}. A maximum practically obtainable polymer thickness for rapid actuation is likely to be $10\mu\text{m}$, implying practically achievable wave amplitudes in the range 1-3 μm .

From these findings, the achievable pumping rates for this configuration seemed rather small, so we considered some alternative concepts. An obvious extension is illustrated in Figure 5.1 (b), where the polymer is deposited on both faces of the channel and the counter electrode is established further along the channel. The pumping rate should be twice that for the single-sided configuration. However, as we showed in Figure 4.16, if polymer oxidation were to proceed to completion, a reflected wave would develop, reversing the flow. The maximum expansion of the polymer is thus limited and this configuration does not give an advantage. It is well-established that the expansion characteristics of ECP can be altered by choice of the anions used to dope the material during synthesis. Small anions are exchangeable so the oxidation process proceeds by anion exchange, giving swelling on oxidation, as we have assumed (Equation 4.1). However, if the polymer is prepared with a large anionic dopant (e.g., dodecylbenzenesulfonate (DBS)), the electrochemical cycling proceeds by cation exchange^{166,167}, in which case the film swells on reduction and shrinks on oxidation:



The possibility of using two differently doped polymers with one expanding on oxidation and one expanding on reduction leads to the possible configurations illustrated in Figures 5.1(c) and (d). The distinction between these is in the electrical connection. In Figure 5.1 (c), the polymer designed to swell on reduction is provided with an electrical connection that extends its whole length. Thus, as the oxidation wave proceeds on the bottom face, the top face would be uniformly swelling. The resultant progressive constriction of the channel would enhance somewhat the

pumping rate. A polymer that swells on reduction will also be decreasing in conductivity as it swells. Thus, with connection at the inlet side of the pump, such a material would swell uniformly on reduction and contract in a wave on oxidation. In a channel, facing a polymer that swells on oxidation, as illustrated in Figure 5.1(d), the behaviour is not expected to be so simple. As we showed in Figure 4.9, the current associated with the oxidation wave proceeding along the bottom face of the channel would be significantly larger at the leading edge of the wave.

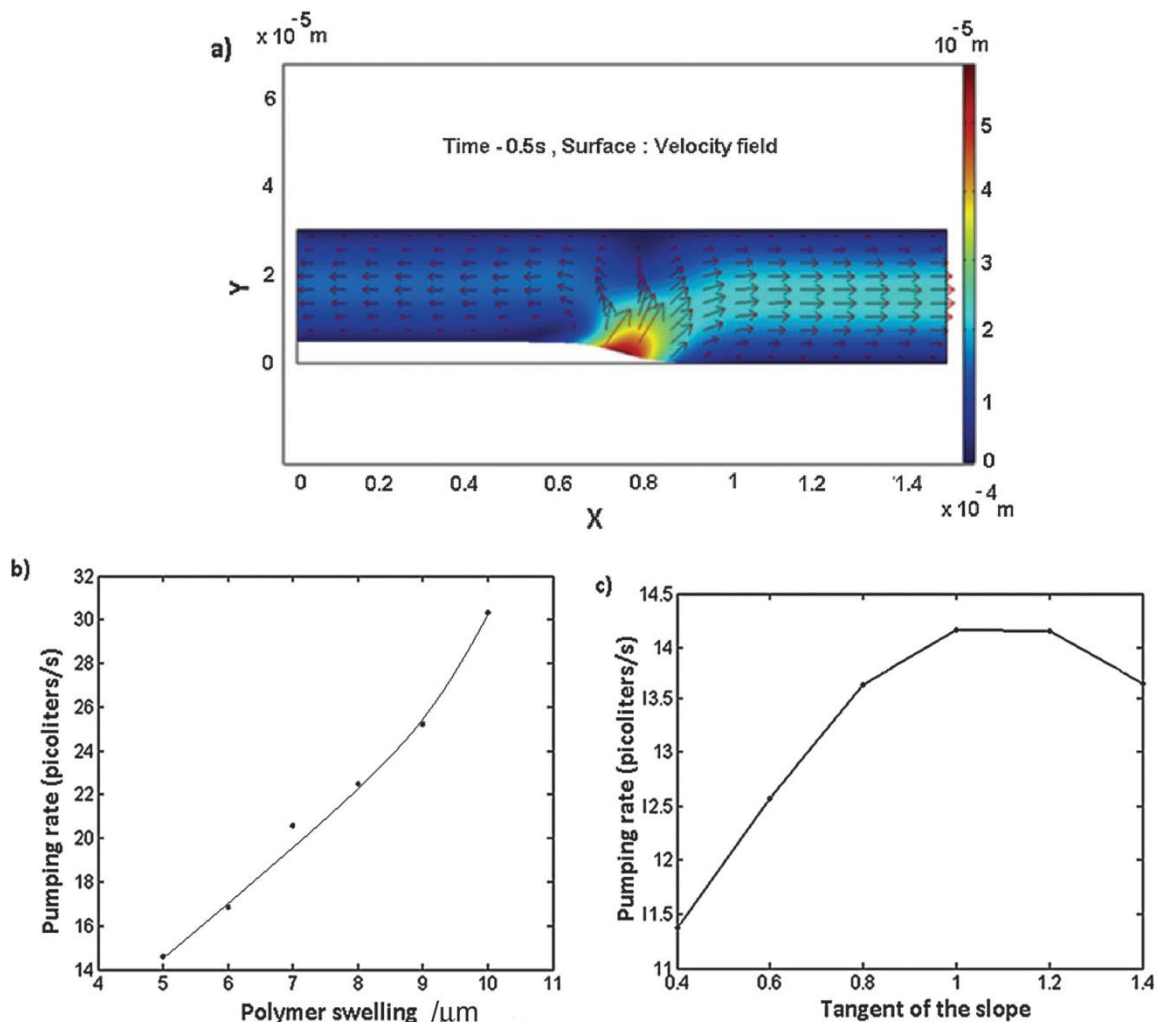


Figure 5.2. Simulation results showing (a) velocity field of the fluid, (b) the variation in flow rate with amount of polymer swelling with wave front-slope 45° , and (c) the variation in flow rate with tangent of the slope angle at the midpoint of the polymer wave front with polymer expansion of $10\mu\text{m}$.

In a configuration, such as the one illustrated in Figure 5.1(d), the polymer on the top surface of the channel, being reduced would be developing a significant electrical

resistance. The top electrode would not be an equipotential plane.

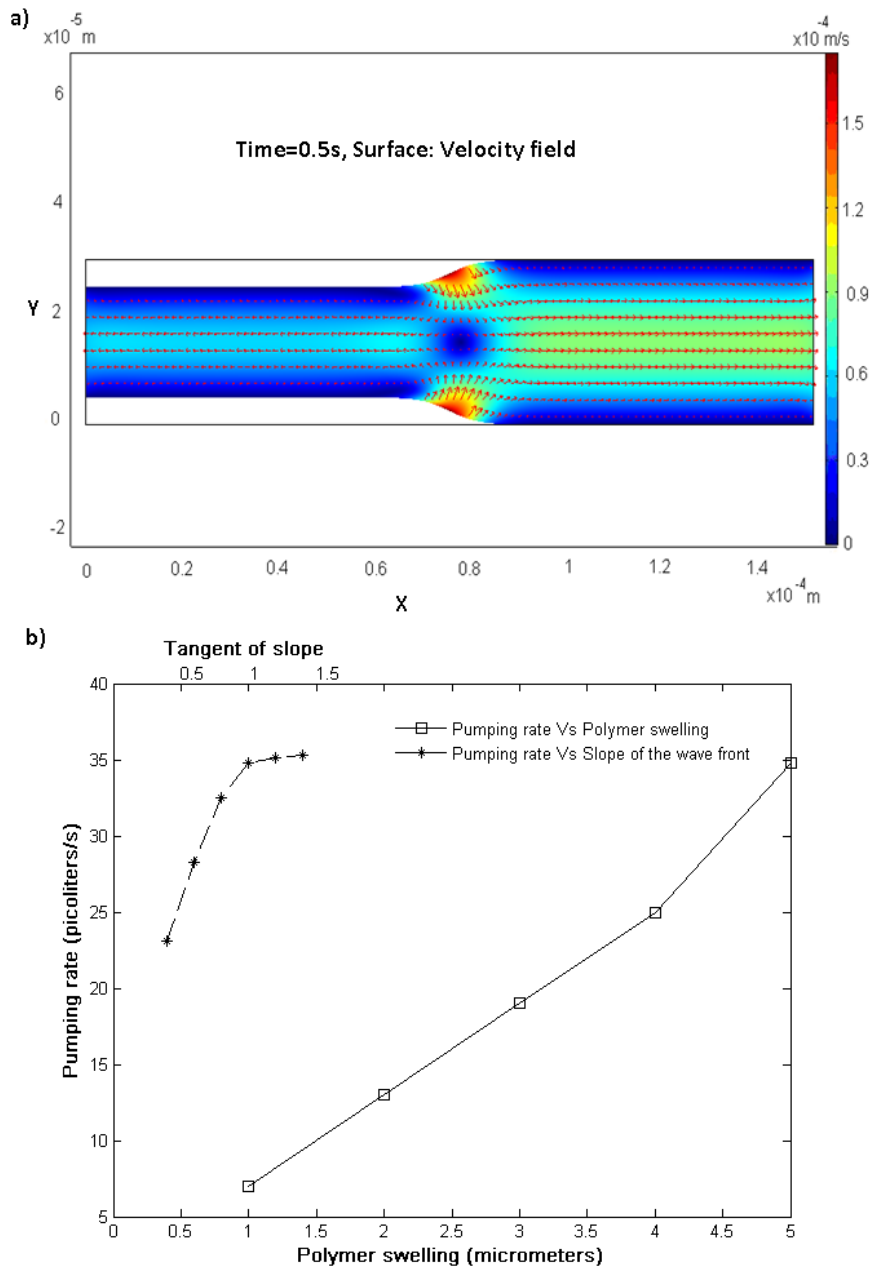


Figure.5.3. Simulation of micropump behavior with ECP swelling on both faces of the channel. The wave propagates the length of the channel in 1s. (a) Velocity field. (b) Dependence of pumping rate on expansion with front-slope 45° and on front-slope with expansion $5\mu\text{m}$.

Thus, the current distribution on the reducing polymer would not be uniform. The effect would be to induce a wave on the top surface of the channel, in step with that on the bottom surface. This is a complicated problem to model and we have not attempted it. Again, we would expect a somewhat increased pumping rate over that

obtainable with the simple configuration of Figure 5.1(a) at most approximately doubled for a given polymer expansion. In support of this assertion, we also present a flow simulation for the case of identical waves passing along both the top and bottom surface of the channel. With each polymer expanding just $5\mu\text{m}$, the flow was increased to 35pL s^{-1} , 77% of the displaced volume. The pump is not particularly efficient, but the predicted performance seems both useful and practically achievable in a very simple device. The simulated velocity field during the oxidation for this configuration is given in Figure 5.3(a). The results also showed that the pumping rate was linearly proportional to the slope of the wave and the amount of polymer swelling, as illustrated in Figure 5.3(b).

5.3. Design of a Micro-Mixer

In the configuration treated in the theoretical description of wave motion, the assumption was made that the counter electrode was a uniform source of ions to balance the ion flux into the active polymer. A suitable ion source would, of course, be a layer of the same type of ECP. If the electrical connections to both electrodes were on the same end of the channel, then with one sign of potential difference, a wave would propagate along one face whilst the opposite face contracted uniformly. If the sign of the potential difference were then to be inverted, a wave would propagate on the second face whilst the first contracted uniformly. Volume is conserved in this configuration so there will be negligible amount of fluid that will be transported out of the chamber. There will, however, be a circulating convective flux established in the chamber with a component of velocity perpendicular to the chamber walls that sweeps through the chamber with the wave. An expected effect is then an enhancement of diffusive mixing of fluids in the chamber

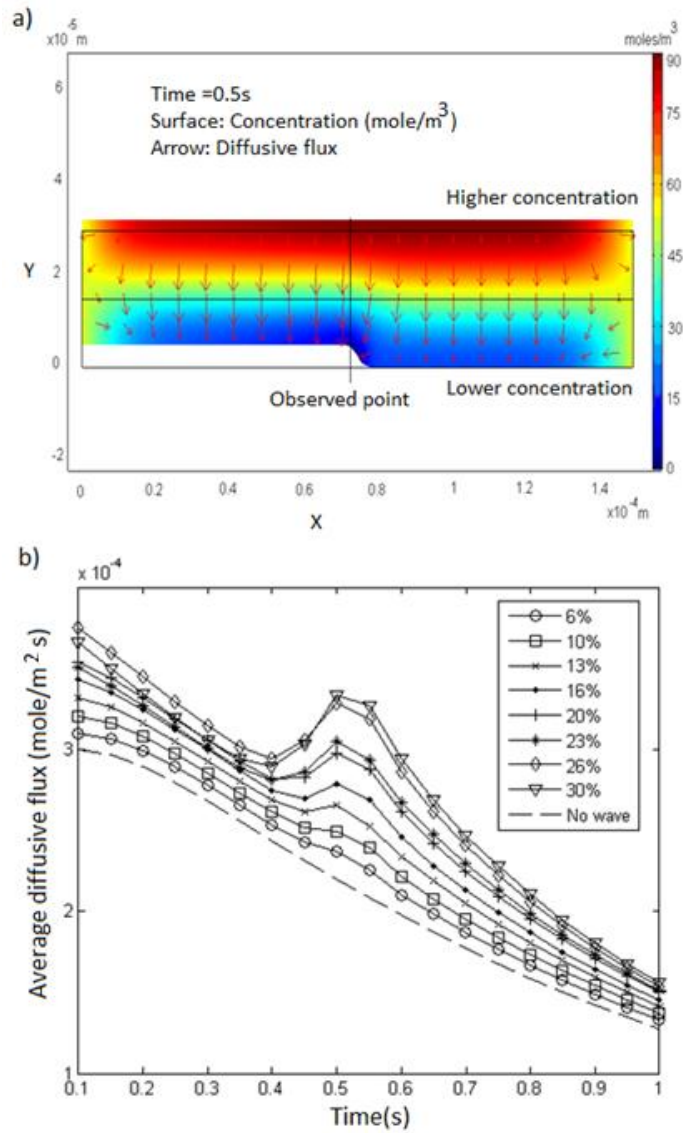


Figure.5.4. Mixing effect in a microchannel having the same type of ECP on both faces. (a) Concentration field and diffusive flux with a wave passing along the bottom face and the top face contracting uniformly. (b) Variation of the diffusive flux across the centre of the channel - the cross point in (a) - with the amount of swelling of the polymer (expressed as a percentage of channel thickness).

To explore this mixing effect, we modelled the mixing chamber as a microchannel filled with two different concentrations of liquids: 0.01 moles/litre in the upper half of the microchannel and 0.1 moles/ litre on the lower half of the microchannel. The mixing of the two different concentrations can be quantified using the diffusive flux at the mid-plane of the chamber, the initial position of the boundary between the two fluids. There are two effects acting to move material towards the centre of the channel as the wave passes. The first is the simple displacement of solution by the wave. The second is the effect of the wave-induced convective motion of the fluid.

The effect of transport of material towards the centre of the channel is to increase the concentration gradient and hence the diffusive flux. To quantify the effect, we calculated the diffusive flux across the midplane of the channel at a position halfway along the channel. As in section 5.2, a sigmoidal wave shape was used, and the wave passed through the channel in 1s. Figure 5.4 illustrates the results. A significant enhancement of diffusive flux could be obtained.

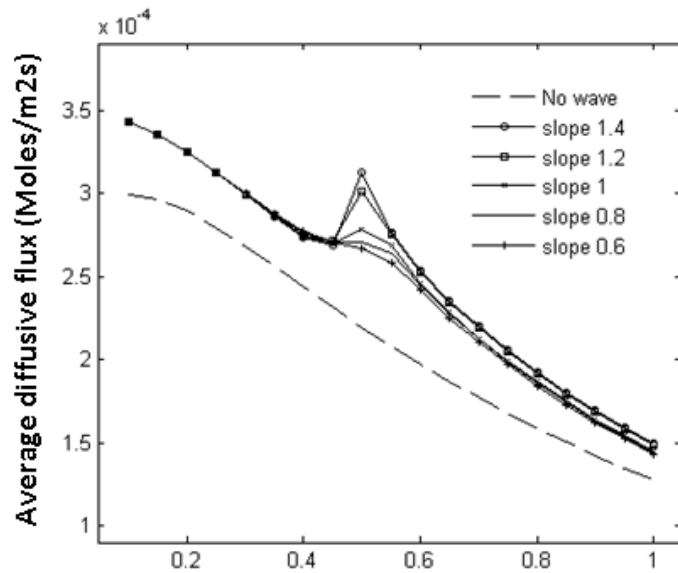


Figure 5.5. Variation of the diffusive flux with the slope of mechanical surface wave.

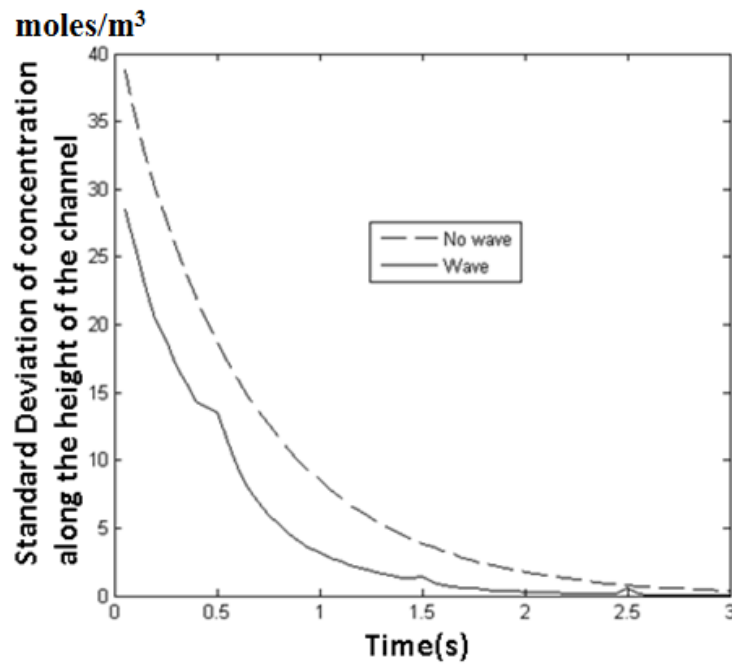


Figure 5.6. Variation of the concentration difference across the channel over multiple cycles of wave.

Figure 5.5 illustrates that higher the slope of the advancing oxidation wave, higher the diffusive flux and hence higher the mixing. Figure 5.6 shows the standard deviation of the concentration over multiple cycles of oxidation wave and that complete mixing could be achieved with just 3 cycles and is faster than the normal diffusive mixing. From the simulations, we can conclude that a micropump and a micromixer with useful performance can be designed that utilise the oxidation wave phenomenon of the ECPs.

CHAPTER 6: MODELLING ELECTROCHEMICALLY ACTIVE CONDUCTING POLYMER -HYDROGEL COMPOSITES

6.1 Introduction

Polyelectrolyte hydrogels are crosslinked polymeric materials known for their swelling properties. These hydrogels swell by osmotic intake of water until reaching equilibrium. The osmotic pressure is due to the Donnan potential created by the free charges in the hydrogel. When water is replaced by ionic salt solution, the swelling of the polyelectrolyte gel reduces as a result of the change in the Donnan equilibrium and repulsion of charges in the hydrogel network^{120,121}. This process is reversible; therefore, if one could remove the ions in the salt solution surrounding the hydrogel, the swelling could increase.

Electrochemically-active conducting polymer (ECP) undergoes a reversible redox reaction during which the charge of the polymer backbone undergoes change. This reaction can be brought about either chemically or electrochemically. During electrochemical actuation, when appropriate potential is applied to the ECP in an electrolyte, the polymer is oxidised or reduced by taking in or releasing electrons to an external circuit. Balancing this electron flux, there is a flux of negative ions into (or out of) the polymer. By this action, the ions can either be pumped into or absorbed from the electrolyte actively by controlling the potential applied to the polymer, thereby changing the ion concentration in the electrolyte surrounding the polymer. Thus, in theory, we can use polyelectrolyte gel as the electrolyte surrounding the ECP and thereby control its swelling by pumping in or out the ions upon electrically switching the redox state of the ECP. In the present chapter, the possibility of causing a significant swelling or contraction of a hydrogel as a consequence of the change in local salt concentration that should accompany the change of redox state of an ECP formed into a composite with the hydrogel is explored. An interpenetrating network of ECP and hydrogel is assumed such that the detailed structure of the composite can be ignored, and the composite can be treated as a uniform medium having properties of ionic and electronic conductivity that vary with position and time. The change in local ionic composition consequent upon the redox switch is calculated and compared with the change required to give a significant expansion or contraction based on the known response of hydrogels.

6.2 Mathematical Modelling

The electrochemical reaction at the ECP – electrolyte interface is assumed given by Equation (6.1).



The negative ions from the electrolyte move into the polymer to balance the positive charge created by the removal of electrons. The reverse reaction happens when an opposite potential is applied. Consider an ECP polyelectrolyte gel composite in which there is an interconnected network of both the polymers. The hydrogel acts as an electrolyte carrying the negative ions required for the reaction. In order to achieve the swelling and shrinking of the hydrogel, ions have to be removed or added by the reaction of the ECP. Two important properties that we have to consider, for this composite to act as an actuator, are the amount of swelling/shrinking that can be achieved and the rate at which it can be achieved.

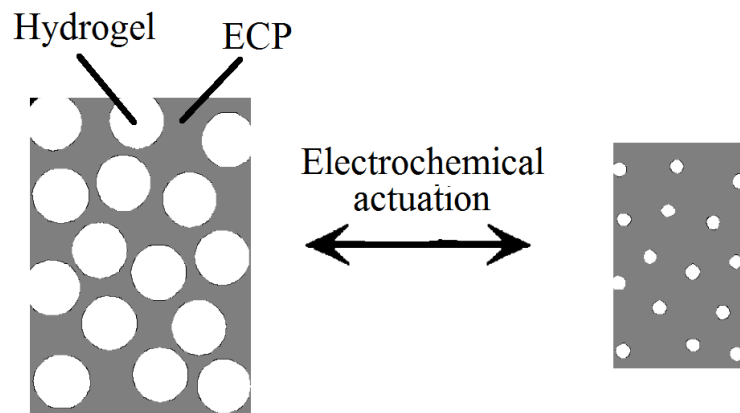


Figure 6.1. Proposed actuation mechanism for the ECP-hydrogel composite.

To understand the behaviour and determine the critical parameters, in this section, we have modelled the polyelectrolyte gel – ECP composite in order to assess its electrochemical behaviour. First we have created a 1-D mathematical model to quantify the concentration changes and the rate at which the change can be achieved with composites having different properties.

The rate at which the ECP will absorb or expel salt will depend on how fast the polymer reaction takes place in the composite. The polymer reaction rate is the rate at which the oxidation of the polymer takes place, represented by Equation 6.2, where M is the ion capacity of the polymer. ζ represents the volume fraction of the hydrogel in the composite.

$$R = (M)(1 - \zeta) \frac{\partial \varepsilon}{\partial t} \quad (6.2)$$

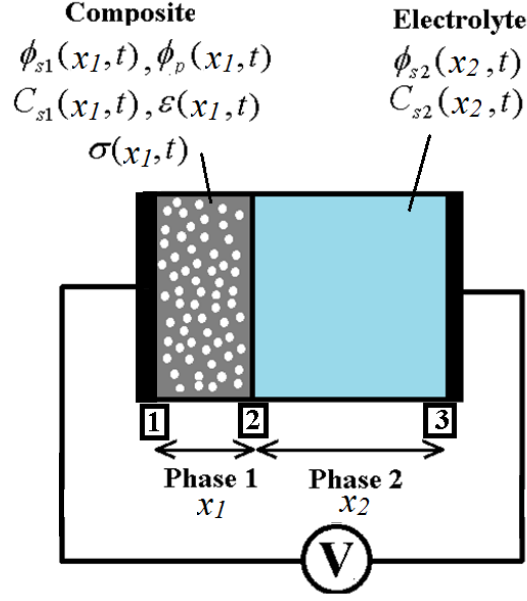
The concentration change in the ECP–hydrogel composite will not only depend on the reaction rate of the ECP but will also depend on the diffusion and migration of the salt in the hydrogel resulting from the concentration gradient and the applied potential gradient. The potential gradient will also change as a result of the concentration change in the hydrogel and the salt solution surrounding the composite. Because of the ECP reaction, there will be a change in its oxidation state and its conductivity, which in turn will affect the potential gradient and concentration. In order to understand this complicated system we have created a 1-D model with two phases: phase 1 with ECP- hydrogel composite and phase 2 with the salt solution. The parameters that have to be considered in phase 1 will be the salt concentration in the hydrogel (C_{s1}), the oxidation state of the ECP (ε), potential in the hydrogel (ϕ_{s1}), and potential in the ECP (ϕ_p). The parameters in the salt solution will be concentration of the solution (C_{s2}) and solution potential (ϕ_{s2}).

The concentration of ions in hydrogel is determined by three factors. The first is the diffusion of the ions due to the concentration gradients in the hydrogel. The second is by the electro-migration of the ions due to the potential gradient due to applied potential. The third is by the uptake of ions by the polymer due to the polymer reaction. Thus, the concentration change in the hydrogel is given by diffusion-electromigration-reaction Equation (6.3)

$$\frac{\partial C_{s1}(x,t)}{\partial t} = U_{B1} \frac{\partial}{\partial x} \cdot \left(\frac{RT}{F} \frac{\partial C_{s1}(x,t)}{\partial x} + C_{s1}(x,t) \frac{\partial \phi_s(x,t)}{\partial x} \right) - M(1 - \zeta) \frac{\partial \varepsilon(x,t)}{\partial t} \quad (6.3)$$

U_{B1} is the mobility constant of the ions in the hydrogel.

Parameters



Boundary conditions

$$\begin{aligned} \text{[1]} \quad & \phi_p = V_0, \phi_{s1} = \phi_p - \Delta\phi + \frac{RT}{F} \ln\left(\frac{C_{s1}(1-\varepsilon)}{\zeta \varepsilon}\right), \frac{\partial C_{s1}}{\partial x} = 0 \\ \text{[2]} \quad & \phi_{s1} = \phi_{s2}, \frac{\partial \phi_p}{\partial x} = 0, \frac{\partial C_{s1}}{\partial x} = \frac{\partial C_{s2}}{\partial x} \\ \text{[3]} \quad & \phi_{s2} = 0, \frac{\partial C_{s2}}{\partial x} = \frac{j_p}{F} \end{aligned}$$

Figure 6.2. Parameters and boundary conditions of the mathematical model.

Because hydrogel does not occupy the total volume of the composite, the apparent concentration of the hydrogel in phase 1 will be the product of the total concentration of the hydrogel in phase1 and the actual volume fraction of the hydrogel (in phase1)

$$C_1(y,t) = C_{s1}(y,t) \zeta \quad (6.4)$$

Thus, we can find the concentration in the actual volume fraction of the hydrogel using Equations 6.3 and 6.4

$$\frac{\partial C_1(x,t)}{\partial t} = U_{B1} \frac{\partial}{\partial x} \cdot \left(\frac{RT}{F} \frac{\partial C_1(x,t)}{\partial x} + C_1(x,t) \frac{\partial \phi_s(x,t)}{\partial x} \right) - M \zeta (1-\zeta) \frac{\partial \varepsilon(x,t)}{\partial t} \quad (6.5)$$

In the composite phase 1, there will be a potential difference at the interface of the ECP and the hydrogel which can be represented by the Nernst Equation:

$$\phi_p(x,t) - \phi_{s1}(x,t) = \Delta\phi - \frac{RT}{F} \ln \left(\frac{C_1(x,t) \cdot (1 - \varepsilon(x,t))}{\zeta \varepsilon(x,t)} \right) \quad (6.6)$$

The conductivity (σ) of the composite (phase 1) is a function of oxidation state of the ECP. During the reaction, the conductivity of the ECP will switch from its lower value (σ_{\min}) to its higher value (σ_{\max}) when the polymer changes from its reduced state to oxidised state. It also depends on how much of polymer volume fraction it contains.

$$\sigma_p(x,t) = \frac{f(\varepsilon(x,t))}{(1 - \zeta)} \quad (6.7)$$

As in chapter 4, we used the empirical sigmoidal function model relating the conductivity σ_p of the polymer to its fraction oxidation state (as proposed by Warren and Madden¹⁵²) to capture the conductivity switch in the model.

$$\sigma_p(x,t) = \left(\frac{\sigma_{\max} - \sigma_{\min}}{1 + e^{(\varepsilon - \varepsilon_T)/W_T}} + \sigma_{\min} \right) / (1 - \zeta) \quad (6.8)$$

Where ε_T is the oxidation state at which the transition occurs and W_T is the transition width.

The rate at which the polymer is oxidised depends on the gradient of the current flow (j_p) across the interface and along the polymer in the x direction. The oxidation rate also depends on the volume fraction (ζ) of the ECP present in the composite and its ion capacity (M).

$$(FM)(1 - \zeta) \frac{\partial \varepsilon(x,t)}{\partial t} = - \frac{\partial j_p}{\partial x} \quad (6.9)$$

The current flow along the ECP depends on the potential gradient across the ECP in the composite due to the applied potential. It also depends on the conductivity of the ECP.

$$j_p = -\sigma_p(x,t) \frac{\partial \phi_p(x,t)}{\partial x} \quad (6.10)$$

From Equations (6.9) and (6.10)

$$(F \cdot M)(1-\zeta) \frac{\partial \mathcal{E}(x,t)}{\partial t} = \frac{\partial}{\partial x} \left(\sigma_p(x,t) \cdot \frac{\partial \phi_p(x,t)}{\partial x} \right) \quad (6.11)$$

In the composite phase 1, there is no net accumulation of charge; hence, the divergence of the total current, which is the sum of the electronic current in the polymer and the ionic current in the hydrogel, is zero. The current flow in the hydrogel (j_{is}) of phase 1 can be calculated from the difference between the ion fluxes of positive and negative ions.

$$j_{is} = (j_i^+ - j_i^-)F$$

$$j_i^+ = -U_{B1}^+ \left(\frac{RT}{F} \frac{\partial C_{s1}^+}{\partial x} + C_{s1}^+ \frac{\partial \phi_s(x,t)}{\partial x} \right)$$

$$j_i^- = -U_{B1}^- \left(\frac{RT}{F} \frac{\partial C_{s1}^-}{\partial x} - C_{s1}^- \frac{\partial \phi_s(x,t)}{\partial x} \right)$$

We assume charge neutrality in the individual phases of the composite and hence $C^+ = C^- = C_{s1}$

The ionic current density is therefore:

$$j_{is} = F \left(\frac{RT}{F} \frac{\partial C_{s1}}{\partial x} (U_{B1}^- - U_{B1}^+) - C_{s1} \frac{\partial \phi_s(x,t)}{\partial x} (U_{B1}^+ + U_{B1}^-) \right)$$

Current in the polymer of phase 1 is given by Equation (6.9). Then the total current is the sum of polymer current and the hydrogel current.

$$j = j_{is} + j_p$$

$$j = F \frac{RT}{F} \frac{\partial C_{s1}}{\partial x} (U_{B1}^- - U_{B1}^+) - FC_{s1} \frac{\partial \phi_s(x,t)}{\partial x} (U_{B1}^+ + U_{B1}^-) - \sigma(x,t) \frac{\partial \phi_p(x,t)}{\partial x} \quad (6.12)$$

The gradient of this total current is zero:

$$\frac{\partial j}{\partial x} = \frac{\partial}{\partial x} \left(F \frac{RT}{F} \frac{\partial C_{s1}}{\partial x} (U_{B1}^- - U_{B1}^+) - FC_{s1} \frac{\partial \phi_s(x,t)}{\partial x} (U_{B1}^+ + U_{B1}^-) - \sigma(x,t) \frac{\partial \phi_p(x,t)}{\partial x} \right) \quad (6.13)$$

$$\frac{\partial j}{\partial x} = \frac{\partial}{\partial x} \left(\frac{1}{\zeta} \frac{RT}{F} \frac{\partial C_1}{\partial x} F (U_{B1}^- - U_{B1}^+) - C_1 \frac{1}{\zeta} \frac{\partial \phi_s(x,t)}{\partial x} F (U_{B1}^+ + U_{B1}^-) - \sigma(x,t) \frac{\partial \phi_p(x,t)}{\partial x} \right) = 0 \quad (6.14)$$

The electrolyte concentration depends on only on diffusion and electro migration of the ions. Also, the mobility constant of the ions in the electrolyte will be different than in the hydrogel phase. The mobility constant of the electrolyte (phase 2) is represented by U_{B2} .

$$\frac{\partial C_{s2}}{\partial t} = U_{B2} \frac{\partial}{\partial x} \cdot \left(\frac{RT}{F} \frac{\partial C_{s2}}{\partial x} + C_{s2} \frac{\partial \phi_{s2}}{\partial x} \right) \quad (6.15)$$

The potential in the solution can be determined from the total current in phase 2, which has zero gradient because there is no charge accumulation.

$$\frac{\partial}{\partial x} \left(-C_1 \frac{\partial \phi_s}{\partial x} (U_{B1}^+ + U_{B1}^-) + \frac{RT}{F} \frac{\partial C_1}{\partial x} (U_{B1}^- - U_{B1}^+) \right) = 0 \quad (6.16)$$

These equations define the hydrogel- ECP composite properties during the electrochemical simulation.

6.3 Numerical Modeling

The nonlinear time dependent partial differential equations in one dimensional space were solved using Comsol multiphysics solver. The equations were normalized using the following parameters. To simplify the equations, the mobility constant for both the positive ion ($U_{AI} = U_{BI}$) and the negative ions are assumed to be the same.

$$\begin{aligned} C_0 &= 1000 \text{ moles m}^{-3}, \text{ (Bulk concentration)} \\ Y_0 &= 5 \times 10^{-4} \text{ m (Thickness of the composite)} \\ U_{BI} &= 4 \times 10^{-9} \text{ (m}^2 \text{ V s}^{-1}, \text{ ionic mobility in the hydrogel)} \end{aligned}$$

$$t_0 = \frac{Y_0^2}{U_{BI}(RT/F)} = 2500 \text{ s}$$

R is the gas constant

T is the temperature in Kelvins

F is Faraday's constant

$$\phi_0 = \frac{RT}{F} = 0.025 \text{ V}$$

$$S_0 = U_{BI} C_0 F = 0.385 \text{ (S/m)}$$

6.4 Results and Discussion

When an appropriate potential is applied, the ECP in the composite starts oxidizing. The oxidation starts from the electrode and proceeds out towards the solution. This reaction is due to the switching of the ECP from its lower conductivity state to its higher conductivity state during oxidation. This phenomenon is similar to the oxidation wave discussed previously in chapter 4. The oxidation wave front is more prominent when the minimum conductivity of the ECP is low. When the minimum conductivity of the polymer is increased, the oxidation wave becomes less prominent and the oxidation takes place uniformly throughout the polymer. A similar effect is observed when the salt concentration of the hydrogel and, hence, its conductivity is decreased. When the polymer starts oxidizing, there is a flow of ions from the hydrogel into the polymer, thereby reducing the salt concentration in the hydrogel. This continues until the entire ECP is oxidised. Once the oxidation reaction is finished, the salt from the surrounding electrolyte starts to diffuse back in the hydrogel as a consequence of the concentration gradient developed by the reaction. Thus, the concentration of the hydrogel relaxes back to its mean concentration. To keep the system balanced, we assume that there is a flux of ions into the electrolyte from the counter electrode at the same rate at which the ions are consumed by the ECP. When the minimum conductivity of the ECP is increased, there is an increase in the change in the concentration of the hydrogel. This reaction is also evident from the increased current density across the interface. These effects are shown in Figure 6.3

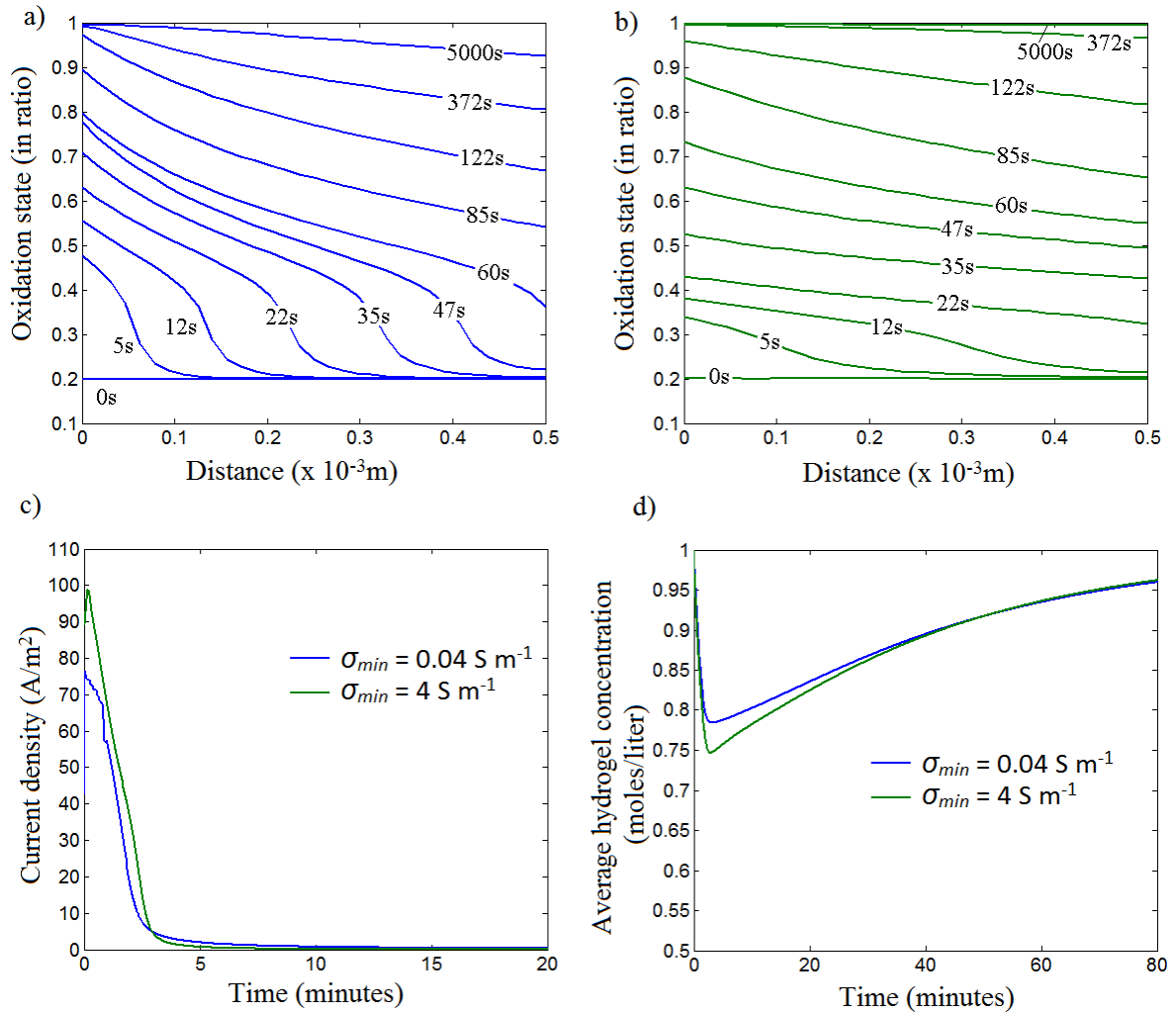


Figure 6.3. Effect of altering the minimum polymer conductivity, (a) ($\sigma_{min} = 0.04 S m^{-1}$) and (b) ($\sigma_{min} = 4 S m^{-1}$) on oxidation wave propagation, (c) on current density across the ECP-hydrogel interface, and (d) on average hydrogel concentration. Other conditions: Hydrogel thickness, $X_1 = 0.5mm$, Electrolyte thickness $X_2 = 1.6 mm$, Volume fraction (ζ) = 0.5, Ion capacity of polymer (M) = 1 mol liter⁻¹ Maximum polymer conductivity, $\sigma_{max} = 40 S m^{-1}$, $\epsilon_T = 0.5$, $W_T = 0.05$, $C_0 = 1 mol liter^{-1}$, Hydrogel mobility $U_{A1} = U_{B1} = 4 \times 10^{-9} m^2 s^{-1} V^{-1}$, Electrolyte mobility = $U_{A2} = U_{B2} = 4 \times 10^{-8} m^2 s^{-1} V^{-1}$, Applied potential $V = 0.125V$.

To see the effect of changes in the overall conductivity of the composite on electrochemical reaction, we simulated cases where there was no switching of the conductivity from the lower conductivity to higher conductivity in the ECP. This case can be achieved practically by mixing conductive fillers in the composite. In this case, the oxidation takes place uniformly throughout the composite. When the conductivity of the composite is very low, the rate of reaction slows down; thus, reaction takes place for a longer time. As a consequence, the change in the ion concentration of the hydrogel is much smaller. However, the alteration of the concentration is maintained for a longer

time period both as a result of the longer reaction time and because of the slower ion flux from the electrolyte caused by the small concentration gradient. Increase in the composite conductivity increases the reaction rate and also increases the changes in the concentration. The effect is diminished once the composite becomes fairly conductive. These effects are illustrated in Figure 6.4

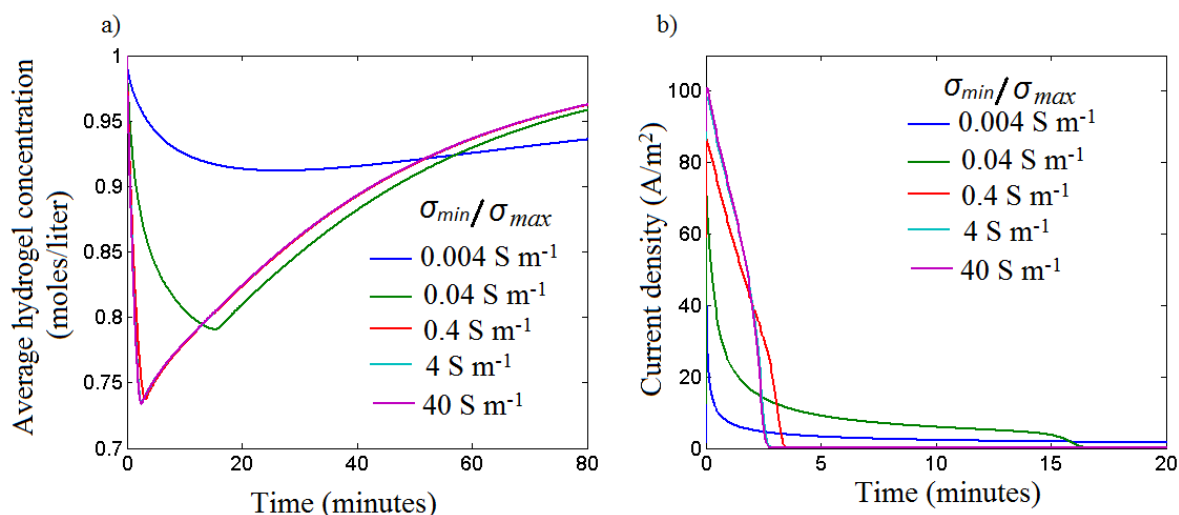


Figure 6.4. Effect of changes in the conductivity of the composite on (a) Average hydrogel concentration and (b) Current density across the ECP-hydrogel interface. Here the composite is assumed to be uniformly conductive throughout the reaction. Other conditions are in Figure 6.3.

The amount of ions absorbed by the ECP mainly depends on the ion capacity of the polymer. Practically, the ion capacity of the composite can be increased either by increasing the ECP content in the hydrogel or by changing the type of the ECP. Different ECPs have different ion capacity ranges. In the simulations, when the ion capacity of the polymer is increased, the change in the concentration of the hydrogel increases. The reaction time and hence the current density across the interface also increases as a result of the increase in the ion capacity. These effects are shown in Figure 6.5. These effects are similar to the experimental observations made by Lin et al¹³⁷ and Moschou et al¹³⁹ where they found an increase in the bending actuation of the ECP-hydrogel composite when the ECP content in the composite was increased. They suggested that change in the bending is due to the increase in the reaction of the ECP and the consequent increased change in the ion concentration of the hydrogel. In their experiments, the composites were placed between two electrodes in an electrolyte solution and were subjected to an electric field.

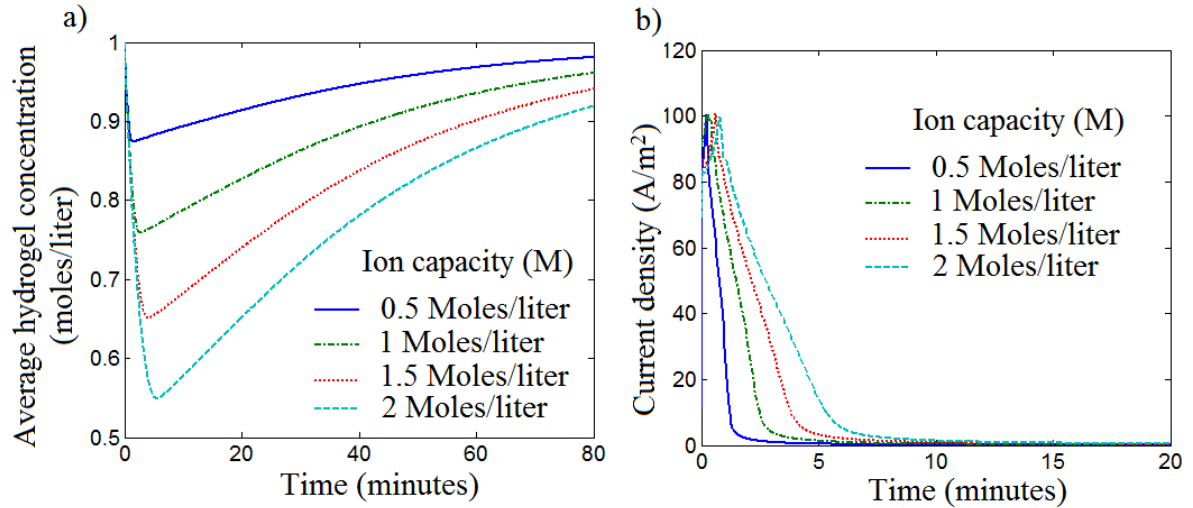


Figure 6.5. Changes in the average hydrogel concentration (a) and current density at the ECP –hydrogel interface and (b) for different ion capacities of the ECP. $\sigma_{min} = 0.04 \text{ S m}^{-1}$, Other parameters are in Figure 6.3

We also looked at the effect of changing the mobility constant of the hydrogel on the electrochemical reaction. Increasing the mobility constant of the hydrogel increased the current density across the hydrogel –ECP interface, thus indicating that more ions are being absorbed by the ECP. Yet increasing the mobility constant also increases the flow of ions into the hydrogel from the surrounding electrolyte. This effect thus reduces the changes in the concentration of the hydrogel. On the other hand, decreasing the mobility constant of the hydrogel decreases the reaction rate, which also reduces the changes in the concentration. Therefore, there is an optimum range of the mobility constant for which the changes in the concentration of the hydrogel will be maximum for a given set of parameters. These effects are shown in Figure 6.6.

A similar effect was observed to result from changes in the volume fraction of the hydrogel in the composite. When the volume fraction of the hydrogel was decreased, the reaction rate increased as a result of the subsequent increase in the volume fraction of the ECP. But increase in the volume fraction of the hydrogel also means there is an increase in the flow of ions from the surrounding electrolyte, and thus a reduction in the changes in ion concentration of the hydrogel. When the volume fraction of the hydrogel is increased, the reaction rate goes down because of the decrease of volume fraction of ECP available for the reaction. Thus the optimum volume fraction of the hydrogel for the

maximum changes in the concentration is around 0.5. These effects are illustrated in Figure 6.7

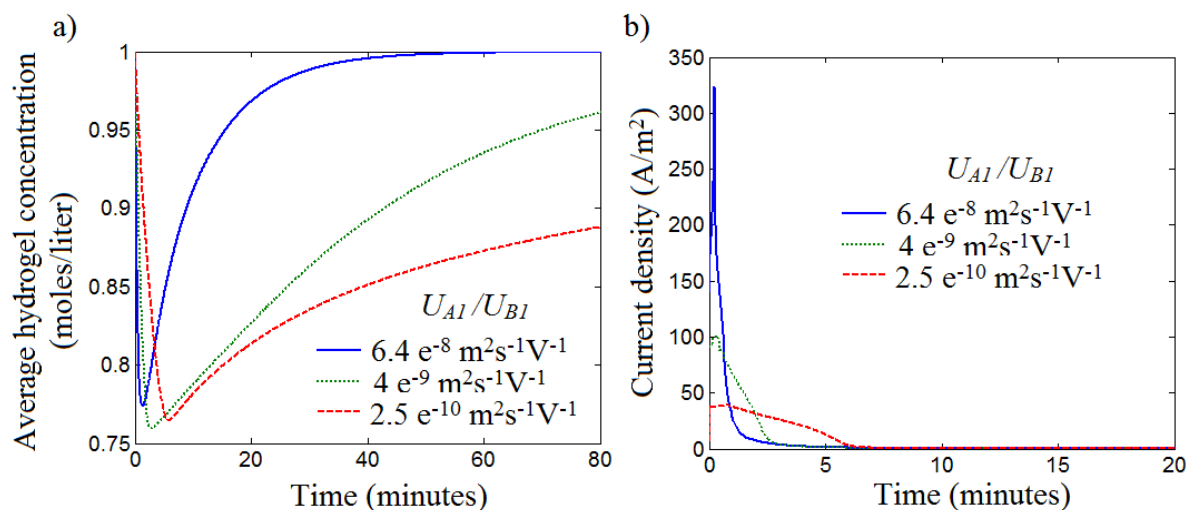


Figure 6.6. Effect of different hydrogel mobility constants on (a) Average hydrogel concentration and (b) Current density at the ECP-hydrogel interface. $\sigma_{min} = 0.04 \text{ S m}^{-1}$, Other parameters are in Figure 6.3

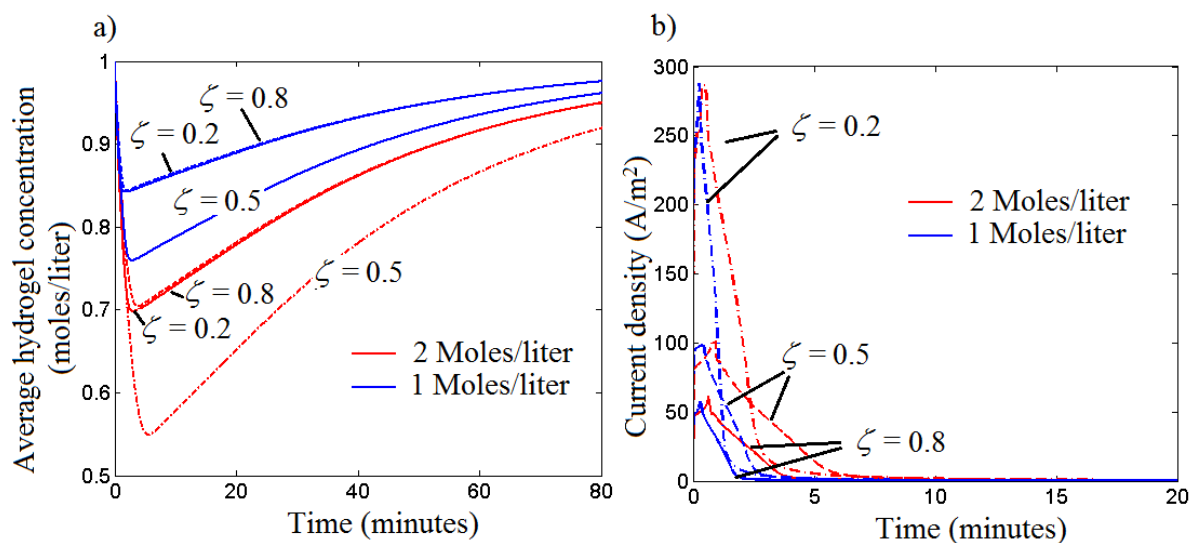


Figure 6.7. Effect of changes in the volume fraction of the hydrogel on (a) Average hydrogel concentration and (b) Current density at the ECP-hydrogel interface. The effects are illustrated for two different ECP ion capacities (Red lines-2 moles/liter Blue lines – 1 moles/liter) $\sigma_{min} = 0.04 \text{ S m}^{-1}$. Other parameters are in Figure 6.3

When the applied voltage is increased there is an increase in the current density across the ECP- hydrogel interface. This effect is due to the increase in the potential gradient across the composite which in turn increases the reaction rate. The changes in the concentration of the hydrogel also increase with the increase in the applied voltage. But this effect

diminishes over the voltage range, as after a certain point, the reaction rate is limited by the ion capacity of the polymer. These effects are illustrated in Figure 6.8

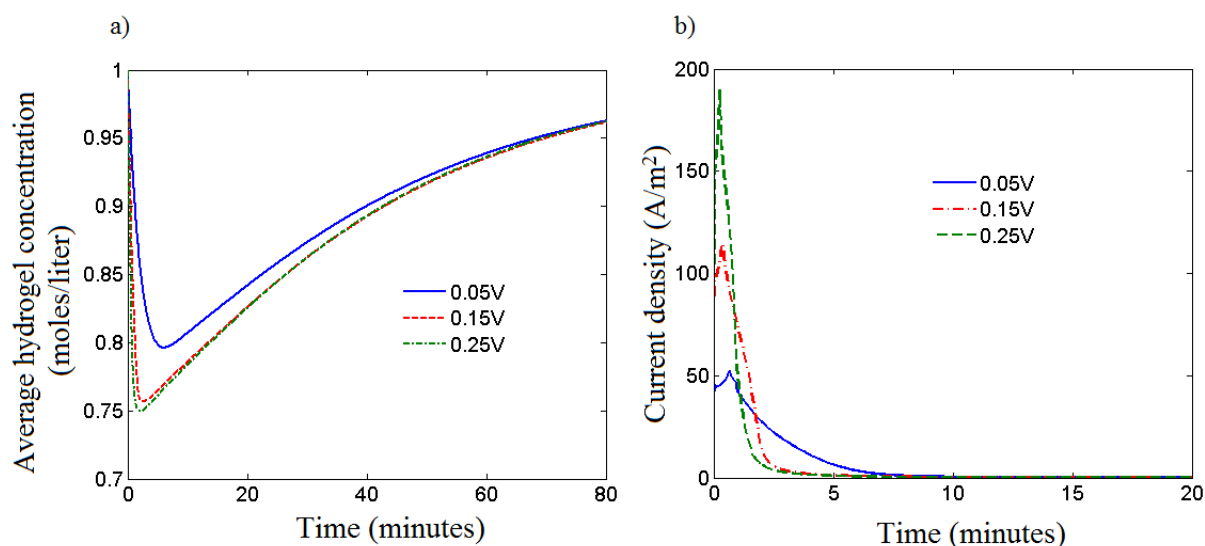


Figure 6.8. Effect of changes in the applied voltage on (a) Average hydrogel concentration and (b) Current density at the ECP-hydrogel interface, $\sigma_{min} = 0.04 \text{ S m}^{-1}$, Other parameters are in Figure 6.3.

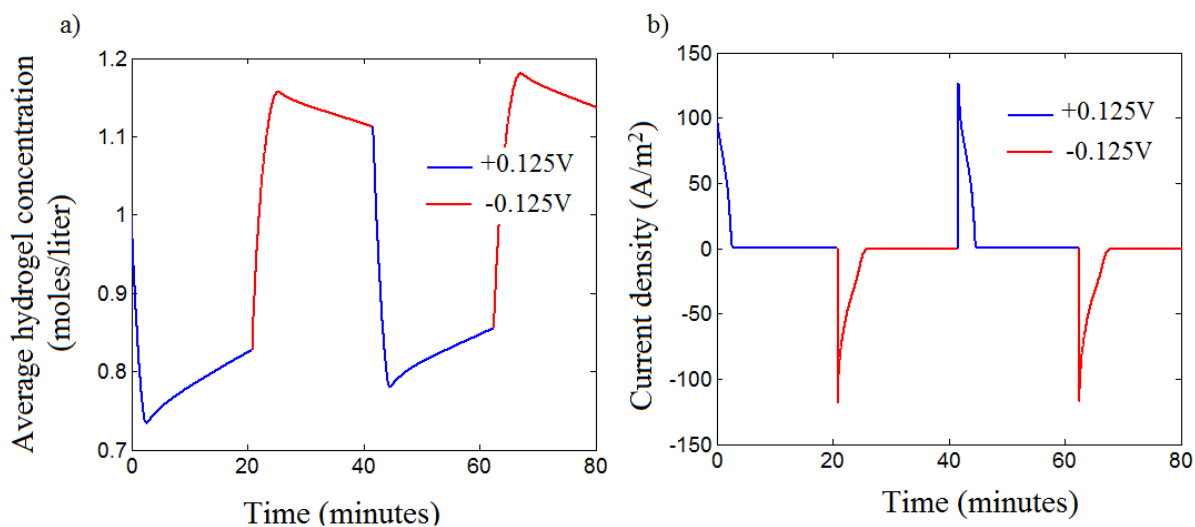


Figure 6.9. Effects of switching between positive and negative potentials on (a) Average hydrogel concentration and (b) Current density at the interface, $\sigma_{min} = 0.04 \text{ S m}^{-1}$, Other parameters are in Figure 6.3.

When the polarity of the potential is reversed, the reduction reaction takes place. In this case the ions are released from the ECP because of the reversal of the polymer to its neutral state. As a consequence there is an increase in the concentration of the hydrogel. The simulated effect of switching between oxidised and reduced state is illustrated in Figure 6.9.

Previous studies have shown that different hydrogels have different swelling properties in ionic solutions. The swelling properties also vary depending on the cross linking density of the hydrogels. Thus, by choosing the type of hydrogel and controlling its cross linking density, we can effectively vary the swelling range of the hydrogel. Travas-Sejdic et al¹²⁰ prepared co-polymers of acrylamide and 2 acrylamido-2methyl-1propane sulphonic acid (poly (AAm/AMPS)) and studied its swelling behavior upon changing the salt concentration of the surrounding electrolyte. They found that when the concentration of the NaCl in the electrolyte was reduced from 1 M to 0.1 M, in some cases, depending on the molar fraction of the charges and the cross linking density, the hydrogel swelled more than 100%. Baker et al¹⁶⁸ synthesized acrylamide based polyampholyte hydrogels and have studied the swelling properties. They found that by decreasing the concentration of the surrounding electrolyte from 1 M to 10^{-5} M the swelling increased by around 100 %. Aalie et al¹⁶⁹ prepared hydrogels based on polyacrylamide and poly(vinyl alcohol). In their experiments, when the salt concentration was reduced from 0.5 M to 0 M the swelling increased by around 30%. In all cases, swelling and deswelling of the hydrogel was not linear with the concentration changes. There was a sudden increase in the swelling of the hydrogel for small changes in the concentration. These findings suggest that small concentration changes can act as a switch, making the hydrogel swell and shrink. The simulation results show that a change in the concentration range of around 0.5 M can be achieved with a polymer of 2 M ion capacity. This change in the concentration range should be sufficient to cause a significant swelling of the hydrogel.

6.5 Conclusions

From the simulations, we can conclude that the changes in the concentration of the hydrogel can be effectively controlled by varying various parameters. The ion capacity of the ECP plays an important role in determining the rate and also the amount of the ion concentration changes that can be achieved. The conductivity of the composite is another important parameter that has to be considered during the composite preparation. The volume fraction and the mobility of the hydrogel also play a significant role. The mathematical model can be used as a design tool to select the type of hydrogels, ECPs, and the concentration ranges needed to design an efficient ECP- hydrogel composite actuator.

CHAPTER 7: ELECTROCHEMICALLY ACTIVE CONDUCTING POLYMER COMPOSITES – PREPARATION AND CHARACTERISTICS

7.1 Introduction

One of the characteristics of Electrochemically active Conducting Polymers (ECP) is their insolubility in most solvents and is, as well as their difficulty in processing. Still, there are several ways by which a ECP can be deposited in a microchannel. Some ECPs like polyaniline can be dissolved in a solvent and can be spin cast directly onto the substrate¹⁷⁰. Other insoluble polymers like PPy can be prepared as a dispersion in a suitable medium by dispersion polymerisation conducted in the presence of a stabilizer¹⁷¹. The dispersed polymer can then be spin coated on to substrates. In other cases, photocrosslinkable monomers may be polymerised directly onto the substrate by exposure to UV. In a recent study, a photo-crosslinkable EDOT monomer was used to pattern PEDOT on a flexible PET film¹⁷².

In other direct methods, ECPs have been electrochemically grown on patterned metal electrodes before these are incorporated into microchannels. Lefevre et al¹⁰⁸ fabricated a ECP based microfluidic actuator using this method. They sputtered a gold layer on a glass wafer and then patterned it using photolithography and wet chemical etching. Then they grew ECP on the patterned gold electrodes using electrochemical polymerisation. This substrate was then used to build a microfluidic actuator. Similar methods that utilise the chemical polymerisation, instead of electrochemical polymerisation have also been used to deposit ECPs on to substrates¹⁷³.

ECPs have also been combined with other processable polymers to form composites that can be easily deposited. Waghuley et al¹⁷⁴ mixed PPy powder with ethyl cellulose binder to form a processable composite. The prepared composite was then screen printed on to a glass substrate to form sensors. Wallace et al¹⁷⁵ prepared a composite in which they stabilised PPy nanoparticles in a poly(ethylene glycol) gel to form a processable composite.

The objective of this section is to explore different methods by which an ECP can be made processable and patternable, so that it can be easily incorporated as actuator element inside microfluidic channels. First, we demonstrated a method to pattern thin films of

polyaniline ECP on glass. Second, we prepared and characterised different ECP based composites that are mechanically stable and can be easily processed. We also have studied their characteristics and electrochemical behaviour.

7.2 Patterning of Polyaniline Thin Films

Polyaniline (PANI) is one of the few ECPs that can be dissolved in a solvent (N-methyl-2-pyrrolidone (NMP) ¹⁷⁶). Thus, PANI can be spin cast onto substrate and can be patterned. In this section, we have used a photolithography technique to pattern thin films of PANI deposited on glass. Previous studies have used similar methods to pattern other polymers. Cui et al¹⁷⁷ used poly(styrenesulfonate) (PSS) doped poly (3, 4-ethylenedioxythiophene) (PEDOT) to pattern a Field Effect Transistor (FET) using Reactive Ion Etching (RIE). In their method, they spin coated the polymer on to the substrate. Dai et al¹⁷⁸ used photoresist patterning to selectively block the substrate and electrochemically polymerised the ECP to form a pattern. In the current study, we used photoresist patterning to protect the ECP layer and have etched the exposed region using Reactive Ion Etching (RIE). We used a photoresist layer, one that was thicker than the ECP layer, so that the ECP layer would be protected. We also used positive photoresist so that it is easier to etch away the remnant photoresist.

7.2.1 Experimental

0.2 grams of polyaniline emeraldine base was dissolved in 25 ml of *N*-Methyl-2-pyrrolidone (NMP) and magnetically stirred for 4 hours. The solution was filtered and then centrifuged. Glass slides were cleaned with detergent, then soaked in Piranha (7:3 H₂SO₄: H₂O₂, CARE: Piranha solutions are highly corrosive and potentially explosive) for 1 hour, rinsed with MilliQ water and dried with N₂ gas. Thin films were cast on the cleaned glass slides using spin coating. The cleaned glass slides were spin coated with the PANI solution at 800 rpm for 2 mins, then dried for 10 minutes in air. To increase the thickness, the same procedure was repeated 2 or 3 more times. A thick layer of positive photo-resist AZ1518 was coated over the PANI film by spin coating (at 1500 rpm for 1 minute). The thickness of the coated photo-resist was measured with a profilometer and was found to be 3 micrometers. It was prebaked at 100 °C and exposed to UV light through a light field mask with the desired pattern for 5 seconds. It was then post baked at 100 °C and developed using the developer (AZ326MIF) to etch away the exposed photo-

resist. The resulting glass slide contained a layer of polyaniline coated with a thick layer patterned photo-resist. It was then subjected to dry etching using March CS-1701 Reactive Ion Etching system. Oxygen was used as the reactive gas with chamber pressure of 415 mtorr. A power of 300 W was applied for 1 minute. The exposed PANI layer was completely removed, leaving behind the PANI layer protected by the photoresist. The residual photoresist was removed using acetone. The sample was then washed with isopropanol and water and then dried with N₂ gas. The step by step procedure is explained in Figure 7.1.

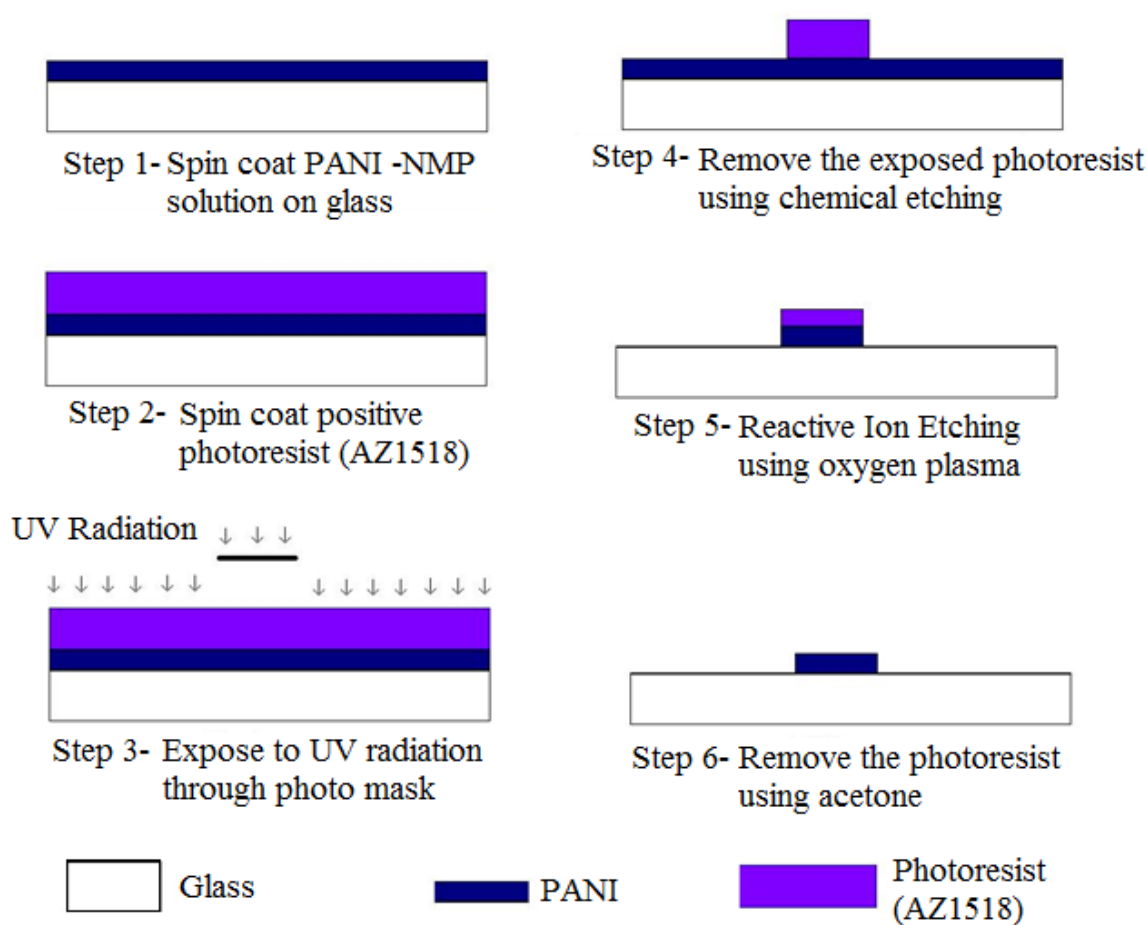


Figure 7.1. Patterning polyaniline (PANI) using photolithography.

7.2.2 Characterisation

Using the described method, a thin film of polyaniline was patterned. A resolution of 100 micrometer was achieved; this was the limitation of the mask and the photolithography equipment used. With higher resolution masks it would be possible to achieve higher resolution patterns. In order to analyse the thickness of the patterned polyaniline, Atomic

Force Microscopy (AFM) was used. The AFM images are shown in Figure 7.2. The thickness of the polyaniline layer was measured to be around 42 nm. The film was continuous and had a definite edge. The AFM measurement also showed some residual photoresist patches on the polyaniline layer.

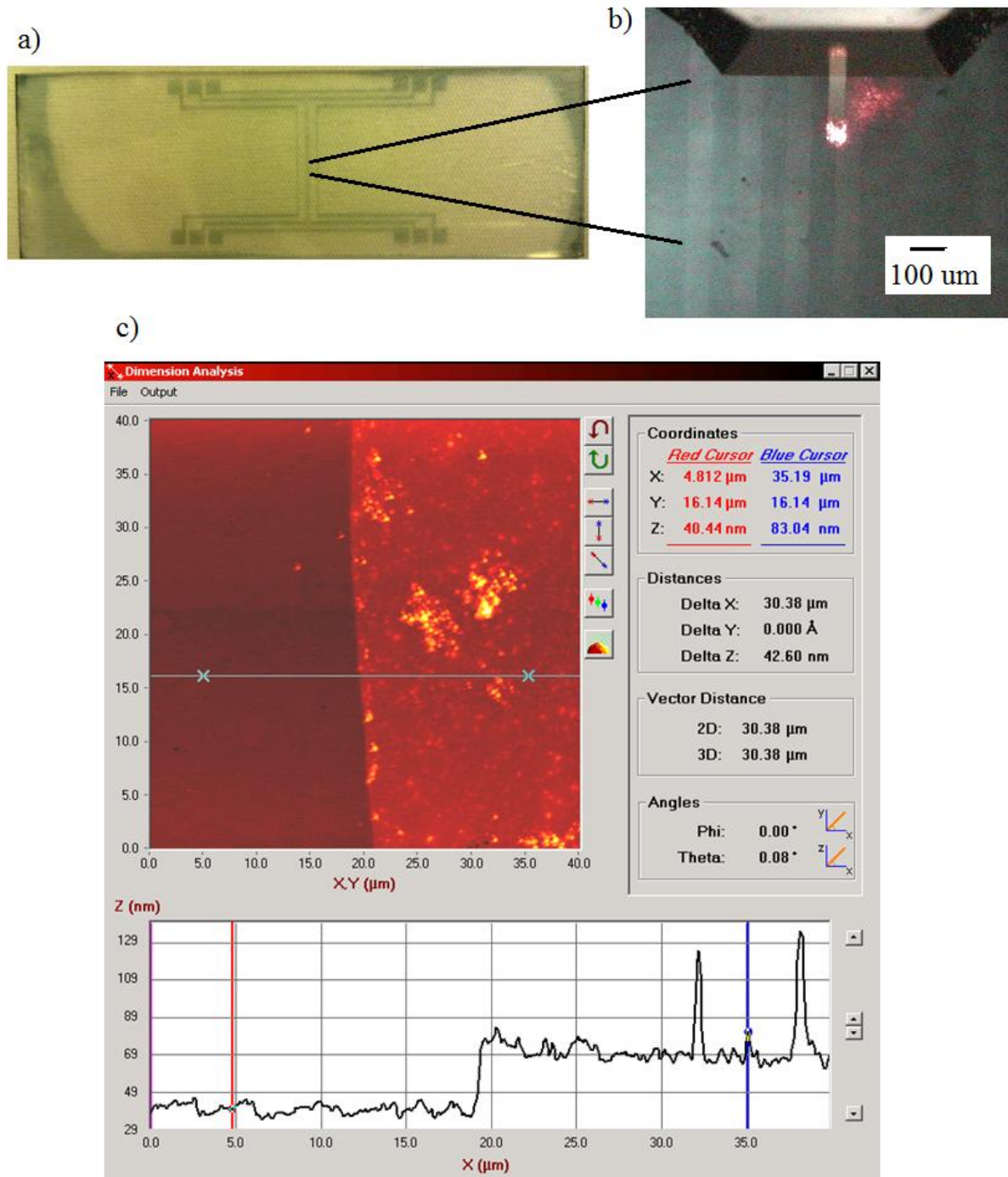


Figure 7.2. A pattern of polyaniline on glass (a) with 100 μm lines, (b) with AFM data, and (c) showing the measured thickness of the polyaniline film to be around 40 nm.

7.3 Polypyrrole-PDMS Composites

PDMS is a flexible, stable, and easily processable polymer. Polypyrrole (PPy), on the other hand, is mechanically poor and brittle and is insoluble in most solvents. Thus, in theory, we can use PDMS as a host matrix for PPy and thereby improve the stability and processability of the PPy. One important aspect to consider is the electrical property of such a composite and whether PPy will retain its electrochemical properties. In their experiments, Cakmak et al¹⁷⁹ prepared a PDMS PPy composite and were able to obtain conductive, mechanically stable, electrochemically active polymer (ECP). They have prepared the composite by coating a thin layer of PDMS on an electrode and electropolymerising pyrrole by applying a voltage of 1.1 V. They were able to achieve a conductivity of 3.9 S/cm. Another study¹⁸⁰ reported the preparation of composites of PDMS with PPy-polyaniline copolymer using a two-step electropolymerisation method. In contrast, we prepared composites by physically mixing PPy powder and carbon fibers with PDMS. Carbon fibres are highly conductive and can therefore increase conductivity and also improve the mechanical stability of the composites.

7.3.1 Experimental

50 mg of commercially available doped PPy powder (Sigma Aldrich) was well grounded and then mixed with various ratios of 1 to 2 mm long carbon fibres. PDMS precursor (Dow Corning) was mixed with curing agent in the ratio of 10:1 and then degassed in vacuum for 1 hour. The PDMS mixture was then mixed well with PPy and carbon fibre mixture in different ratios, followed by casting it on glass and curing it in oven at 60 °C for 1 hour. The resulting composite films were peeled off the glass and characterised.

7.3.2 Characterisation

The composite films we prepared were elastic and conductive. The conductivity of the composites increased with the increase in the amount of carbon fibre added to the composite. The conductivity of the composite increased from 3×10^{-4} S/cm when no carbon fibres were added to 1×10^{-3} S/cm when 100 mg of carbon fibres were added to the 50 mg of PDMS. The microscopic images of the composites showed that the carbon fibres became well connected when the amount of carbon fibres added was increased from 20 to 50 mg, at which point the conductivity of the composite increased 10 fold from 5×10^{-4} to 6×10^{-3} S/cm. The conductivities obtained for different composites are

listed in Table 7.1. Though the composites were conductive, the conductivity ranges were very low compared to the conductivity of PPy powder which was in the range of 1 to 10 S/cm.

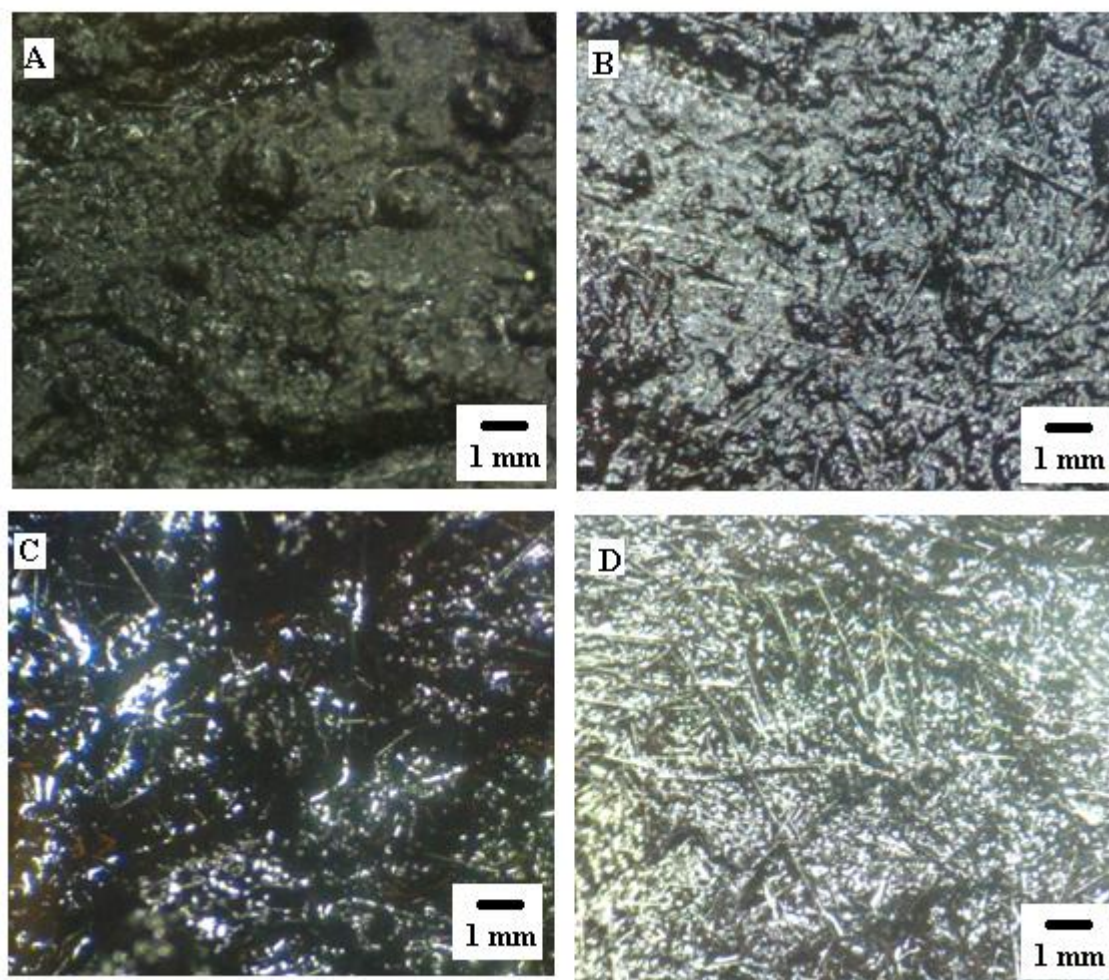


Figure 7.3. Microscopic images of ECP–PDMS composites with different carbon fibre content: (a) with no carbon fibres, (b) with 20 mg, (c) with 50 mg, and (d) 100 mg. In all cases PDMS was 50 mg and PPy was 50 mg.

Table 7.1

Conductivity of the ECP–PDMS Composites with Different Carbon Fibre Content

Type	Polypyrole	Carbon fibres	Conductivity (S/cm)
a	50 mg	0 mg	3×10^{-4}
b	50 mg	20 mg	5×10^{-4}
c	50 mg	50 mg	6×10^{-3}
d	50 mg	100 mg	1×10^{-3}

In order to characterise, the composite films were stuck onto a glassy carbon electrode (30 mm^2) using adhesive tape (Kapton polyimide tape with silicone adhesive) and then subjected to cyclic voltammetry in a 0.1 M NaCl solution (Ag/AgCl reference) in a standard electrochemical cell. The scan rate was set to 0.1 V/s and the potential range from -0.6 to +1.2 V. This potential range is within the PPy oxidation and reduction range. The cyclic voltammograms (CV) obtained are shown in Figure 7.4

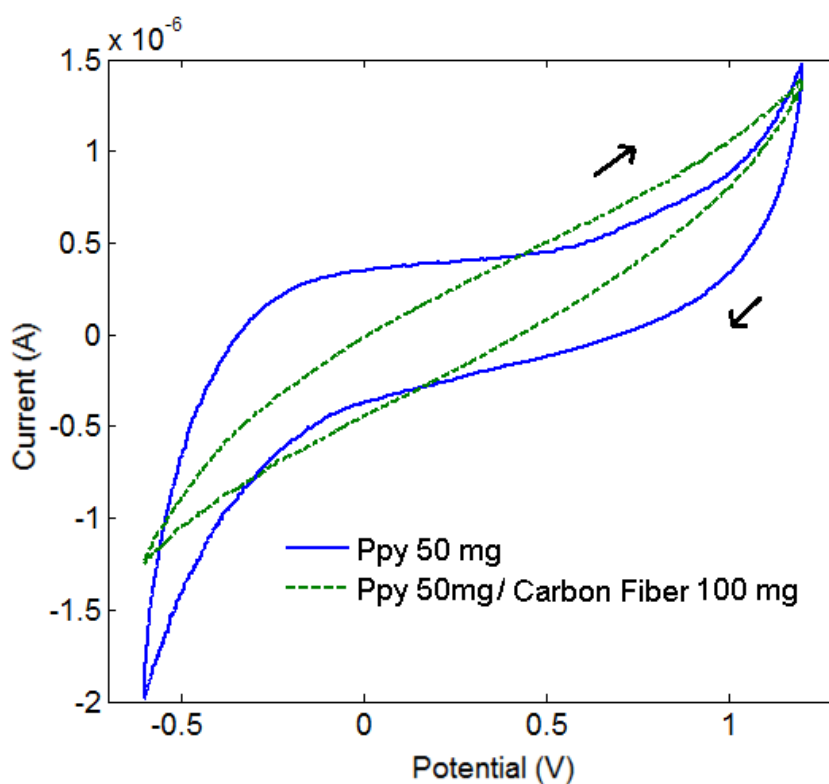


Figure 7.4. Cyclic voltammograms of PPy-PDMS composites with and without carbon fibers; all mixtures had 50 mg PDMS.

CVs of the composites with only PPy had very low current and showed no electrochemical activity of PPy in this voltage range. The CV obtained had a broad peak and current was due to the capacitive charging of the PPy –PDMS double layer. When the carbon fibres were added to the composite the current as a result of the capacitive charging decreased because of the increased conductivity and the reduction in the double layer capacitance.

SEM images of the composites showed PDMS completely covering PPy. This quality of the composite might explain low conductivity and the absence of electrochemical activity.

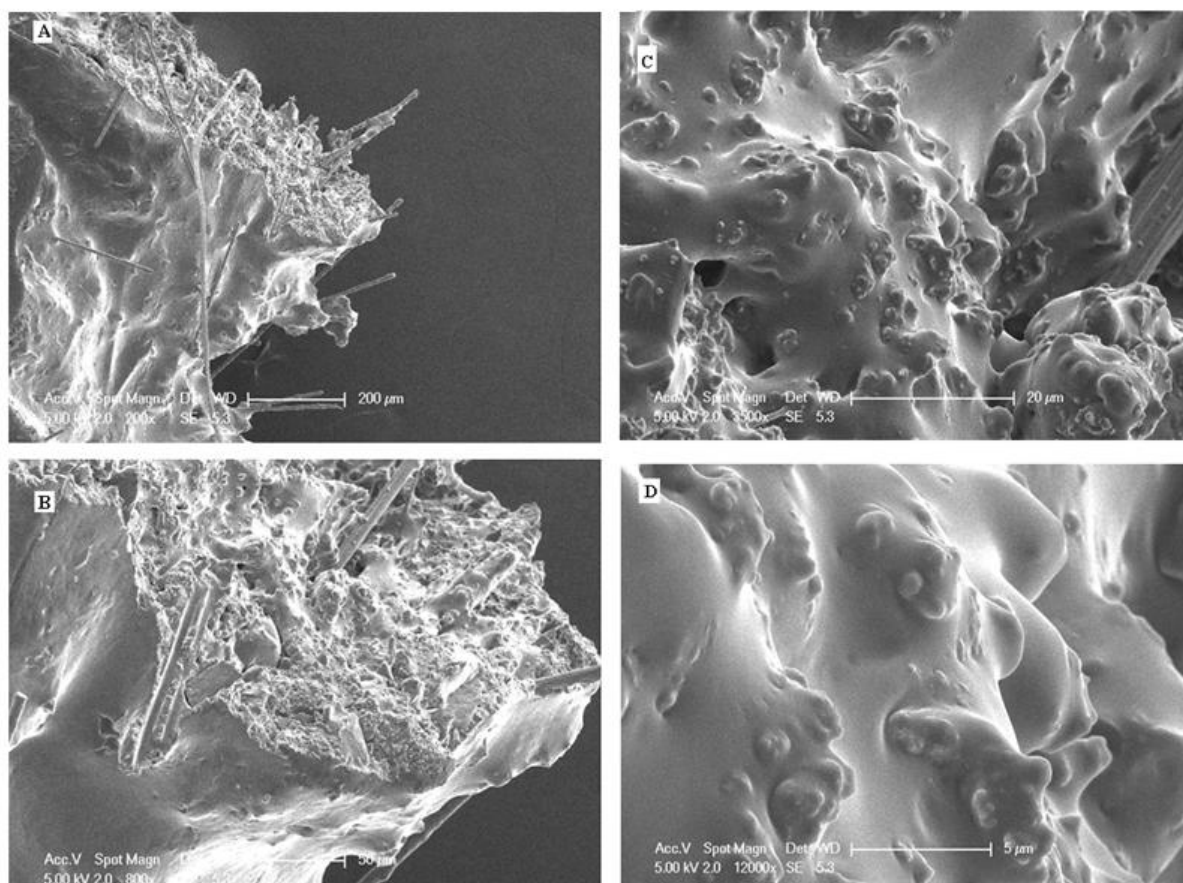


Figure 7.5. SEM images of ECP –PDMS composites at different magnifications.

7.4 Polypyrrole-Carbon Fibre Composites

In this section, we explored different methods to prepare ECP coated carbon fibre composites. Carbon fibres are highly conductive and have good mechanical properties, properties which make them amenable to serving as conductive filler to polymer

composites. It has been reported that the electrical properties of the ECPs can be improved by adding carbon based additives¹⁸¹. ECP-coated carbon nanotubes have been used as super capacitive materials¹⁸². Kim et al¹⁴⁴ deposited thin layers of PPy on carbon fibres for a similar super capacitive application. An et al¹¹⁷ noted that the number of electrochemical cycles of the ECPs can be improved by adding carbon additives. In this section, we prepared ECP-coated carbon fibres by two different methods.

7.4.1 Chemical Polymerisation

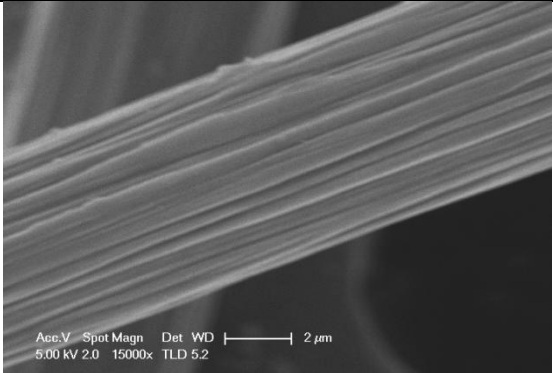
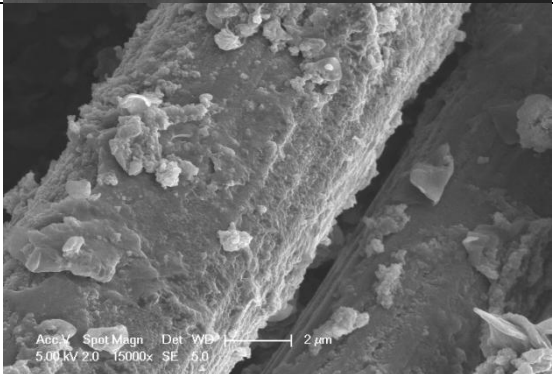
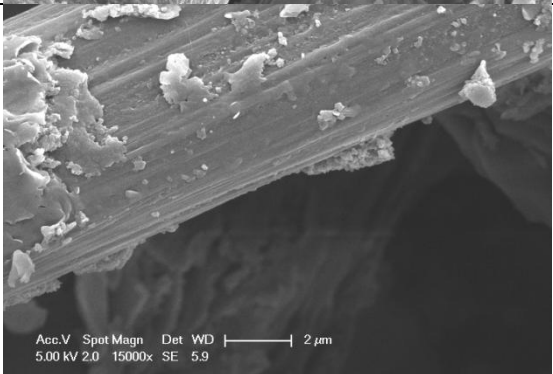
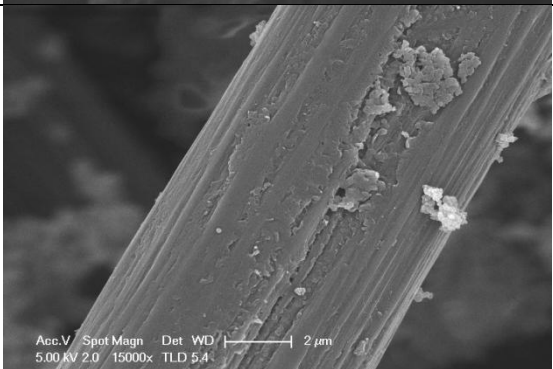
In the first method, ECP-carbon fiber composites were prepared chemically using Ferric Chloride (FeCl_3) as oxidant and Dodecyl Benzene Sulphonate (DBS) as surfactant. This method was adopted from a previous study by An et al¹¹⁷ where they used chemical polymerization method to prepare a carbon aerogel -PPy composite. Carbon fibers of length 1 to 2 mm long were washed and soaked in dilute nitric acid (3 M) and then washed thoroughly and dried in vacuum oven. Carbon fibers were dispersed in 20 ml of distilled water containing DBS and kept in ultrasound for 10 mins. 0.4 g of distilled pyrrole monomer was then added and stirred. Different quantities of FeCl_3 were dissolved in 20 ml of distilled water, which was then added to the mixture slowly and the set up was put in ultrasound bath for 10 mins. The mixture was continuously stirred for 12 hours. After that time, the solid agglomerate was removed using centrifuge and then washed thoroughly with distilled water and dried in vacuum oven for 12 hours. Different amounts of oxidant and surfactants were added for different samples.

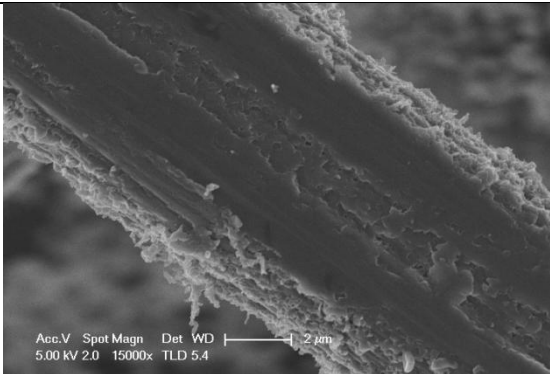
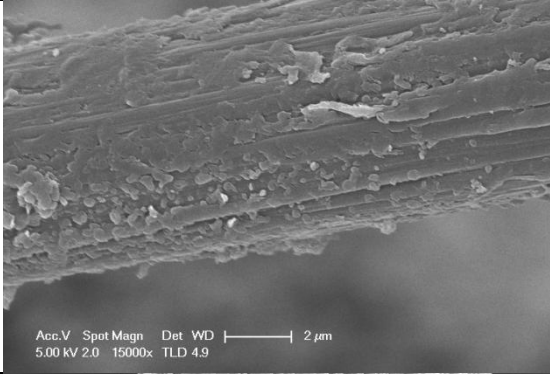
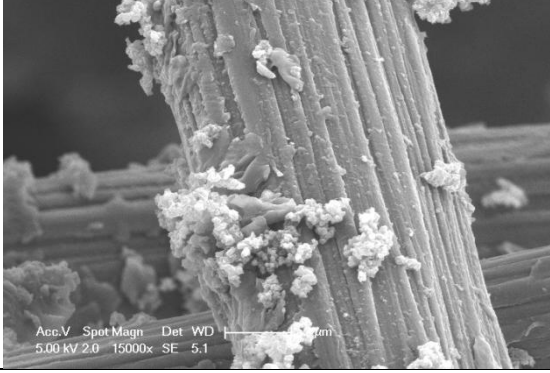
7.4.2 Characterization

Chemically polymerized carbon fiber-ECP composites were studied using Scanning Electron Microscope (SEM). SEM images (Figure 7.4) show that a layer of PPy has formed over the carbon fiber due to chemical polymerization. The thickness of the layer was higher when both the oxidant and the surfactant concentration were higher. When the concentration of the oxidant was reduced, there was a significant decrease in the thickness of the PPy layer formed. The changes in the concentration of the surfactant also affected the polymerisation process. An et al¹¹⁷ proposed a mechanism by which the surfactant would interact with the reaction mechanism and would change the morphology of the ECP. Decrease in the concentration of the surfactant also decreased the thickness of the polymer deposited. All the experimental parameters and the SEM images are given in Figure 7.2.

Table 7.2

Different Morphology of the ECP Formation with Respect to Changes in Concentration of Oxidant and Surfactant

Sample	Carbon fibers	FeCl ₃ (oxidant)	DBS (surfactant)	SEM
1	Bare fiber			
2	0.1 g	0.972 g in 20 ml	1.4 g in 20 ml	
3	0.1 g	0.486g in 20 ml	1.4 g in 20 ml	
4	0.1g	0.972 g in 20 ml	0.7 g in 20 ml	

5	0.1g	0.486 g in 20 ml	0.7 g In 20 ml	
6	0.1g	0.972 g in 20 ml	0.35 g in 20 ml	
7	0.1g	0.486 g in 20 ml	0.35 g in 20 ml	

In order to characterise the ECP coated carbon fibres and also to check if the ECP is electrochemically active we used Scanning Ion Conductance Microscopy (SICM) to perform electrochemical studies on a single fibre. In this experiment a single PPy coated carbon fibre was isolated and placed on an Indium Tin Oxide (ITO) electrode. Cyclic voltammetry was performed with the SICM pipette filled with 0.1 M NaCl as an electrolyte. A droplet was formed over the fibre with the pipette containing counter and reference electrodes. Ag/AgCl electrodes were used as both counter and reference electrodes while ITO as working electrode. (For more information regarding the SICM used, refer Laslau et al¹⁸³) The current showed a clear oxidation peak of PPy at 0.4 V. CVs were also performed on a single carbon fibre and the ITO electrode as controls. The results and the setup are shown in Figure 7.7

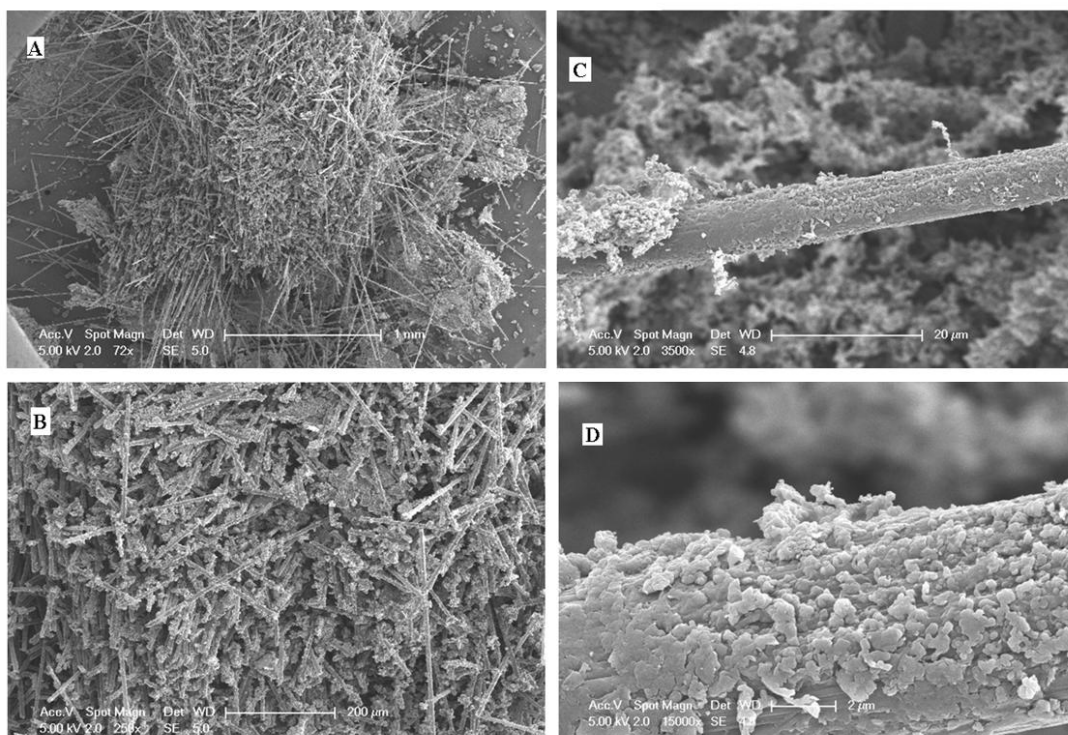


Figure 7.6. SEM images showing carbon fibre coated with PPy (Sample 2: FeCl_3 – 0.972g in 20 ml, DBS -1.4 g in 20 ml, Py- 0.4 g) for different magnifications.

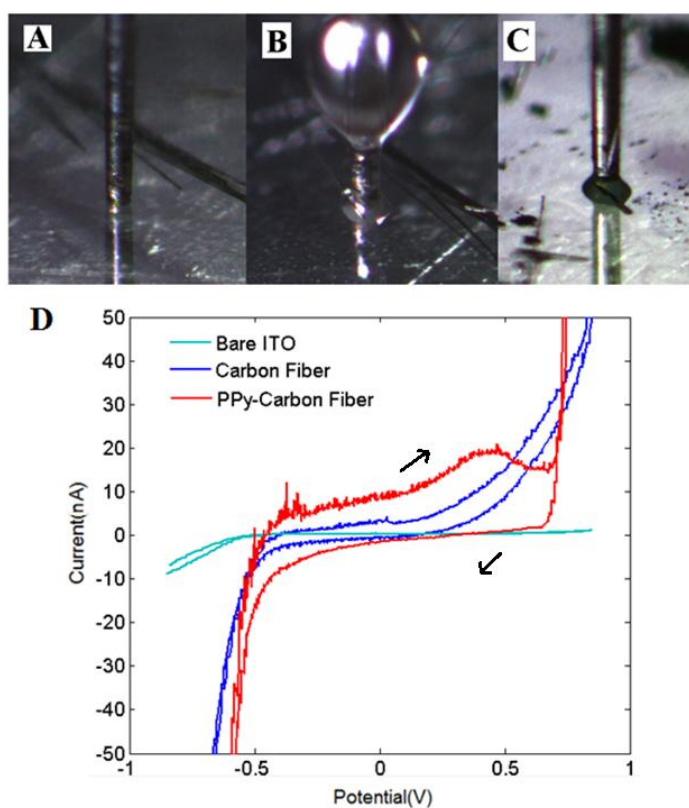


Figure 7.7. Setup showing the SICM pipette on the ITO electrode (a), carbon fiber(b), carbon fiber coated with PPy(c), and the cyclic voltammeties obtained (d).

7.4.3 Electrochemical Polymerization

In the second method, ECPs were polymerized on the carbon fibers electrochemically. A bunch of carbon fibres was used as working electrode and platinum mesh as the counter electrode. The electrolyte solution was prepared with 0.5 M pyrrole in propylene carbonate (PC) with 0.5 M trifluoromethanesulfonate (Triflate) salt. A constant potential of 0.85 V (Ag/AgCl) was applied for 3 hours. After the process, the carbon fibres were found to be covered with a black powdery PPy. The fibres were analysed using Raman spectroscopy to confirm the presence of PPy.

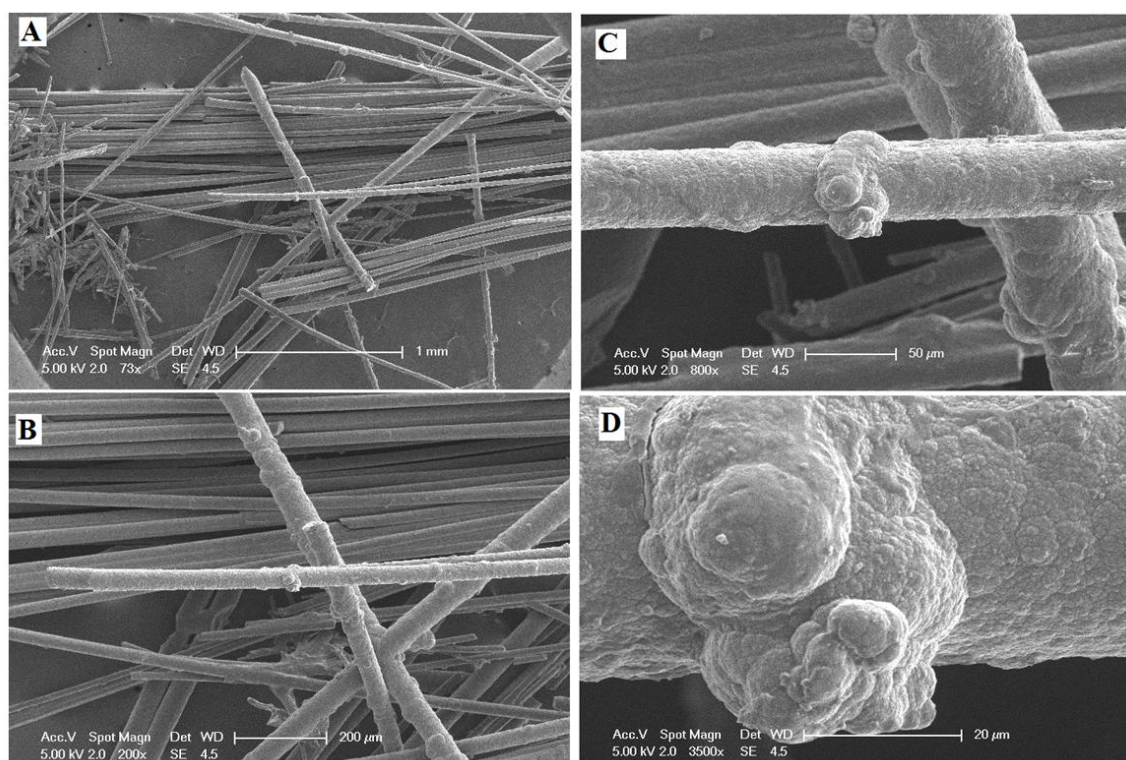


Figure 7.8. SEM images showing carbon fibre coated with PPy by electrochemical polymerisation method in different magnifications.

The fibres coated with PPy were analysed using SEM. SEM pictures showed cauliflower structures of PPy and that the thickness of the carbon fibres has increased quite significantly from 5 micron (bare fibres, refer table 7.2) to 50 microns (PPy coated). The surface morphology of the PPy was smooth. Figure 7.8 shows SEM images of the electrochemically prepared PPy carbon fibre composites.

7.5 Polypyrrole-Hydrogel Composites

As discussed in the previous chapters, hydrogels swell by osmotic intake of water. The swelling is sensitive to the ion concentration and the pH of the surrounding electrolyte. In chapter 6, we explored the idea of using ECP actuation as a mechanism to pump or remove ions from the hydrogel. From the simulation results, we concluded that by incorporating ECPs into the hydrogel and actuating it, it is possible to significantly alter ion concentration of the hydrogel. In chapter 2, we reviewed in detail various methods to prepare and characterise the ECP-hydrogel composites. In this section, we prepared polyelectrolyte hydrogel composites using various methods and have characterised them for their electrochemical properties. First we synthesised a PAA-p (HEMA) based hydrogel. Then, we prepared five different types of composites, as described in section 7.5.3.

7.5.1 Hydrogel Synthesis

Photo crosslinkable hydrogel containing PAA-HEMA was synthesized by a method described by Onuki et al¹⁸⁴. The characteristics of the resulting hydrogel depends on several formulation factors, including the polymer concentration in the aqueous phase, the degree of modification with HEMA, and the initiator concentration. Details are given below.

7.5.1.1 Materials. PAA (molecular weight 450,000), 2, 2-dimethoxy-2-phenylacetophenone (DMPA), and 1-ethyl-3-(3-dimethylaminopropyl)carbodiimide hydrochloride (EDC) were purchased from Sigma. HEMA was purified to eliminate the inhibitor by filtration through a basic Al₂O₃ column. All other reagents were of chemical grade.

7.5.1.2 Synthesis of photocrosslinkable polymers. PAA-HEMA was synthesized as follows: 7.22 g of HEMA was added to 2.00 g of PAA dissolved in purified water (40 mL), and the mixture was stirred for 30 min on ice. EDC (0.80 g) dissolved in purified water was added to the mixture, which was then stirred for 4 hours at room temperature to complete the reaction. The reaction mixture was dialyzed using cellulose tube in the dark 5 times against purified water and then lyophilized using a freeze-dryer under reduced pressure. A white cotton-like substance was obtained as final product.

7.5.1.3 Preparation of photocrosslinked hydrogels. 100 mg of the photocrosslinkable PAA-HEMA was dissolved in 1 mL phosphate-buffered saline (PBS, pH 7.4); then 1 mg DMPA dissolved in 50 μ L ethanol was added to the aqueous solution. The mixture was then UV irradiated. The wavelength of illumination ranged from 200 to 400 nm and the irradiation time was 25 min.

7.5.2 Hydrogel Characterisation

The synthesised hydrogel was studied for its swelling behaviour. The hydrogel precursor was poured into a microfluidic chamber (see section 3.1) and then exposed to UV for 20 minutes. The photocrosslinked hydrogel was then sealed in the chamber with a PDMS layer. Solutions with different salt concentration and pH were introduced into the chamber and the swelling behaviour of the hydrogel was analysed using an optical microscope. Similar to other hydrogels, the synthesised PAA-P (HEMA) was sensitive to concentration and pH changes. When the concentration of the surrounding electrolyte was reduced, the water uptake capacity of the hydrogel increased. The hydrogel volume increased by more than 50% for ion concentration changes from 0.8 M to 0 M. When the pH of the solution was increased, the hydrogel de-swelled. The swelling of the hydrogel was calculated as a ratio of the measured volume to the maximum volume.

$$\text{Swelling \%} = \frac{\text{Measured volume}}{\text{Maximum volume}} \times 100$$

The swelling percentages for different salt concentration and pH and over time are given in the Figure 7.9.

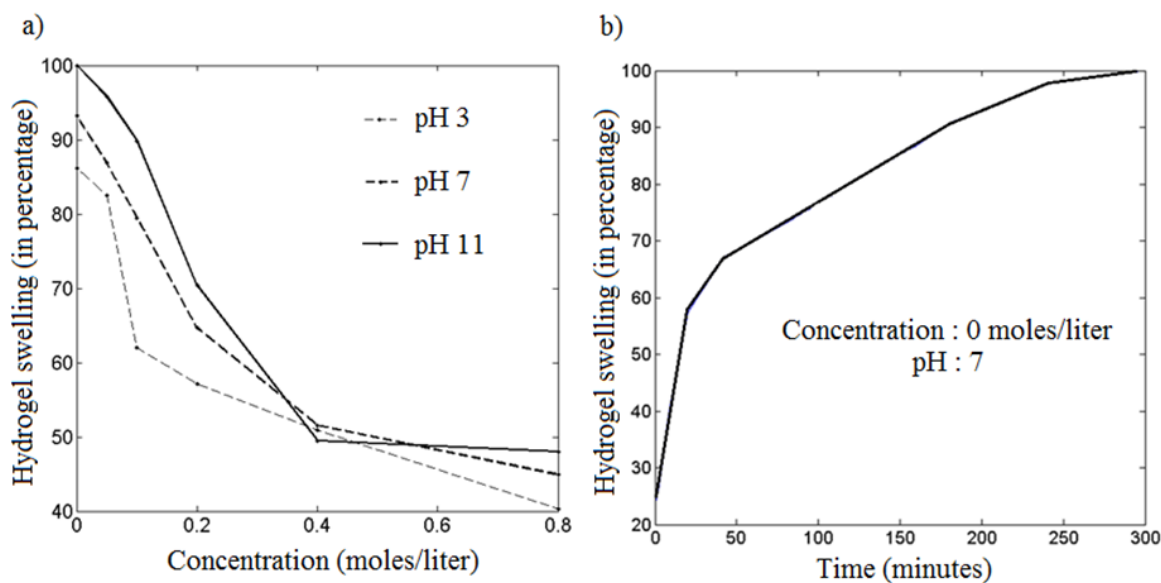


Figure 7.9. Hydrogel swelling for (a) different salt concentration and pH and (b) hydrogel swelling over time.

7.5.3 Hydrogel-Polypyrrole Composite Preparation

Five different hydrogel-PPy composites were prepared and characterised in two different settings. Our objective was to prepare a composite that is easily processable and that can be incorporated within the microfluidic cell. Thus, our focus was on the physical mixing method. We also explored the electrochemical polymerisation and chemical polymerisation processes to prepare the composites in order to compare the efficiency of the physical mixing process with other available process methods.

7.5.3.1 Physical mixing method 1. In the first method the 50 mg of hydrogel precursor with the photo initiator was mixed with commercially available PPy powder to form a homogenous mixture. The mixture was poured onto glassy carbon electrode (30 mm²) and was crosslinked using UV to form the composite. We then characterised the composite using cyclic voltammetry (CV) in a standard electrochemical cell (Figure 3.5a).

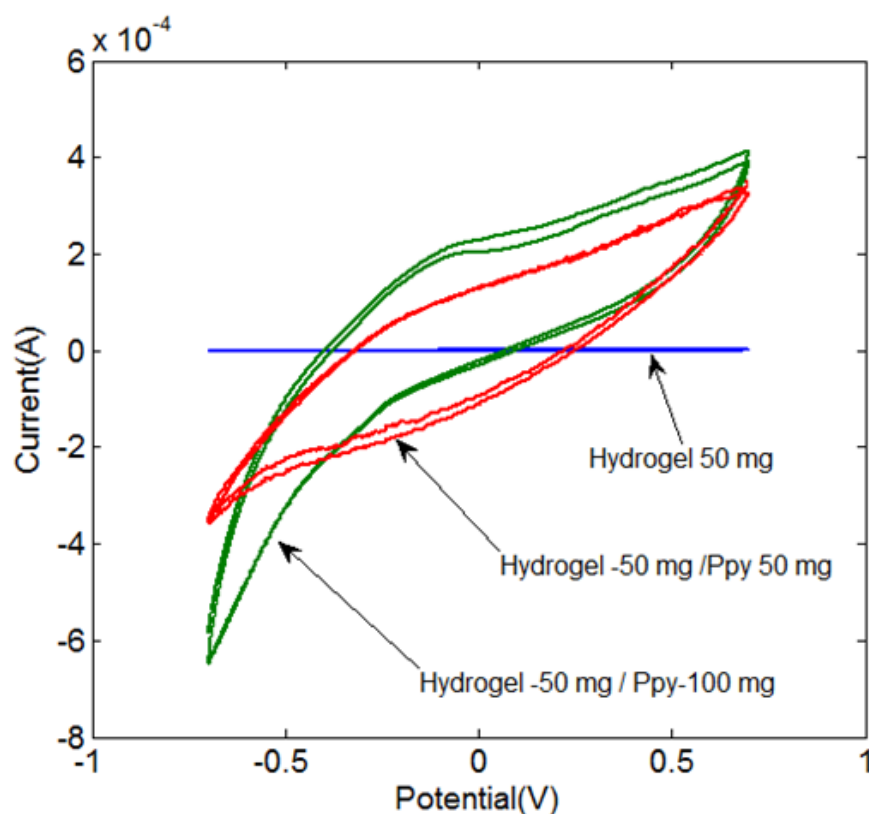


Figure 7.10. CVs for different hydrogel / PPy ratios, NaCl – 0.1M, Scan rate 0.1V/s.

Two different composites were prepared with different amounts of PPy powder; one with 50 mg of PPy in 50 mg of hydrogel and another with 100 mg of PPy in 50 mg of hydrogel. The CVs were performed with 0.1M NaCl solution, platinum wire counter electrode and Ag/AgCl reference electrode. The CVs of both the composites showed no significant PPy oxidation or reduction peak but composite had a much higher current compared to pure hydrogel. When the amount of PPy was increased, the current increased and the composite showed increased electrochemical activity.

7.5.3.2 Physical mixing method 2. In the second method, carbon fibers coated with PPy, prepared in the section 7.4 (sample 2 of chemical polymerisation method), was added to the 50 mg of hydrogel precursor and photo initiator and was poured on glassy carbon electrode (30 mm²) crosslinked using UV. Similar to the previous study, the composites were characterised using cyclic voltammetry in a standard electrochemical cell with 0.1 M NaCl with platinum wire counter electrode and Ag/AgCl reference electrode (Figure 3.5a).

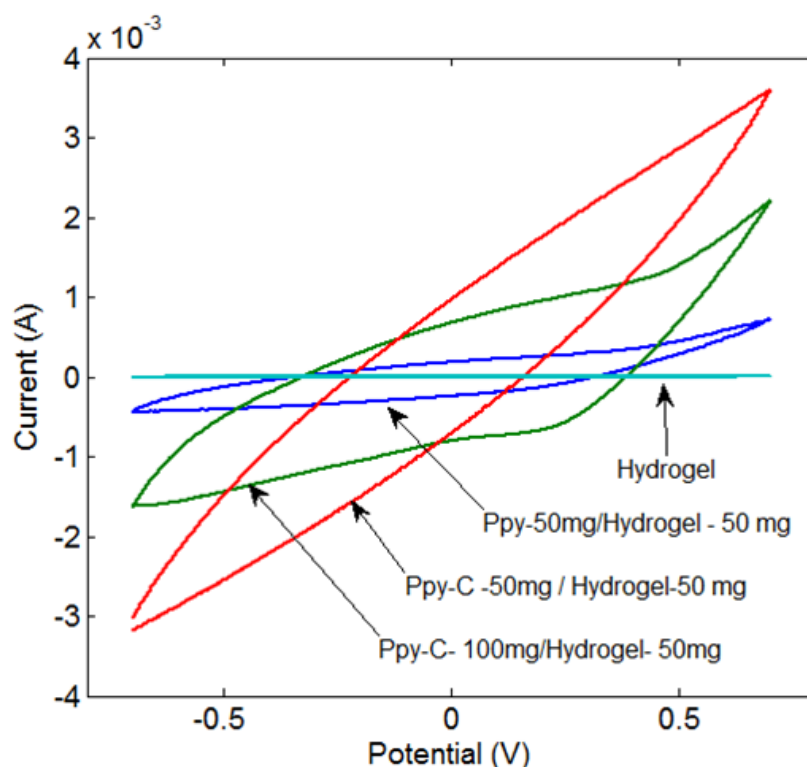


Figure 7.11. CVs for different Hydrogel Ppy composites. The ratios were NaCl – 0.1M Scan rate 0.1V/s.

The composite showed a significant increase in the current due to the addition of the polypyrrole coated carbon fibres as compared to composites with only PPy powder. When the amount of fibres was increased, the CV became broader, showing an increased electrochemical activity (capacitive). This reaction might suggest that when there is less volume fraction of PPy coated carbon fibres, the electrochemistry of thin PPy layer on the carbon fibers was not significant enough; when the amount of Ppy coated fibers was increased, the PPy layers got more connected and hence showed an increase in the electrochemical behaviour.

7.5.3.3 Physical mixing method in microfluidic electrochemical cell. In this method, the composites were prepared in a microfluidic electrochemical cell (fabrication method outlined in section 3.1). Thickness of the cell used in these studies were 1 mm. As before, hydrogel precursor with photo initiator was mixed with PPy powder and in order to increase the connectivity, graphite powder was added along with the PPy powder. Graphite is highly conductive and electrochemically less active. We prepared four different composites in the electrochemical cell. One was hydrogel with just PPy powder

and three other composites with additional graphite powder in different quantities. In all cases 50 mg of hydrogel was added to 50 mg of PPy powder. The prepared precursor, mixed with the solids, was laid down in the microchannel and was exposed to UV. The composite formed was then subjected to electrochemical studies using the setup described in section 3.3.

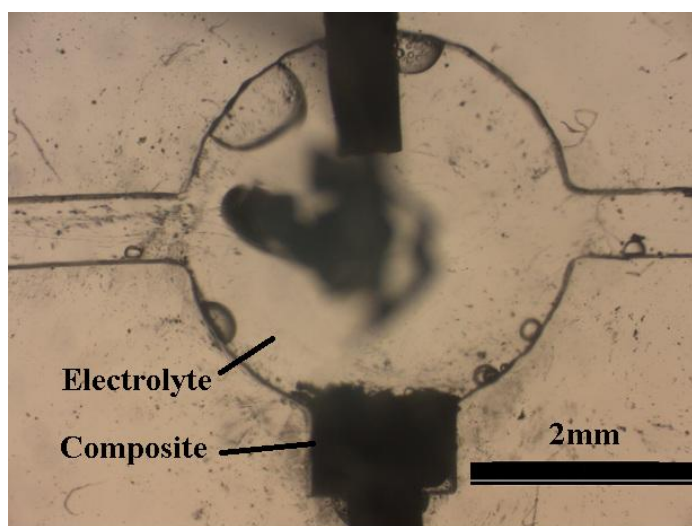


Figure 7.12. ECP-graphite-hydrogel composite in the microfluidic electrochemical cell.

The cyclic voltammetry was performed to characterise the composite. A carbon working electrode of surface area 0.8 mm^2 was used along with another carbon counter electrode and Ag/AgCl reference electrode. 0.1M NaCl was used as electrolyte and the scan rate was maintained at 0.1V/s. When the composite was composed only of hydrogel and PPy, it had a characteristic oxidation peak of PPy at 0.4 V. When the graphite powder was added the peak disappeared but the current increased. However, increasing the proportion of the graphite powder further reduced the current significantly. This effect is due to the fact that the volume fraction of the hydrogel goes down with increasing amount of graphite and PPy. Thus, there is less amount of hydrogel (hence the ions) to react with the PPy, reducing the current. This effect has been captured in the modelling results shown in section 6.

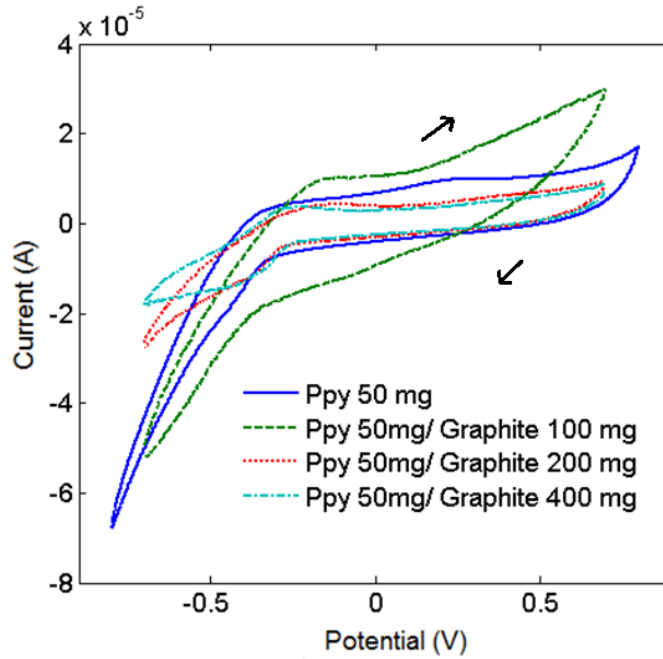


Figure 7.13. CVs for different Graphite-PPy ratios, NaCl – 0.1M Scan rate 0.1V/s.

To find how much salt ECPs take or expel during the reaction, we looked at the charge consumed by the ECPs during electrochemical reaction. To calculate the charge consumed during oxidation we have integrated the anodic cycle of the cyclic voltammetry. Using this method, the charge consumed by the composite with only PPy was calculated, as per Equation 7.1:

$$Q = \frac{\int i \, dv}{dv/dt} \quad (7.1)$$

where $\frac{dv}{dt}$ is the scan rate

$$Q = \frac{0.01.2}{0.1} = 0.12C$$

From the charge consumed we can calculate the number of electrons.

$$\text{No of electrons} = \frac{\text{Total charge } Q}{\text{Charge of electron}} = \frac{0.12}{1.6 \times 10^{-19}} = 7.5 \times 10^{17} \text{ electrons}$$

To compensate the loss of electrons, ideally there will be an equal number of ions moving into the composite, which is 7.5×10^{17} negative ions. This result is equal to 1.2×10^{-6}

moles of ions. We can calculate the volume of the composite from the microscopic image, which is roughly equal to 2.5 mm^3 . From these calculations, the total ion capacity of the composite in the microchamber is about 0.5×10^{-6} moles/cubic mm or 0.5M. From the mathematical model in chapter 6, the change in the concentration predicted for 0.5M ion capacity range of the composite is around 10% (Figure 6.4).

We also subjected the composite to constant potential in order to study if there was any mechanical actuation due to the change in the ion concentration of the composite due to PPy oxidation and reduction.

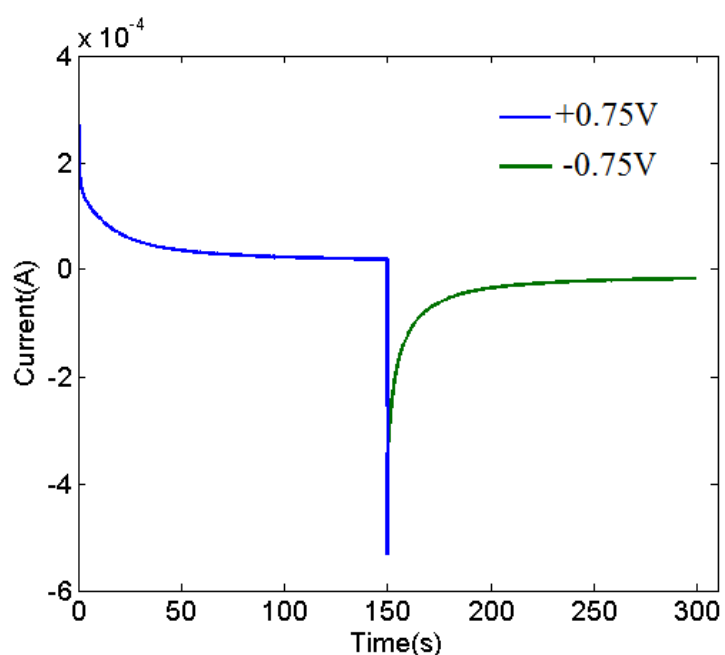


Figure 7.14. I-t response curve of composite prepared by physical mixing method. PPy-50mg Graphite 100 mg.

The composites were applied a positive potential of 0.75 V. The composites were monitored with optical microscope to record any mechanical actuation. The polarity was reversed after 150 s and held at -0.75 V for 150 s. The composite showed no significant actuation. From the predicted concentration changes and the observed swelling behaviour of the hydrogel we can conclude that the ion capacity of the composite achieved through physical mixing method was not enough to cause the swelling.

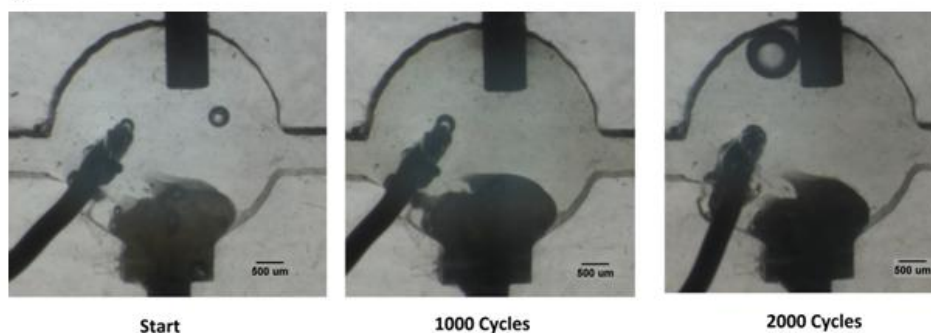
The current response during this study is shown in the i-t curve shown in Figure 7.14. The current range obtained was higher than the CV because of the capacitive charging. The

current range obtained in the experiments were comparable to the current ranges predicted by the model for a 0.5M ion capacity range composite.

7.5.3.4 Electrochemical polymerisation in microfluidic electrochemical cell. In

order to compare the physical mixing method with other methods, in this section, we prepared PPy-hydrogel composites through electrochemical polymerisation. In this method, PAA- HEMA hydrogel was first prepared in the PDMS microchamber with carbon working and counter electrode and Ag/AgCl reference electrode. A solution containing 0.4 M pyrrole and 0.4 M KCL was introduced in the chamber and polypyrrole was electropolymerised using cyclic voltammetry. The scan rate was maintained at 0.05 V/s and voltage was cycled for 2000 cycles. The PPy growth was slow and the hydrogel gradually turned black as a result of PPy growth.

a)



b)

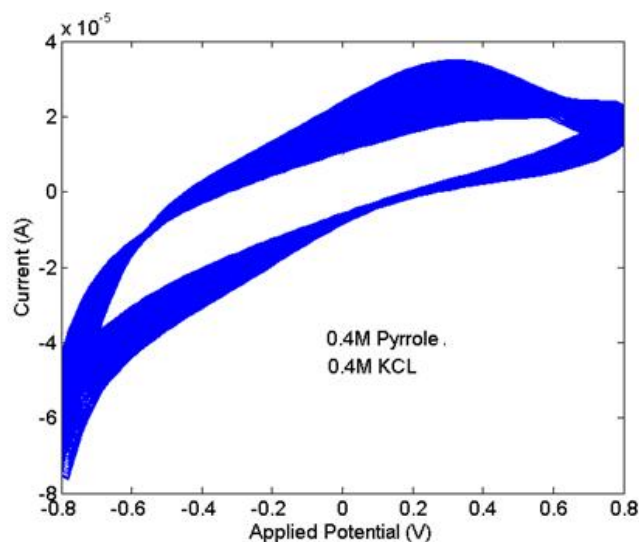


Figure 7.15. Electrochemical growth of PPy in an electrochemical cell (a) time lapse images showing PPy growing in the hydrogel and (b) Cyclic voltammetry of PPy growth. Scan rate 0.05 V/s

The growth cyclic voltammetry showed gradual increase in the current due to the growth of the polymer. The CV also showed the oxidation peak at 0.4 V, which is characteristic for PPy. The ion capacity calculated from the CV was around 1.2×10^{-6} moles/ mm^3 .

After 2000 cycles the electrolyte was flushed with water and the chamber was filled with 0.1 M NaCl and was subjected to constant potential to study its mechanical actuation behaviour. The composite was subjected to +0.75 V for 90 s and the polarity was reversed. The composite showed no significant actuation behaviour. The i-t response curve recorded during the experiment is given in Figure 7.16.

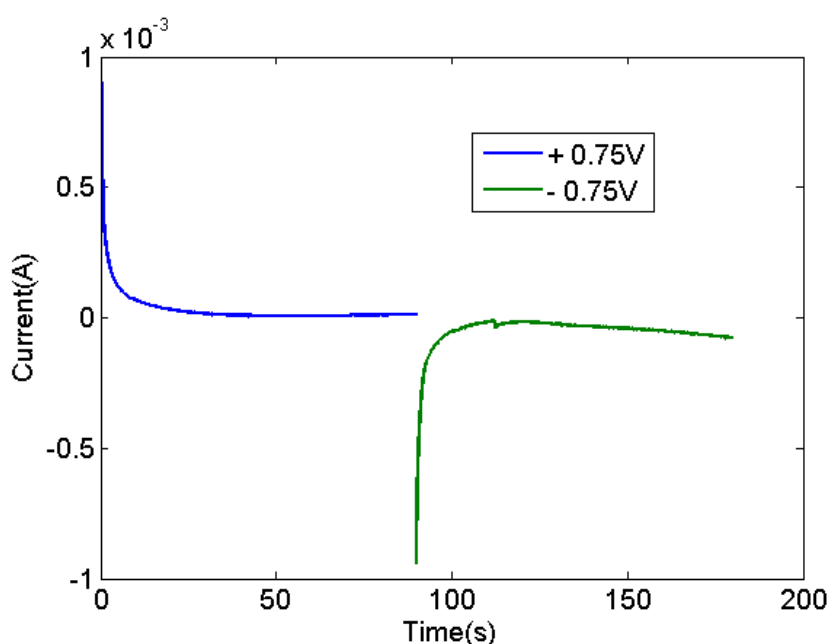


Figure 7.16. i-t response curve of the electrochemically prepared composite.

7.5.3.5 Chemical polymerisation in microfluidic electrochemical cell. In this method, the composites were prepared by chemical oxidation of hydrogel containing pyrrole monomer. In order to chemically prepare the composite, hydrogel was first prepared in PDMS microchamber same as by the previous techniques and then soaked in pyrrole solution for 3 hours. An oxidant, ammonium per sulphate (APS), was then introduced in the chamber and soaked for 3 more hours. This process was repeated for few more cycles. After each cycle, i.e. after either soaking it in APS or pyrrole, the contents (oxidant / pyrrole solution) were flushed out and filled with solution containing 0.1 M NaCl and was subjected to cyclic voltammetry. Carbon working electrode of surface area 0.8 mm^2 was used with another carbon electrode and counter and Ag/AgCl

wire as reference. The scan rate was maintained at 0.1 V/s. Figure 7.17 shows, depending on the last cycle, the CV peaks of both PPy and APS. The current due to PPy increased after every cycle of filling in pyrrole, showing the increase in the volume fraction of the ECP.



Figure 7.17. Chemically prepared PPy hydrogel composite.

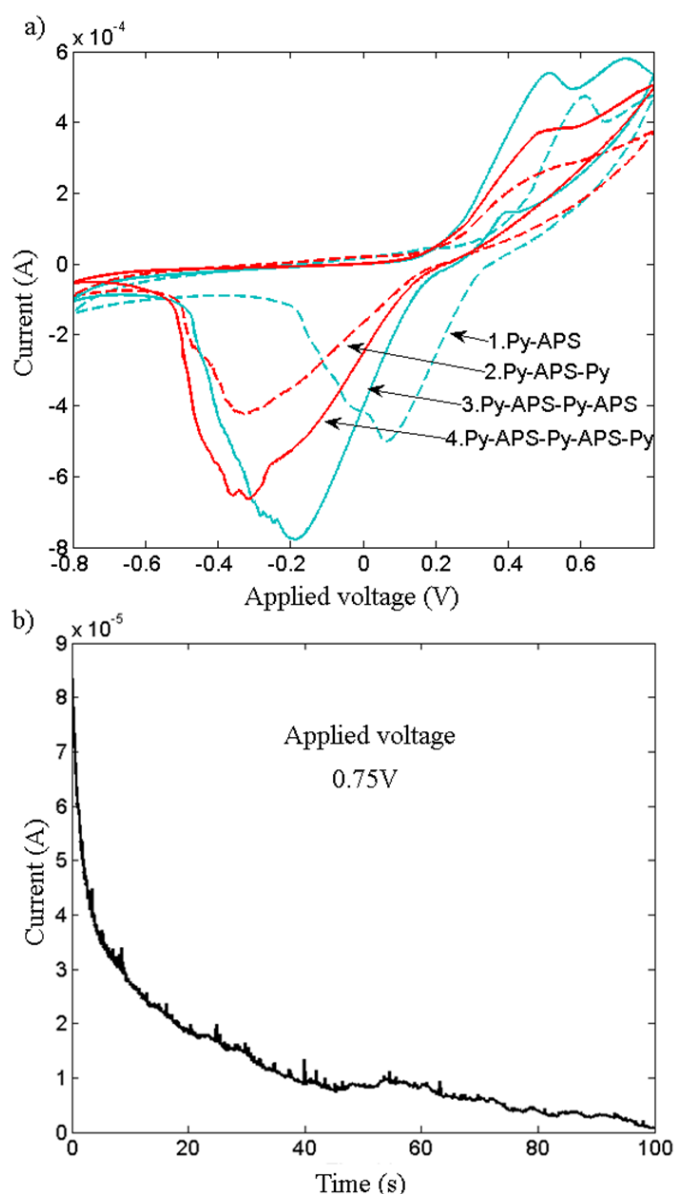


Figure 7.18. Cyclic voltammetry of the chemically prepared ECP – hydrogel composites, 0.1 M NaCl, scan rate 0.1 V/s. Red line- Cycle ended with pyrrole, Blue line – Cycle ended with APS (a) and the i-t curve for the same composite after final oxidation (b).

The cyclic voltammetry showed that the depending on the cycle the oxidation and reduction peaks were different. After each APS cycle there were distinct peaks showing oxidation and reduction of the APS. The APS residue also pronounced and shifted the PPy oxidation and reduction peaks. After each of the pyrrole cycle the CV peaks looked more similar to PPy oxidation and reduction peaks. And after each couple of cycle the peak current increased indicating the increase in the volume fraction of the ECP. The ion capacity calculated from the CV was around 0.8×10^{-5} moles per mm^3 . It should be noted that this value may not truly reflect the ion capacity of the PPy, as there is an amplification of current due to the presence of APS molecules.

7.6 Discussion

Although we were able to prepare and characterise PPy-hydrogel composites, none of the composites had significant mechanical actuation. This result might be attributable to the insufficient availability of active PPy in the composite. In case of physical mixing methods, the ion capacity measurements from CV showed that only a fraction of PPy added to the mixture was electrochemically active. There are several reasons as to why this low level of activity might happen. When mixed with hydrogel, the electrical connectivity of the PPy can become poor. A break in the electrical connectivity near the electrode can disconnect entire PPy network in the composite. However, this result cannot be the case for the composites prepared with sufficient amount of graphite powder. One must note that increasing the graphite and PPy content will also significantly reduce the volume fraction of the hydrogels. When the volume fraction of the hydrogel is reduced, it affects the mechanical actuation of the composite in two ways. First, it reduces the amount of hydrogel that is available to absorb the electrolyte and cause the swelling, thus affecting the mechanical actuation more directly. Second, when the hydrogel volume fraction is reduced the ECP networks that are in the inner layers of composites are cut off from the electrolyte solution. Thus, the entire composite becomes similar to a solid ECP. In our experiments, the prepared composites were very thick in the order of millimetres; because of this thickness, the oxidation process may slow down significantly.

CHAPTER 8: CONCLUSION

In the introduction, the main objectives of this thesis were set out to 1) understand the phenomenon of oxidation wave in Electrochemically active Conducting Polymers (ECP) by building a 2-D numerical model. 2) Computationally design a microfluidic mixer and a pump that utilizes the ECP oxidation wave and find its efficiency to mix or pump electrolytes. 3) Build a 1D numerical model of a ECP hydrogel composite and find the concentration changes in the composite during electrochemical actuation. And 4) explore the experimental methods to prepare and characterise various ECP composites and study the electrochemical actuation behaviour in a microfluidic channel. With respect to these objectives, those concerned with modelling have been achieved, but the attempts at experimental implementation have been less successful, though much has been learned.

The key contributions of the thesis are listed below

1. An efficient solution for 2D Nernst Plank equations was developed to understand the oxidation wave propagation in ECP. The mathematical model developed in chapter 4 showed that the key element determining the wave propagation is the proportion of the ionic flux in the solution near the interface that is carried by electro-migration rather than diffusion. The model also showed that it is possible to control the shape and the velocity of the wave front by controlling the relative conductivities of the electrolyte and of polymer in its oxidised and reduced state. The important attributes of the reported experimental results on the oxidation wave propagation in ECP have been captured in the model. The Scharfetter and Gummel numerical method in a 2D domain developed to solve the drift diffusion equations has many advantages, as it conserves mass and is numerically stable. This method is robust and can also be extended to cover more difficult problems such as electrolytes with more than one species. Another unique aspect of the model is that it takes into consideration the effects of changes in the geometry of the electrochemical cell, which is important for designing practical microfluidic applications.
2. A mixer and a pump design which uses the expansion or contraction of ECP caused by oxidation wave propagation as a way to stimulate the electrolyte in direct contact with the polymer was developed. For practical implementation of such a pump or mixer, the results of chapter 5 showed that an expansion of 10% of a layer 50 μ m thick within a timescale of 1s would be needed. Whilst such expansions have readily been observed for

ECP actuated in non-aqueous or special electrolytes, most ECP show rather smaller effects in aqueous saline electrolytes of the type that might need to be moved in devices designed for biological measurement.

3. A 1D mathematical model was developed to predict the compositional changes that occur during the electrochemical reaction of ECP– hydrogel composites. Chapter 6 showed that significant actuation could potentially be obtained for a composite of an ECP and a suitably chosen hydrogel. The key was to disperse the ECP throughout the hydrogel such that an ion capacity of at least 2 M was obtained whilst maintaining electronic and ionic connectivity of the composite. The attempts at formulation presented in chapter 7 showed that, with PPy- hydrogel composites in aqueous chloride electrolyte, an ion capacity of 0.5 M could fairly readily be achieved.

8.1 Future Work

Our preliminary experimental studies are just the beginning of a practical device building process. From the experimental studies on the ECP-hydrogel composites, we can conclude that the type of hydrogel plays an important role in determining the amount of actuation that can be achieved. More studies could be done on synthesising a hydrogel that is more suited for this particular application. A hydrogel that is more sensitive to concentration changes and has sharp changes in the swelling properties is the key to construct a successful actuator. This hydrogel would mean that the ion capacity of the composite does not need to be very high to cause a minor change in the concentration. Low ion capacity range was the main issue in our experimental design to build actuators. The mathematical model can be used to calculate the concentration ranges of the electrolytes required to cause sufficient changes. Studies can also be performed to utilise the pH sensitivity property of the hydrogel. In this case, the ECP actuation can be utilised to cause a change in the pH of the hydrogel. Hydrogels that are more sensitive to pH change can be synthesised. The mathematical model can be modified to estimate the changes in positive ion concentration rather than the negative ion and thus can be used to predict the changes in the pH of the hydrogel.

There are also other parameters that can be explored, such as the type of the ECPs, solvent, and the ions used in the experiments. Our experimental studies have been done only on PPy with aqueous NaCl as electrolyte. Although water is the most practical and

most used solvent in biological studies, other solvents can also be used to validate the mathematical models and to demonstrate the actuation properties. Ion exchange properties of the polymers vary widely depending on the type of polymer and the type of ions. Thus, a detailed study can be done to identify the type of the polymer, salt, and the solvent that has a maximum ion exchange property in the hydrogels.

Once a processable, high actuation ECP composite material has been developed, it can be used to build a practical microfluidic pump or a mixer. A simple peristaltic pump can be built using the oxidation wave model developed. It should be noted that the peristaltic wave phenomenon is due to the switching of the ECP from its low to high conductivity state. An ECP composite prepared using conductive filling material will be conductive regardless of the state of oxidation of ECP will not have a propagating wave of compositional change. Hence it is important to prepare a composite with a switchable conductivity for this particular design. However, using high actuation composite materials, many different pump and mixer designs can be built. The UV curable hydrogel composites can be patterned using photolithography techniques to build actuators for microfluidic devices.

REFERENCES

- 1 Whitesides G M, The origins and the future of microfluidics. *Nature* 442, 368-373 (2006).
- 2 Karnik R, Yue M, Li D, Yang P, Majumdar, A Electrostatic Control of Ions and Molecules in Nanofluidic Transistors. *Nano letters*, 943-948 (2005).
- 3 Tan T C, Lee A I, Vittorio C, Abraham P L, Design of microfluidic channel geometries for the control of droplet volume, chemical concentration, and sorting. *Lab on a Chip* (2004).
- 4 Khandurina J, Jacobson S C, Waters L C, Foote R S, Ramsey J M Integrated System for Rapid PCR-Based DNA Analysis in Microfluidic Devices. *Analytical chemistry*, 2995-3000 (2000).
- 5 Ottino J M, Wiggins S, Introduction: Mixing in microfluidics. *Philos. Trans. R. Soc. Lond. Ser. A-Math. Phys. Eng. Sci.* 362, 923-935 (2004)
- 6 Ou J, Moss G R, Rothstein J P Enhanced mixing in laminar flows using ultrahydrophobic surfaces. *Phys. Rev. E* 76 (2007)
- 7 Swickrath M J, Burns S D, Wnek G E, Modulating passive micromixing in 2-D microfluidic devices via discontinuities in surface energy. *Sens. Actuator B-Chem.* 140, 656-662 (2009)
- 8 Stroock A D, Dertinger S K W, et al, Chaotic mixer for microchannels. *Science* 295, 647-651 (2002)
- 9 Tabeling P, Chabert M, Dodge A, Jullien C, Okkels F, Chaotic mixing in cross-channel micromixers. *Philos. Trans. R. Soc. Lond. Ser. A-Math. Phys. Eng. Sci.* 362, 987-1000 (2004)
- 10 Schwesinger N, Frank T, Wurmus H, A Modulator microfluid system with an integrated micromixer. *Journal of Micromechanics and Microengineering* 6, 99-102 (1996)
- 11 Ryu K S, Shaikh K, Goluch E, Fan Z F, Liu C Micro magnetic stir-bar mixer integrated with parylene microfluidic channels. *Lab on a Chip* 4, 608-613, (2004)
- 12 Tierno P, Johansen T H and Fischer T M, Magnetically driven colloidal microstirrer. *J. Phys. Chem. B* 111, 3077-3080 (2007)
- 13 Tsai T H, Liou D S, Chen P H, Yang C T in *2009 4th IEEE International Conference on Nano/Micro Engineered and Molecular Systems, Vols 1 and 2* 69-74 (2009)
- 14 Smela E, Conjugated polymer actuators. *MRS Bull.* 33, 197-204 (2008)
- 15 Baughman, R. H. Conducting polymer artificial muscles. *Synthetic Metals* 78, 339-353 (1996)
- 16 Sui J, Travas-Sejdic J, Chu S Y, Li K C, Kilmartin P A, The Actuation Behavior and Stability of p-Toluene Sulfonate Doped Polypyrrole Films Formed at Different Deposition Current Densities. *Journal of Applied Polymer Science* 111, 876-882 (2009)
- 17 Shoa T. N. et al. Electromechanical coupling in polypyrrole sensors and actuators. *Sens. Actuator A-Phys.* 161, 127-133 (2010)
- 18 Low L M, Seetharaman S, He K Q, Madou M J, Microactuators toward microvalves for responsive controlled drug delivery. *Sens. Actuator B-Chem.* 67, 149-160 (2000)
- 19 Ramirez-Garcia S. et al., Towards the development of a fully integrated polymeric microfluidic platform for environmental analysis. *Talanta* 77, 463-467 (2008)
- 20 Wu Y. et al. TITAN: a conducting polymer based microfluidic pump. *Smart Mater. Struct.* 14, 1511-1516 (2005)
- 21 Hara S, Zama T, Takashima W, Kaneto K TFSI-doped polypyrrole actuator with 26% strain. *J. Mater. Chem.* 14, 1516-1517 (2004)
- 22 Beebe D J et al. Functional hydrogel structures for autonomous flow control inside microfluidic channels. *Nature* 404, 588-590 (2000)
- 23 Bhat N V, Shaikh Y B Synthesis and structural investigation of conductive composites from cellophane and polypyrrole. *J. Appl. Polym. Sci.* 53, 187-191 (1994)
- 24 Gilmore K, Hodgson A J, Luan B, Small C J, Wallace G G. Preparation of hydrogel/conducting polymer composites. *Polymer Gels and Networks* 2, 135-143 (1994)
- 25 Guiseppi-Elie A, Wilson Ann M, Sujdak Andrew S. in *Tailored Polymeric Materials for Controlled Delivery Systems* Vol. 709 ACS Symposium Series Ch. 15, 185-202, American Chemical Society, (1998)
- 26 Small C J, Too C O, Wallace G G Responsive conducting polymer-hydrogel composites. *Polymer Gels and Networks* 5, 251-265 (1997)
- 27 Kim B C, Spinks G, Too C O, Wallace G G, Bae Y H Preparation and characterisation of processable conducting polymer-hydrogel composites. *Reactive and Functional Polymers* 44 (2000)
- 28 IEEE website in *IEEE Global History Network* (IEEE)
- 29 Feynman R P in *Engineering and Science*, Caltech (1959)
- 30 Nathanson H C, Newell W E, Wickstrom R A, Davis J R Jr The resonant gate transistor.

- 31 *Electron Devices, IEEE Transactions on* 14, 117-133 (1967)
- 32 Roylance L, Angell J in *Solid-State Circuits Conference. Digest of Technical Papers, IEEE International*. 220-221 (1978)
- 33 Fan L S, Tai Y C, Muller R S IC-processed electrostatic micromotors. *Sensors and Actuators* 20, 41-47 (1989)
- 34 Petersen K E Silicon as a mechanical material. *Proceedings of the IEEE* 70, 420-457 (1982)
- 35 Sharpe W. *et al.* Strain Measurements of Silicon Dioxide Microspecimens by Digital Imaging Processing. *Experimental Mechanics* 47 (2007)
- 36 French P J, Sarro P M Surface versus bulk micromachining: the contest for suitable applications. *Journal of Micromechanics and Microengineering* 8, 45 (1998)
- 37 Bustillo J M, Howe R T, Muller R S Surface micromachining for microelectromechanical systems. *Proceedings of the IEEE* 86, 1552-1574 (1998)
- 38 Kovacs G T A, Maluf N I, Petersen K E Bulk micromachining of silicon. *Proceedings of the IEEE* 86, 1536-1551 (1998)
- 39 Howard R E, Liao P F, Skocpol W J, Jackel L D, Craighead H G Microfabrication as a Scientific Tool. *Science* 221, 117-121 (1983)
- 40 Papakonstantinou P, Vainos N A, Fotakis C Microfabrication by UV femtosecond laser ablation of Pt, Cr and indium oxide thin films. *Applied Surface Science* 151, 159-170, (1999)
- 41 Takai M, Bollmann D, Habeger K Maskless patterning of indium tin oxide layer for flat panel displays by diode pumped laser irradiation. *Applied Physics Letters* 64, 2560-2562 (1994)
- 42 Yuan D Laser direct-write microfabrication and patterning *PhD thesis, University of Michigan, (2008)*
- 43 Chong T C, Hong M H, Shi L P Laser precision engineering: from microfabrication to nanoprocessing. *Laser & Photonics Reviews* 4, 123-143, (2010)
- 44 Osellame R, Hoekstra H J W M, Cerullo G, Pollnau M Femtosecond laser microstructuring: an enabling tool for optofluidic lab-on-chips. *Laser & Photonics Reviews* 5, 442-463, (2011)
- 45 Bassous E, Taub H H, Kuhn L Ink jet printing nozzle arrays etched in silicon. *Applied Physics Letters* 31, 135-137 (1977)
- 46 Terry S C, Jerman J H, Angell J B A gas chromatographic air analyzer fabricated on a silicon wafer. *Electron Devices, IEEE Transactions on* 26, 1880-1886 (1979)
- 47 DeWitt S H Micro reactors for chemical synthesis. *Current Opinion in Chemical Biology* 3, 350-356 (1999)
- 48 Dittrich P S, Manz A Lab-on-a-chip: microfluidics in drug discovery. *Nat Rev Drug Discov* 5, 210-218 (2006)
- 49 Kraly J R, Holcomb R E, Guan Q, Henry C S Review: Microfluidic applications in metabolomics and metabolic profiling. *Analytica Chimica Acta* 653, 23-35 (2009)
- 50 Psaltis D, Quake S, Yang C Developing optofluidic technology through the fusion of microfluidics and optics. *Nature* 442, 381-386 (2006)
- 51 Chin C D *et al.* Microfluidics-based diagnostics of infectious diseases in the developing world. *Nat Med* 17, 1015-1019 (2011)
- 52 Ma C *et al.* A clinical microchip for evaluation of single immune cells reveals high functional heterogeneity in phenotypically similar T cells. *Nat Med* 17, 738-743, (2011)
- 53 Devadhasan J, Kim S, An J Fish-on-a-chip: a sensitive detection microfluidic system for alzheimer's disease. *Journal of Biomedical Science* 18, 33 (2011)
- 54 Yager P. *et al.*, Microfluidic diagnostic technologies for global public health. *Nature* 442, 412-418 (2006)
- 55 Kamei T. *et al.*, Microfluidic Genetic Analysis with an Integrated a-Si:H Detector. *Biomedical Microdevices* 7, 147-152 (2005)
- 56 Jha S K, Joo G S, Ra G S, Lee H H, Kim Y S Development of PCR Microchip for Early Cancer Risk Prediction. *Sensors Journal, IEEE* 11, 2065-2070 (2011)
- 57 Lion N. *et al.* Microfluidic systems in proteomics. *Electrophoresis* 24, 3533-3562, (2003)
- 58 Vinuselvi P. *et al.* Microfluidic Technologies for Synthetic Biology. *International Journal of Molecular Sciences* 12, 3576-3593 (2011)
- 59 Wlodkowic D, Cooper J M Tumors on chips: oncology meets microfluidics. *Current Opinion in Chemical Biology* 14, 556-567 (2010)
- 60 Choban E R, Markoski L J, Wieckowski A, Kenis P J A Microfluidic fuel cell based on laminar flow. *Journal of Power Sources* 128, 54-60 (2004)
- 61 Wei Z. *et al.* A Laminar Flow Electroporation System for Efficient DNA and siRNA Delivery. *Analytical Chemistry* 83, 5881-5887 (2011)
- Maenaka H, Yamada M, Yasuda M, Seki M Continuous and Size-Dependent Sorting of

- Emulsion Droplets Using Hydrodynamics in Pinched Microchannels. *Langmuir* 24, 4405-4410 (2008)
- 62 Nam-Trung N, Zhigang W Micromixers—a review. *Journal of Micromechanics and Microengineering* 15, R1 (2005)
- 63 Stiles T *et al.* Hydrodynamic focusing for vacuum-pumped microfluidics. *Microfluidics and Nanofluidics* 1, 280-283 (2005)
- 64 Malecha K, Golonka L J, Baldyga J, Jasinska M, Sobieszuk P Serpentine microfluidic mixer made in LTCC. *Sensors and Actuators B: Chemical* 143, 400-413 (2009)
- 65 Kim D S, Lee S H, Kwon T H, Ahn C H A serpentine laminating micromixer combining splitting/recombination and advection. *Lab on a Chip* 5, 739-747 (2005)
- 66 Lin Y, Gerfen G J, Rousseau D L, Yeh S R Ultrafast Microfluidic Mixer and Freeze-Quenching Device. *Analytical Chemistry* 75, 5381-5386 (2003)
- 67 Che-Hsin L *et al.* A rapid three-dimensional vortex micromixer utilizing self-rotation effects under low Reynolds number conditions. *Journal of Micromechanics and Microengineering* 15, 935 (2005)
- 68 Xize N, Yi-Kuen L Efficient spatial-temporal chaotic mixing in microchannels. *Journal of Micromechanics and Microengineering* 13, 454 (2003)
- 69 Luong T D, Phan V N, Nguyen N T High-throughput micromixers based on acoustic streaming induced by surface acoustic wave. *Microfluidics and Nanofluidics* 10, 619-625,(2011)
- 70 Campisi M, Accoto D, Damiani F, Dario P A soft-lithographed chaotic electrokinetic micromixer for efficient chemical reactions in lab-on-chips. *Journal of Micro - Nano Mechatronics* 5, 69-76 (2009)
- 71 Chen C K, Cho C C Electrokinetically driven flow mixing utilizing chaotic electric fields. *Microfluidics and Nanofluidics* 5, 785-793(2008)
- 72 Affanni A, Chiorboli G Development of an enhanced MHD micromixer based on axial flow modulation. *Sensors and Actuators B: Chemical* 147, 748-754 (2010)
- 73 Francais O *et al.* A Thermally-Driven Micromixer Based on Fluid Volume Variation. *ASME Conference Proceedings* 685-692 (2006)
- 74 Prettyman J B, Eddington D T Leveraging stimuli responsive hydrogels for on/off control of mixing. *Sensors and Actuators B: Chemical* 157, 722-726 (2011)
- 75 Himstedt H H. *et al.* Magnetically Activated Micromixers for Separation Membranes. *Langmuir* 27, 5574-5581 (2011)
- 76 Ryu K S, Shaikh K, Goluch E, Fan Z, Liu C Micro magnetic stir-bar mixer integrated with parylene microfluidic channels. *Lab on a Chip* 4, 608-613 (2004)
- 77 Williams A, Akle B, Vlachos P Active Laminar Mixing Induced by Surface Disturbance. *ASME Conference Proceedings* 2006, 1077-1085,(2006)
- 78 Chao C S, Huang P-C, Chen M K, Jang L S Design and analysis of charge-recovery driving circuits for portable peristaltic micropumps with piezoelectric actuators. *Sensors and Actuators A: Physical* 168, 313-319,(2011)
- 79 Hwang S F, Shiu Y S Fabrication and characterization of two-chamber and three-chamber peristaltic micropumps. *International Journal of Precision Engineering and Manufacturing* 11, 613-618 (2010)
- 80 Trenkle F, Haerberle S, Zengerle R Normally-closed peristaltic micropump with re-usable actuator and disposable fluidic chip. *Sensors and Actuators B: Chemical* 154, 137-141, (2011)
- 81 Ohuchi K, Tsuchiya K, Uetsuji Y *Micro-NanoMechatronics and Human Science (MHS), 2010 International Symposium on.* 269-274 (2010)
- 82 Fang Y, Tan X A novel diaphragm micropump actuated by conjugated polymer petals: Fabrication, modeling, and experimental results. *Sensors and Actuators A: Physical* 158 (2010)
- 83 Kwon G H, Jeong G S, Park J Y, Moon J H, Lee S H. A low-energy-consumption electroactive valveless hydrogel micropump for long-term biomedical applications. *Lab on a Chip* 11, 2910-2915 (2011)
- 84 Ates M, Sarac A S Conducting polymer coated carbon surfaces and biosensor applications. *Progress in Organic Coatings* 66, 337-358,(2009)
- 85 Wanekaya A K *et al.* Field-Effect Transistors Based on Single Nanowires of Conducting Polymers. *The Journal of Physical Chemistry C* 111, 5218-5221 (2007)
- 86 Gao J, Heeger A J, Lee J Y, Kim C Y Soluble polypyrrole as the transparent anode in polymer light-emitting diodes. *Synthetic Metals* 82, 221-223,(1996)
- 87 Svirskis D, Travas-Sejdic J, Rodgers A, Garg S Electrochemically controlled drug delivery based on intrinsically conducting polymers. *Journal of Controlled Release* 146, 6-15, (2010)

- 88 Qin H, Liu Z, Yin W, Zhu J, Li Z A cobalt polypyrrole composite catalyzed cathode for the direct borohydride fuel cell. *Journal of Power Sources* 185, 909-912 (2008)
- 89 Pei Q, Zuccarello G, Ahlskog M, Ingnas O Electrochromic and highly stable poly(3, 4-ethylenedioxythiophene) switches between opaque blue-black and transparent sky blue. *Polymer* 35, 1347-1351 (1994)
- 90 Sadki S, Schottland P, Brodie N, Sabouraud G The mechanisms of pyrrole electropolymerization. *Chemical Society Reviews* 29, 283-293 (2000)
- 91 Genies E M, Bidan G, Diaz A F Spectroelectrochemical study of polypyrrole films. *Journal of Electroanalytical Chemistry and Interfacial Electrochemistry* 149, 101-113, (1983)
- 92 Bjorklund R B Kinetics of pyrrole polymerisation in aqueous iron chloride solution. *Journal of the Chemical Society, Faraday Transactions 1: Physical Chemistry in Condensed Phases* 83, 1507-1514 (1987)
- 93 Rosseinsky D R *et al.* Mechanisms of the chemical and electrochemical polymerizations of pyrrole compared by product spectrometry and conductivity loss effected by pyridine inhibition or by over-oxidation. *Electrochimica Acta* 36, 733-738, (1991)
- 94 Beck F, Oberst M, Jansen R On the mechanism of the film forming electropolymerization of pyrrole in acetonitrile with water. *Electrochimica Acta* 35, (1990)
- 95 Kilmartin P A, Travas-Sejdic J in *Nanostructured Conductive Polymers.* 599-630 John Wiley & Sons, Ltd (2010)
- 96 Pei Q, Ingnas O Electrochemical applications of the bending beam method 2. Electroshrinking and slow relaxation in polypyrrole. *The Journal of Physical Chemistry* 97, 6034-6041 (1993)
- 97 Gandhi M R, Murray P, Spinks G M, Wallace G G Mechanism of electromechanical actuation in polypyrrole. *Synthetic Metals* 73, 247-256 (1995)
- 98 Suárez M F, Compton R G In situ atomic force microscopy study of polypyrrole synthesis and the volume changes induced by oxidation and reduction of the polymer. *Journal of Electroanalytical Chemistry* 462, 211-221 (1999)
- 99 Bay L, Jacobsen T, Skaarup S, West K. Mechanism of Actuation in Conducting Polymers: Osmotic Expansion. *The Journal of Physical Chemistry B* 105, 8492-8497 (2001)
- 100 Smela E Conjugated Polymer Actuators for Biomedical Applications. *Advanced Materials* 15, 481-494 (2003)
- 101 Smela E Microfabrication of PPy microactuators and other conjugated polymer devices. *Journal of Micromechanics and Microengineering* 9, 1 (1999)
- 102 Fredrik Pettersson P, Ingnas O in *1st Annual International Special Topic Conference on Microtechnologies in Medicine & Biology.* (ed David BEEBE) 334-335.
- 103 Casadevall i Solvas X, Lambert R, Kulinsky L, Rangel R, Madou M Micromixing and flow manipulation with polymer microactuators. *Microfluidics and Nanofluidics*, 1-12
- 104 Fuchiwaki M, Naka Y, Tanaka K Bimorph Type Soft Actuator Based on Conducting Polymer and Its Application to Micro Pump. *ASME Conference Proceedings* (2007)
- 105 Alici G, Mui B, Cook C. Bending modeling and its experimental verification for conducting polymer actuators dedicated to manipulation applications. *Sensors and Actuators A: Physical* 126, 396-404 (2006)
- 106 Alici G, Metz P, Spinks G M A methodology towards geometry optimization of high performance polypyrrole (PPy) actuators. *Smart Materials and Structures* 15, 243 (2006)
- 107 Yao Q, Alici G, Spinks G M Feedback control of tri-layer polymer actuators to improve their positioning ability and speed of response. *Sensors and Actuators A: Physical* 144, 176-184 (2008)
- 108 Lefevre F, Izquierdo R, Schougaard S B *Circuits and Systems and TAISA Conference, 2008. NEWCAS-TAISA 2008 Joint 6th International IEEE Northeast Workshop on.* 318-322 (2008)
- 109 Kim J H *et al.*, Performance characteristics of a polypyrrole modified polydimethylsiloxane (PDMS) membrane based microfluidic pump. *Sensors and Actuators A: Physical* 148, 239-244, (2008)
- 110 Wei W, Shuxiang G in *Robotics and Biomimetics (ROBIO), 2010 IEEE International Conference.* 1577-1583 (2010)
- 111 Naka Y, Fuchiwaki M, Tanaka K A micropump driven by a polypyrrole-based conducting polymer soft actuator. *Polymer International* 59, 352-356, (2010)
- 112 Causley J, Stitzel S, Brady S, Diamond D, Wallace G. Electrochemically-induced fluid movement using polypyrrole. *Synthetic Metals* 151, 60-64 (2005)
- 113 Thomas Steen H *et al.*, An all-polymer micropump based on the conductive polymer poly(3,4-ethylenedioxythiophene) and a polyurethane channel system. *Journal of Micromechanics and*

- Microengineering* 17, 860 (2007)
- 114 Habu Y, Narkis M, Titelman G I, Siegmann A Polyaniline–DBSA polymer blends prepared via aqueous dispersions. *Synthetic Metals* (1999)
- 115 Jayashree anand, S P, Sathyanarayana D N Conducting polyaniline blends and composites. *Prog. Polym. Sci* (1998)
- 116 Eli ruckenstein J S P New method for the preparation of thick conducting polymer composites. *Journal of Applied Polymer Science* (1991)
- 117 An H. *et al.* Polypyrrole/carbon aerogel composite materials for supercapacitor. *Journal of Power Sources* 195, 6964-6969, doi:DOI: 10.1016/j.jpowsour.2010.04.074 (2010)
- 118 Park J H, Ko, J M, Park O O, Kim D.-W Capacitance properties of graphite/polypyrrole composite electrode prepared by chemical polymerization of pyrrole on graphite fiber. *Journal of Power Sources* 105, 20-25 (2002)
- 119 Coffey B, Madsen P V, Poehler T O, Searson P C High charge density conducting polymer/graphite fiber composite electrodes for battery applications. *Journal of The Electrochemical Society* 142, 321-325 (1995)
- 120 Travas-Sejdic J, Easteal A Swelling equilibria and volume phase transition of polyelectrolyte gel with strongly dissociated groups. *Polymer Gels and Networks* 5, 481-502 (1998)
- 121 Horkay F, Tasaki I, Basser P J Osmotic swelling of polyacrylate hydrogels in physiological salt solutions. *Biomacromolecules* 1, 84-90, doi:10.1021/bm9905031 (2000)
- 122 Tao Y, Zhao J X, Wu C X Polyacrylamide hydrogels with trapped sulfonated polyaniline. *European Polymer Journal* 41, 1342-1349 (2005)
- 123 Tang Q *et al.* Polyaniline/polyacrylamide conducting composite hydrogel with a porous structure. *Carbohydrate Polymers* 74, 215-219 (2008)
- 124 Tang Q, Lin J, Wu J, Zhang C, Hao S Two-steps synthesis of a poly(acrylate-aniline) conducting hydrogel with an interpenetrated networks structure. *Carbohydrate Polymers* 67, 332-336 (2007)
- 125 Owino J H O, Arotiba O A, Baker, P G L, Guiseppi – Elie A, Iwuoha E I Synthesis and characterization of poly (2-hydroxyethyl methacrylate)-polyaniline based hydrogel composites. *Reactive and Functional Polymers* 68, 1239-1244 (2008)
- 126 Aouada F A *et al.* Electrochemical and mechanical properties of hydrogels based on conductive poly(3,4-ethylene dioxithiophene)/poly(styrenesulfonate) and PAAm. *Polymer Testing* 25, 158-165 (2006)
- 127 Wieczorek W, Florjanczyk Z, Stevens J R Proton conducting polymer gels based on a polyacrylamide matrix. *Electrochimica Acta* 40, 2327-2330 (1995)
- 128 Siddhanta S K, Gangopadhyay R Conducting polymer gel: formation of a novel semi-IPN from polyaniline and crosslinked poly(2-acrylamido-2-methyl propanesulphonic acid). *Polymer* 46, 2993-3000, doi:10.1016/j.polymer.2005.01.084 (2005)
- 129 Tang Q *et al.* Superabsorbent conducting hydrogel from poly(acrylamide-aniline) with thermo-sensitivity and release properties. *Carbohydrate Polymers* 73, 473-481 (2008)
- 130 Kim B C, Spinks G M, Wallace G G, John R Electroformation of conducting polymers in a hydrogel support matrix. *Polymer* 41, 1783-1790 (2000)
- 131 Brahim S, Guiseppi-Elie A Electroconductive hydrogels: Electrical and electrochemical properties of Polypyrrole-Poly(HEMA) composites. *Electroanalysis* 17, 556-570 (2005)
- 132 Li Y, Neoh K G, Kang E T Controlled release of heparin from polypyrrole-poly(vinyl alcohol) assembly by electrical stimulation. *Journal of Biomedical Materials Research Part A* 73A, 171-181 (2005)
- 133 Chansai P, Sirivat A, Niamlang S, Chotpattananont D, Viravaidya-Pasuwat K Controlled transdermal iontophoresis of sulfosalicylic acid from polypyrrole/poly(acrylic acid) hydrogel. *International Journal of Pharmaceutics* 381, 25-33 (2009)
- 134 Lira L M, Córdoba de Torresi S I Conducting polymer-hydrogel composites for electrochemical release devices: Synthesis and characterization of semi-interpenetrating polyaniline-polyacrylamide networks. *Electrochemistry Communications* 7, 717-723 (2005)
- 135 Tang Q, Wu J, Lin J A multifunctional hydrogel with high conductivity, pH-responsive, thermo-responsive and release properties from polyacrylate/polyaniline hybrid. *Carbohydrate Polymers* 73, 315-321 (2008)
- 136 Lin J, Tang Q, Wu J, Li Q. A multifunctional hydrogel with high-conductivity, pH-responsive, and release properties from polyacrylate/polypyrrole. *Journal of Applied Polymer Science* 116, 1376-1383 (2010)
- 137 Lin J *et al.* Electric field sensitivity of conducting hydrogels with interpenetrating polymer

- network structure. *Colloids and Surfaces A: Physicochemical and Engineering Aspects* 346, 177-183 (2009)
- 138 A. K. Bajpai, J. B., Soni S N Preparation and characterization of electrically conductive composites of poly(vinyl alcohol)-g-poly(acrylic acid) hydrogels impregnated with polyaniline (PANI). *eXPRESS Polymer Letters* 2, 26-39 (2008)
- 139 Moschou E A, Peteu S. F, Bachas L G, Madou M J, Daunert S Artificial muscle material with fast electroactuation under neutral pH conditions. *Chemistry of Materials* 16, 2499-2502 (2004)
- 140 Moschou E A, Madou M J, Bachas L G, Daunert S Voltage-switchable artificial muscles actuating at near neutral pH. *Sensors and Actuators B: Chemical* 115, 379-383 (2006)
- 141 Tingyang D X Q, Shen C, Wang J, Lu Y High-strength multifunctional conducting polymer hydrogels. *Advanced Materials Research Vols*, 123-125 (2010)
- 142 Yamauchi T *et al.* Preparation of composite materials of polypyrrole and electroactive polymer gel using for actuating system. *Synthetic Metals* 152, 45-48 (2005)
- 143 Tanaka T, Nishio I, Sun S-T, Ueno-Nishio S Collapse of gels in an electric field. *Science* 218, 467-469 (1982)
- 144 Han Il K *et al.* Volume behavior of interpenetrating polymer network hydrogels composed of polyacrylic acid- co -poly(vinyl sulfonic acid)/polyaniline as an actuator. *Smart Materials and Structures* 15, 1882 (2006)
- 145 Brahim S, Narinesingh D, Guiseppi-Elie A Polypyrrole-hydrogel composites for the construction of clinically important biosensors. *Biosensors and Bioelectronics* 17, 53-59 (2002)
- 146 Kim D.-H, Abidian M, Martin D C Conducting polymers grown in hydrogel scaffolds coated on neural prosthetic devices. *Journal of Biomedical Materials Research Part A* 71A, 577-585 (2004)
- 147 Ogawa J, Kanno I, Kotera H, Wasa K, Suzuki T Development of liquid pumping devices using vibrating microchannel walls. *Sens. Actuator A-Phys.* 152, 211-218 (2009)
- 148 Wang S S, Huang X Y, Yang C Valveless micropump with acoustically featured pumping chamber. *Microfluidics and Nanofluidics* 8, 549-555
- 149 Tezuka Y, Aoki K Direct demonstration of the propagation theory of a conductive zone in a polypyrrole film by observing temporal and spatial variations of potentials at addressable microband array electrodes. *J. Electroanal. Chem.* 273, 161-168 (1989)
- 150 Tezuka, Y, Ohyama S, Ishii T, Aoki K Observation of propagation speed of conductive front in electrochemical doping process of polypyrrole films. *Bulletin of the Chemical Society of Japan* 64, 2045-2051 (1991)
- 151 Lacroix J C, Fraoua K, Lacaze P C Moving front phenomena in the switching of conductive polymers. *Journal of Electroanalytical Chemistry* 444, 83-93 (1998)
- 152 Warren M R, Madden J D Electrochemical switching of conducting polymers: A variable resistance transmission line model. *Journal of Electroanalytical Chemistry* 590, 76-81 (2006)
- 153 Wang, X Z, Smela E Experimental Studies of Ion Transport in PPy(DBS). *J. Phys. Chem. C* 113, 369-381 (2009)
- 154 Wang X Z, Shapiro B, Smela E Visualizing ion currents in conjugated polymers. *Advanced Materials* 16, 1605 (2004)
- 155 Wang X Z, Shapiro B, Smela E Development of a Model for Charge Transport in Conjugated Polymers. *J. Phys. Chem. C* 113, 382-401 (2009)
- 156 Brumleve T R, Buck R P Transmission-line equivalent-circuit models for electrochemical impedances. *Journal of Electroanalytical Chemistry* 126, 73-104 (1981)
- 157 Brumleve T R, Buck R P Numerical-solution of nernst-planck and poisson equation system with applications to membrane electrochemistry and solid-state physics. *Journal of Electroanalytical Chemistry* 90, 1-31 (1978)
- 158 Scharfetter D I, Gummel H K Large-signal analysis of a silicon read diode oscillator. *IEEE Trans. Electron Devices* ED16, 64-77 (1969)
- 159 Cohen H, Cooley J W Numerical solution of time-dependent Nernst-Planck equations. *Biophys. J.* 5, 145-162 (1965)
- 160 Feldman B J, Burgmayer P, Murray R W The potential dependence of electrical-conductivity and chemical charge storage of poly(pyrrole) films on electrodes. *Journal of the American Chemical Society* 107, 872-878 (1985).
- 161 Feldberg S W Reinterpretation of polypyrrole electrochemistry - consideration of capacitive currents in redox switching of conducting polymers. *Journal of the American Chemical Society* 106, 4671-4674 (1984)

- 162 Albery W J, Elliott C M, Mount A R A transmission-line model for modified electrodes
and thin-layer cells. *Journal of Electroanalytical Chemistry* 288, 15-34 (1990)
- 163 Albery W J, Mount A R Transmission-line model for conducting polymers including
cations and donnan exclusion. *Journal of the Chemical Society-Faraday Transactions* 89,
 2487-2497 (1993)
- 164 Newman J S, Thomas-Alyea K E *Electrochemical Systems*. 3rd edn, 286-9 John Wiley
 (2004)
- 165 Chu S Y *et al.* The effect of monomer and electrolyte concentrations during synthesis on the
actuation of PPy(CF₃SO₃) films in aqueous electrolytes. *Synthetic Metals* 158, 38-44 (2008)
- 166 Takashima W, Pandey S S, Kaneto K Investigation of bi-ionic contribution for the
enhancement of bending actuation in polypyrrole film. *Sensors and Actuators B: Chemical* 89,
 48-52 (2003)
- 167 Han G, Shi G High-response tri-layer electrochemical actuators based on conducting
polymer films. *J. Electroanal. Chem.* 569, 169-174 (2004)
- 168 Baker J P, Stephens D R, Blanch H W, Prausnitz J M Swelling equilibria for acrylamide-
based polyampholyte hydrogels. *Macromolecules* 25, 1955-1958 (1992)
- 169 Aalaie J, Vasheghani-Farahani E, Semsarzadeh M A, Rahmatpour A Gelation and Swelling
Behavior of Semi-Interpenetrating Polymer Network Hydrogels Based on Polyacrylamide and
Poly(vinyl alcohol). *Journal of Macromolecular Science, Part B* 47, 1017-1027 (2008)
- 170 Chinn D, Janata, J Spin-cast thin films of polyaniline. *Thin Solid Films* 252, 145-151 (1994)
- 171 Armes S P, Aldissi M Preparation and characterization of colloidal dispersions of
polypyrrole using poly(2-vinyl pyridine)-based steric stabilizers. *Polymer* 31, 569-574 (1990)
- 172 Kim J, You J, Kim E Flexible Conductive Polymer Patterns from Vapor Polymerizable and
Photo-Cross-Linkable EDOT. *Macromolecules* 43, 2322-2327(2010)
- 173 Mazur M, Krysiński P Bulk- and surface-initiated chemical in situ polymerisation of 2,5-
dimethoxyaniline and 2-methoxyaniline on thiol-coated gold electrodes. *Electrochimica Acta*
 46, 3963-3971 (2001)
- 174 Waghuley S A, Yenorkar S M, Yawale S S, Yawale S P Application of chemically
synthesized conducting polymer-polypyrrole as a carbon dioxide gas sensor. *Sensors and*
Actuators B: Chemical 128, 366-373 (2008)
- 175 Lee E S, Park J H, Wallace G G, Bae Y H In situ formed processable polypyrrole
nanoparticle/amphiphilic elastomer composites and their properties. *Polymer International* 53,
 (2004)
- 176 Lee Y M, Kim J H, Kang, J S, Ha S Y Annealing Effects of Dilute Polyaniline/NMP
Solution. *Macromolecules* 33, 7431-7439 (2000)
- 177 Cui T, Liang G, Varahramyan K An organic poly(3, 4-ethylenedioxythiophene) field-
effect transistor fabricated by spin coating and reactive ion etching. *Electron Devices, IEEE*
Transactions on, 50, 1419-1422 (2003)
- 178 Dai L, Mau A W H, Gong X, Griesser H J Electrochemical generation of conducting
polymer patterns on plasma modified surfaces. *Synthetic Metals* 85, 1379-1380 (1997)
- 179 Çakmak G, Küçükyavuz Z, Küçükyavuz S Flexible and conducting composites of
polypyrrole and polydimethylsiloxane. *J. Appl. Polym. Sci.* 93, 736-741 (2004)
- 180 Cakmak G, Küçükyavuz Z, Küçükyavuz S Conductive copolymers of polyaniline,
polypyrrole and poly(dimethylsiloxane). *Synthetic Metals* 151, 10-18 (2005)
- 181 Muthulakshmi B, Kalpana D, Pitchumani S, Renganathan N G Electrochemical deposition
of polypyrrole for symmetric supercapacitors. *Journal of Power Sources* 158, 1533-1537,
 (2006)
- 182 Jurewicz K, Delpoux S, Bertagna V, Béguin F, Frackowiak E Supercapacitors from
nanotubes/polypyrrole composites. *Chemical Physics Letters* 347, 36-40 (2001)
- 183 Laslau C, Williams D E, Kannan B, Travas-Sejdic J Scanned Pipette Techniques for the
Highly Localized Electrochemical Fabrication and Characterization of Conducting Polymer
Thin Films, Microspots, Microribbons, and Nanowires. *Advanced Functional Materials* (2011)
- 184 Onuki Y, Nishikawa M, Morishita M, Takayama K Development of photocrosslinked
polyacrylic acid hydrogel as an adhesive for dermatological patches: Involvement of
formulation factors in physical properties and pharmacological effects. *International Journal*
of Pharmaceutics 349, 47-52, (2008)